

THE UNIVERSITY OF CALGARY.

STRUCTURAL AND CONFORMATIONAL ENERGY STUDIES OF  
LIGANDS OF ANGIOTENSIN CONVERTING ENZYME AND  
THERMOLYSIN

BY

Alice Vrielink

A THESIS

SUBMITTED TO THE FACULTY OF GRADUATE STUDIES  
IN PARTIAL FULFILLMENT OF THE REQUIREMENTS FOR THE  
DEGREE OF MASTER OF SCIENCE

DEPARTMENT OF CHEMISTRY

CALGARY, ALBERTA

DECEMBER, 1985

© Alice Vrielink, 1985

Permission has been granted to the National Library of Canada to microfilm this thesis and to lend or sell copies of the film.

The author (copyright owner) has reserved other publication rights, and neither the thesis nor extensive extracts from it may be printed or otherwise reproduced without his/her written permission.

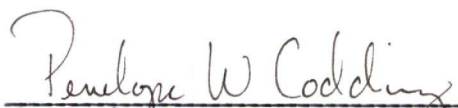
L'autorisation a été accordée à la Bibliothèque nationale du Canada de microfilmer cette thèse et de prêter ou de vendre des exemplaires du film.

L'auteur (titulaire du droit d'auteur) se réserve les autres droits de publication; ni la thèse ni de longs extraits de celle-ci ne doivent être imprimés ou autrement reproduits sans son autorisation écrite.

ISBN 0-315-30026-4

THE UNIVERSITY OF CALGARY  
FACULTY OF GRADUATE STUDIES

The undersigned certify that they have read, and recommend to the Faculty of Graduate Studies for acceptance, a thesis entitled "Structural and Conformational Energy Studies of Ligands of Angiotensin Converting Enzyme and Thermolysin" by Alice Vrieling in partial fulfillment of the requirements for the degree of Master of Science.

  
\_\_\_\_\_  
Supervisor, Dr. P.W. Coddling  
Department of Chemistry

  
\_\_\_\_\_  
Dr. R.E. Huber  
Department of Chemistry

  
\_\_\_\_\_  
Dr. R.S. Roche  
Department of Chemistry

  
\_\_\_\_\_  
Dr. G. Moore  
Department of Medical Biochemistry

Date January 2, 1986

## ABSTRACT

Angiotensin converting enzyme (ACE) is a regulatory zinc peptidase in the renin-angiotensin system that converts the decapeptide, angiotensin I to the octapeptide, angiotensin II. Angiotensin II acts to increase blood pressure through a negative feedback loop. Treatment of hypertension has involved the development of inhibitors of ACE. The crystal structure determination of two ACE inhibitors, S,S-1-[3-(benzoylthio)-2-methyl-1-oxopropyl]-indoline-2-carboxylic acid, WY44088, and S,S-1-[3-mercapto-2-methyl-oxopropyl]-indoline-2-carboxylic acid, WY44221, as well as the substrate analogue of angiotensin I, hippuryl-L-histidyl-L-leucine, have been carried out. Structural comparisons of these compounds with captopril [54] show, in the case of the inhibitors, major differences in the configuration about the peptide bond; captopril adopts a *trans* configuration, whereas, the two indoline inhibitors adopt a *cis* configuration. The substrate analogue, however, has the same peptide bond configuration as captopril.

Conformational energy calculations using the molecular mechanics program, YETI, [51], have been carried out on two inhibitor complexes of thermolysin. These calculations show that the important residues for ligand binding to the active site are Arg 203, which forms hydrogen bonds to the inhibitor, and the S<sub>1</sub>' subsite, which enhances the binding through hydrophobic interactions with the inhibitor. Asn 112 may further enhance the binding through hydrogen bonds, however, this interaction appears to be less important than that with Arg 203. The zinc atom also plays an important role in ligand binding; the coordination geometry about the metal ion is optimally tetrahedral for

the inhibitors studied.

Molecular mechanics calculations were also carried out on the complex of the ACE inhibitor, WY44221, and thermolysin. A minimum energy conformation was found which has a *cis* configuration about the peptide bond.

One important residue in the active site of the enzyme is Arg 203 which forms a three center hydrogen bond with the carboxyl group of WY44221. The minimized structure has optimally a distorted tetrahedral geometry about the zinc atom. These studies show that thermolysin could be a reasonable model for studying the active site of angiotensin converting enzyme and can aid in the design of new ACE inhibitors.

## ACKNOWLEDGEMENTS

I would like to thank the following people for their assistance and support throughout this work:

- my supervisor, Dr. Penelope Coddling, without whose guidance and patience this work would not have been possible and whose love for science has been a constant inspiration to me. Not only has she been a model supervisor but an invaluable friend with whom I have spent many happy moments.

- Dr. D.H. Kim of Wyeth Pharmaceuticals for providing the two ACE inhibitors, WY44221 and WY44088.

- Dr. M.N.G. James of the University of Alberta for allowing me to use the interactive computer graphics facility in his laboratory.

- Dr. Ron Corbett for his assistance with the kinetic experiments.

- Mr. Ian Olthof for his assistance with the implementation of the molecular mechanics program.

- Ms. Anne Baird for the typing of this manuscript.

- The Alberta Heritage Foundation for Medical Research for providing the financial assistance in the form of a studentship and the University of Calgary for financial support in the form of graduate teaching assistantships.

To my mother and father,  
Mr. and Mrs. F.E. Vrielink.  
Thank you for your constant support  
and encouragement.

"There has been a great deal of speculation in traditional philosophy [read: chemistry] which might have been avoided if the importance of structure, and the difficulty of getting behind it, had been realized."

Bertrand Russell

## TABLE OF CONTENTS

	Page
ABSTRACT .....	iii
ACKNOWLEDGEMENTS .....	v
TABLE OF CONTENTS .....	viii
LIST OF TABLES .....	xi
LIST OF FIGURES .....	xiv
I. Introduction .....	1
II. Theory .....	11
1. Structure Solution .....	11
2. Structure Refinement .....	17
3. Molecular Mechanics .....	21
III. Crystal Structure Determination .....	26
1. Methods .....	26
2. Structure Solution of WY44088 .....	27
2.1 Experimental .....	27
2.2 Results .....	30
3. Structure Solution of WY44221 .....	40
3.1 Experimental .....	40
3.2 Results .....	42
4. Structure Solution of Hippuryl-L-histidyl-	
L-leucine .....	50

	Page
4.1 Experimental .....	50
4.2 Results .....	52
IV. Molecular Mechanics Experimental .....	68
1. Methods .....	68
2. Minimization of the Complex of Thermolysin and PPP .....	72
2.1 Experimental .....	72
2.2 Results .....	73
3. Minimization of the Complex of Thermolysin and BAG .....	84
3.1 Experimental .....	84
3.2 Results .....	85
4. Minimization of the Complex of Thermolysin and WY44221 .....	96
4.1 Kinetic Study of the Inhibition of Thermolysin by WY44221 .....	96
4.2 Experimental .....	98
4.3 Results .....	100
V. Discussion .....	110
1. Comparison of the X-Ray Structures .....	110
2. Molecular Mechanics Calculations of Thermolysin Inhibitors .....	115
3. Minimization of the Complex of Thermolysin and WY44221 .....	118

	Page
Appendix I      Torsion Angles for Amino Acid Residues ....	121
References .....	122

## LIST OF TABLES

Table		Page
1	Crystal Data for WY44088 .....	33
2	Fractional Atomic Coordinates and Equivalent Isotropic Temperature Factors for the Non- Hydrogen Atoms of WY44088 .....	34
3	Fractional Atomic Coordinates and Equivalent Isotropic Temperature Factors for the Hydrogen Atoms of WY44088 .....	35
4	Anisotropic Temperature Factors for the Non- Hydrogen Atoms of WY44088 .....	36
5	Bond Distances for WY44088 .....	37
6	Bond Angles for WY44088 .....	38
7	Torsion Angles for WY44088 .....	31
8	Crystal Data for WY44221 .....	44
9	Fractional Atomic Coordinates and Equivalent Isotropic Temperature Factors for WY44221 .....	45
10	Anisotropic Temperature Factors for the Non- Hydrogen Atoms of WY44221 .....	46
11	Bond Distances for WY44221 .....	47
12	Bond Angles for WY44221 .....	48
13	Torsion Angles for WY44221 .....	49
14	Crystal Data for hip-L-his-L-leu .....	56
15	Fractional Atomic Coordinates and Equivalent Isotropic Temperature Factors for the Non- Hydrogen Atoms of hip-L-his-L-leu .....	57

Table	Page
16 Fractional Atomic Coordinates and Equivalent Isotropic Temperature Factors for the Hydrogen Atoms of hip-L-his-L-leu .....	59
17 Anisotropic Temperature Factors for the Non- Hydrogen Atoms of Hip-L-his-L-leu .....	61
18 Distances for hip-L-his-L-leu .....	63
19 Bond Angles for hip-L-his-L-leu .....	65
20 Hydrogen Bond Parameters for hip-L-his-L-leu .....	67
21 Refinement Parameters Used in the Molecular Mechanics Calculations .....	71
22 Minimization Data for the Complex of Thermolysin and PPP .....	80
23 Comparison of Torsion Angles Before and After Minimization for the Complex of Thermolysin and PPP .....	81
24 Distances and Angles for the Zinc Atom Coordination Sphere for the Complex of Thermolysin and PPP .....	83
25 Minimization Data for the Complex of Thermolysin and BAG .....	91
26 Comparison of Torsion Angles Before and After Minimization for the Complex of Thermolysin and BAG .....	92
27 Distances and Angles for the Zinc Atom Coordination Sphere for the Complex of Thermolysin and BAG .....	94

Table	Page
28 Hydrogen Bond Interactions Before and After Minimization for the Complex of Thermolysin and BAG .....	95
29 Minimization Data for WY44221 .....	106
30 Comparison of Torsion Angles Before and After Minimization for the Complex of Thermolysin and WY44221 .....	107
31 Distances and Angles for the Zinc Atom Coordination Sphere for the Complex of Thermolysin and WY44221 .....	109

## LIST OF FIGURES

Figure		Page
1	Inhibitors of angiotensin converting enzyme .....	5
2	View of the active site of thermolysin .....	8
3	Molecular structure and atomic labelling scheme for WY44088 .....	32
4	Molecular structure and atomic labelling scheme for WY44221 .....	43
5	Molecular structure and atomic labelling scheme for hip-L-his-L-leu .....	54
6	Packing diagram of hip-L-his-L-leu showing the water sheath around the molecules .....	55
7	Stereoscopic drawings of the X-Ray and minimized complexes of thermolysin and PPP .....	76
8	Hydrogen bond interactions between PPP and Arg 203 after minimization .....	77
9	Stacking Interactions between the $\beta$ phenyl ring of PPP and Phe 114 of the enzyme after minimization .....	78
10	Superposition of the metal coordination geometry before and after refinement of the complex of thermolysin and PPP .....	79
11	Stereoscopic drawings of the X-ray and the minimized complexes of thermolysin and BAG .....	88
12	Hydrogen bonding residues for the complex of thermolysin and BAG minimizations .....	89

Figure		Page
13	Superposition of the metal coordination geometry before and after refinement of the complex of thermolysin and BAG .....	90
14	Plot of $k_{cat}/K_m$ versus the negative logarithm of the inhibitor concentration .....	97
15	Stereoscopic drawings of the X-ray and the minimized structures of WY44221 .....	103
16	Superposition of the metal coordination geometry before and after refinement of the complex of thermolysin and WY44221 .....	104
17	Hydrogen bonding interactions between Arg 203 and WY44221 for the modelled and the minimized complexes of thermolysin and WY44221 .....	105
18	Molecular Superposition of Captopril and WY44088 .....	112
19	Molecular Superposition of Captopril and WY44221 .....	113
20	Molecular Superposition of Captopril and hip-L-his-L-leu .....	114

## I. Introduction

The renin-angiotensin system is a closed loop, negative feedback system which modulates the constriction of blood vessels and blood volume homeostasis. The system is activated through the release of the proteolytic enzyme, renin, in the kidney. Renin specifically cleaves angiotensinogen, a protein that circulates in the blood, to form the inactive decapeptide, angiotensin I, Asp-Arg-Val-Tyr-Ile-His-Pro-Phe-His-Leu. Subsequently, angiotensin converting enzyme, (E.C.3.4.15.1, ACE), found mainly in the lungs, hydrolyzes the Phe-His peptide bond, releasing the dipeptide, His-Leu, and leaving the active octapeptide, angiotensin II, Asp-Arg-Val-Tyr-Ile-His-Pro-Phe. Angiotensin II acts as a potent vasopressor, increasing blood pressure both by the constriction of blood vessels and through the secretion of aldosterone which causes an increase in blood volume. The increase in blood pressure and volume is a negative feedback that stops any further release of renin. Malfunctions in the system can cause blood pressure to rise above the normal levels resulting in hypertension.

Inhibition of the renin angiotensin system has been therapeutically useful in the treatment of hypertensive diseases. The inhibition can occur, however, at a number of different sites, namely: renin inhibitors, angiotensin II antagonists, and ACE inhibitors. The work described in this thesis deals with inhibitors of ACE; these drugs bind to ACE and prevent the formation of angiotensin II. Reviews of the renin-angiotensin system and the drugs affecting it are given by Ashworth [1] and Ganong [2].

ACE requires the presence of a zinc atom and is a member of a group of zinc metalloexo- and endo-peptidases including thermolysin and

pancreatic carboxypeptidase A. The enzyme has a molecular weight of 124,000 Daltons and contains 1 gram atom of zinc per mole of protein. Studies done with the chromophoric substrate, furanacryloyl-Phe-Gly-Gly, showed no enzyme hydrolysis after the removal of the zinc atom by 1,10-phenanthroline; however, substrate binding to the enzyme was still observed [3]. The zinc atom is, therefore, not required for substrate binding but is important for enzymatic activity either because it polarizes the carbonyl bond of the scissile peptide linkage or it promotes the attack of water via a zinc hydroxide [4,5,6].

The X-ray structure of the enzyme has not yet been determined. ACE is usually found bound to cell membranes; it is, therefore, difficult to isolate and may not be active when crystallized unless the crystals contain a membrane-like environment. Chemical modifications of different residues have, however, been used to identify the amino acids that are essential for the catalytic activity of ACE [7]. The essential residues in the active site are tyrosine, arginine, glutamic acid, and lysine.

The development of specific ACE inhibitors has been the target of much research over the past number of years. The initial success was the design, by Cushman and Ondetti of the Squibb Institute for Medical Research [8,9], of an orally effective ACE inhibitor. Their design strategies were based on the known chemical and kinetic properties of ACE and on its similarities to pancreatic carboxypeptidase A. Based on the knowledge that ACE releases dipeptides from the carboxylic acid end of molecules and pancreatic carboxypeptidase A releases single amino acids, and that both enzymes contain a zinc atom essential for activity, the active sites of the two enzymes were assumed to be similar. Using

the binding interaction of the potent carboxypeptidase A inhibitor, D-benzyl-succinic acid, ( $K_i = 4.5 \times 10^{-7}$  M) [10] as a model and, accounting for the different specificities of the two enzymes, a number of ACE inhibitors were designed. 2-D-methyl-3-mercaptopropanoyl-L-proline (commonly known as captopril) was the most active with an  $IC_{50}$  value, the concentration for 50% inhibition, of  $1.1 \times 10^{-8}$  M. The basic structural requirements that Ondetti and Cushman postulated for ACE inhibitors are: a pyrrolidine ring, a carboxylic acid group at one end of the molecule, an amide group, a methyl group  $\alpha$  to the carbonyl bond, a group which coordinates to the zinc atom (such as the sulfhydryl group of captopril), and an S,S absolute configuration of the two chiral centers.

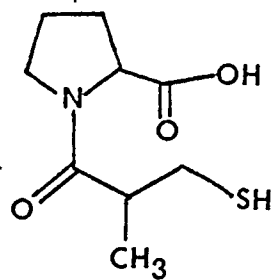
The successful design of captopril provided a model for the active site of the enzyme. The active site, proposed by Ondetti and Cushman [8,9], consists of a positively charged basic residue (arginine), that interacts with the carboxyl group of the substrate, a zinc ion that coordinates to the inhibitor or substrate molecule at a distance of a dipeptide from the arginine residue, a group (lysine), that will form a hydrogen bond to the amide carbonyl group, and two circular clefts that accommodate substituents on the dipeptide backbone.

Based on these minimum structural requirements, analogues of captopril have been prepared which are better inhibitors of ACE [11-14]. These new compounds provide a better delineation of the shape of the active site. For example, Kim and coworkers at Wyeth Laboratories [15] prepared analogues of captopril that contained an additional hydrophobic group. The X-ray structures of two of these inhibitors are described in this work. They are S,S-1-[3-(benzoylthio)-2-methyl-1-

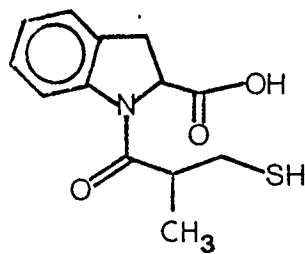
oxopropyl]-indoline-2-carboxylic acid (WY44088), which has an activity nearly equal to that of captopril ( $IC_{50} = 3.8 \times 10^{-8}$  M) and S,S-1-[3-mercapto-2-methyl-1-oxopropyl]-indoline-2-carboxylic acid, (WY44221), which is three times more active than captopril ( $IC_{50} = 3.7 \times 10^{-9}$  M) (see Figure 1). On the basis of the activity of these analogues, Kim proposed that the active site of ACE has a hydrophobic pocket that was not included in the Ondetti and Cushman model. This pocket could enhance the binding of inhibitors and thus increase their inhibitory potency.

The active site model of ACE can be further probed by comparing the shapes and potential energy profiles of different inhibitors to determine the common minimum energy structure for ACE inhibition. Andrews and coworkers did such a study on a series of potent ACE inhibitors having  $IC_{50}$  values in the nanomolar range [16]. Two inhibitors included in the series were WY44221 and captopril. Molecular mechanics calculations were performed on the isolated molecules. The results of these calculations indicate that there is an energy barrier of 2.1 kcal/mole between the *cis* and *trans* peptide bond conformers of captopril favoring the *trans* conformer. This barrier of rotation for WY44221 is 3.6 kcal/mole favoring the *cis* conformer due to the unfavorable interactions between the aromatic ring and the methyl carbon atom. From these potential energy calculations, it was concluded that the *trans* structure is the biologically active form. This was confirmed by the syntheses of two rigid *trans* ACE inhibitors by Merck ( $IC_{50} = 6 \times 10^{-10}$  M) [17] and Ciba Geigy ( $IC_{50} = 3 \times 10^{-9}$  M) [16].

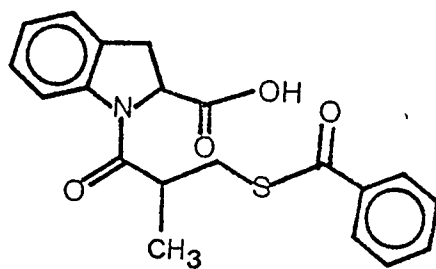
These calculations were, however, only done on the isolated inhibitors. Conformations of the inhibitors that are less stable in the



captopril



WY44221



WY44088

Figure 1

Inhibitors of angiotensin converting enzyme.

case of the isolated molecule can be stabilized by hydrogen bonding and van der Waals interactions with protein residues in the active site of an enzyme.

Molecular modelling studies using interactive computer graphics have been used as a tool for studying the molecular interactions of proteins with different ligands [18] and for predicting relative binding affinities [19]. These modelling studies would be useful in the study of inhibitors of ACE. These studies can be extended by using molecular mechanics to refine the modelled complexes to determine the low energy binding conformation of the complexes and the interactions contributing to this conformation.

Since the X-ray structure of ACE is not available, another enzyme must be chosen as a model for use in the calculations. The requirements for the model enzyme are:

1. It must be a zinc peptidase.
2. It must show some inhibition by ACE inhibitors.
3. The residues present in the active site must be implicated in the ACE mechanism.
4. It must have a well refined crystal structure.

The enzyme which meets these criteria and thus is most suited to act as a model for ACE is thermolysin. Thermolysin is a zinc-requiring endopeptidase of molecular weight 34,000 and is specific for peptide bonds on the imino side of hydrophobic residues. The atomic structure of native thermolysin has been refined by a restrained least squares procedure to a resolution of 1.6 Å and a crystallographic residual of 0.23 [20]. This, therefore, gives a very detailed and accurate description of the atomic structure of the active site of thermolysin.

Binding studies of a number of inhibitors to thermolysin have also been investigated crystallographically and provide extensive information about the interactions between inhibitor and enzyme [4,5,21-24]. These crystallographically determined complexes show very little conformational changes in the enzyme structure as a result of the binding of the inhibitors. Thermolysin also bears close similarities to a number of zinc enzymes in terms of its function and mechanistically important residues [25,26]. The residues in the active site of thermolysin which correspond to those postulated for the active site of ACE [8,9] include Arg 203, Asn 112 and Glu 143. Both enzyme active sites also contain a zinc atom. Thermolysin also contains a hydrophobic pocket which is referred to as the S<sub>1</sub> subsite. Kinetic binding studies, to be described in this work, show that ACE inhibitors do inhibit peptide cleavage by thermolysin. These factors make thermolysin a good model enzyme for elucidating the active site binding conformation of ACE inhibitors.

Thermolysin consists of two roughly spherical domains separated by a cleft across the middle of the molecule which contains the active site. The zinc atom essential for activity is contained in the active site and is tetrahedrally coordinated to NE2 of His 142, NE2 of His 145, OE1 of Glu 166, and H<sub>2</sub>O 0392 (this numbering corresponds to that found in the Brookhaven Protein Data Bank [27]). A diagram of the native enzyme showing the zinc coordination and the important active site residues is in Figure 2. Binding of an inhibitor to thermolysin replaces the water molecule by an oxygen atom on the inhibitor molecule. In some inhibitor complexes pentacoordination of the zinc ion is observed [4,21,24].

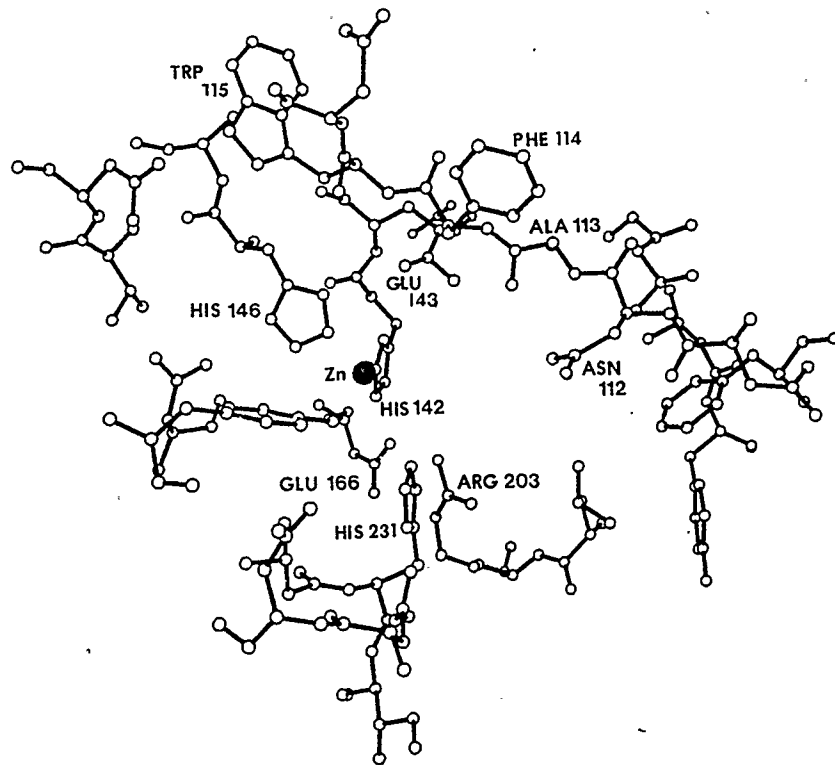


**Figure 2**

View of the active site of thermolysin.

The residues involved in zinc coordination and other important components of the active site are shown.

The binding features of the active site of thermolysin have been well characterized. The enzyme contains a hydrophobic pocket, denoted  $S_1$ , which binds phenyl rings or leucine side chains and is considered to be the primary substrate recognition site. An  $S_2$  hydrophobic subsite binds the tryptophan residue of the inhibitor, N-(1-carboxyl-3-phenylpropyl)-L-leucyl-tryptophan, CLT, [21] and the phosphoramidon inhibitor [23]. A water molecule is found in the active site that hydrogen bonds to the main chain nitrogen atom of Trp 115 and, often, to atoms on the inhibitor molecules. Residues in the active site which interact closely with the bound inhibitors are Asn 111, Asn 112, Ala 113, Trp 115, Glu 143, Tyr 157, His 231 and Arg 203 (see Figure 2).

Molecular modelling studies were carried out by Hangauer et al. [18] using the model substrate Z-Phe-Phe-Leu-Trp to elucidate the mechanism of action of thermolysin. These studies predicted that a transition state is formed in which the zinc ion is pentacoordinate. This hypothesis was substantiated by the crystal structure of the pentacoordinate complex of the inhibitor, CLT, and thermolysin. This inhibitor has a very low inhibition constant,  $K_i = 5 \times 10^{-8}$  M, which may be attributed to the pentacoordination of the zinc atom.

Molecular mechanics calculations of the structures of the inhibitor-thermolysin complexes are necessary in order to give a precise description of the essential binding interactions. Comparison of the results of these calculations with the crystal structures will also serve as a test of the validity of the calculation; the minimization results should not differ greatly from the crystal structures. Then, using thermolysin as the enzyme model for ACE, these calculations can be performed on modelled complexes of thermolysin-ACE inhibitors, to give

the active site binding conformation of these inhibitors.

## II. Theory

### 1. Structure Solution

The science of X-ray crystallography uses the internal ordered structure of a crystal and the properties of X-ray radiation to determine the positions of individual atoms and thus obtain a three dimensional representation of a molecule. The electron density distribution,  $\rho(r)$ , of a crystal, is calculated by the three dimensional Fourier series:

$$\rho(r) = \frac{1}{V} \sum_{hkl} F(hkl)e^{i2\pi(hx+ky+lz)} \quad (1)$$

where  $F(hkl)$  is the structure factor amplitude of the reflection,  $hkl$ , and  $\phi(hkl)$  is the phase angle. The structure factor is made up of two components, the amplitude  $|F(hkl)|$  and the phase and is expressed as:

$$F(hkl) = |F(hkl)|e^{i\phi(hkl)} \quad (2)$$

The X-ray experiment measures the intensities of the diffracted radiation from which the structure factor amplitudes can be calculated. The relationship between the measured intensity and the structure factor amplitude is given by:

$$|F(hkl)| = \sqrt{\frac{KI(hkl)}{Lp}} \quad (3)$$

where  $I(hkl)$  is the measured intensity and  $L$  is the Lorentz factor which corrects for the difference in the length of time required for any

single reciprocal lattice point to pass through the sphere of reflection. The polarization factor,  $p$ , is due to the polarized nature of the diffracted X-ray beam and accounts for the variation in the reflection efficiency with the reflection angle;  $K$  is the scale factor which related  $|F(hk\ell)|$  to the absolute number of electrons. The phase information, however, is missing from the data and obtaining that phase is the fundamental problem of X-ray crystallography, which is commonly known as the "phase problem".

In a centrosymmetric crystal lattice the presence of a center of inversion that relates the atomic positions restricts the possible values of the phase angle,  $\phi(hk\ell)$ , to either 0 or  $\pi$ . In this case the exponential term in equations 1 and 2 have only 2 values;  $\pm 1$  and the structure factor  $F(hk\ell)$  is related by a sign (+ or -) to the observed intensity. In noncentrosymmetric crystal lattices, the phase values are unrestricted and no simplification of equations 1 and 2 results.

The direct method is a mathematical technique used to solve the phase problem. It is particularly useful in solving crystal structures which have no unique atoms of high electron density and, therefore, is applicable to the structure determination of organic molecules. Hauptman and Karle [28], predicted that the phase information was contained in the measured intensities and could be determined, without any previous knowledge of the structure, by mathematical techniques developed from inequality theory and probability theory. The two assumptions of the direct method are:

1. The electron density can never be negative.
2. A correlation between the phases and the amplitudes is possible if the atoms in the structure are identical, spherically

symmetrical, and do not overlap in space.

Harker and Kasper [29] used these assumptions to develop a set of inequality expressions relating structure factors so that the phase of one reflection can be determined from the phase of another reflection. Hauptman and Karle applied the inequality expressions to generate a phase addition formula which, for centrosymmetric structures, is of the form:

$$s[E(hk\ell)] \approx s\left[\sum_{h'k'\ell'} E(h'k'\ell')E(h-h',k-k',\ell-\ell')\right] \quad (4)$$

where  $s$  means "the sign of",  $E(hk\ell)$  is the normalized structure factor, and the  $hk\ell$ 's are the indices of three reflections [28]. The summation is over all vector pairs with known signs whose indices add to give  $h$ ,  $k$ , and  $\ell$ . Equation 4 is also known as the Sigma 2 or the phase determining equation. As was pointed out earlier, the signs,  $(\pm 1)$ , can be used to represent the phase angle for centrosymmetric crystals.

The normalized structure factors are given by the equation:

$$|E(hk\ell)|^2 = \frac{K|F(hk\ell)|_0^2}{\epsilon \sum_{i=1} g_i(hk\ell)} \quad (5)$$

where  $K$  is a scale factor associated with  $|F(hk\ell)|$ , and  $g_i$  is the temperature corrected atomic scattering factor. The factor  $\epsilon$  takes into account the fact that, due to the symmetry of the space group, reflections in certain reciprocal lattice zones or rows will have a

higher average intensity than the general reflections. These values may be obtained from the International Tables [30]. The intensity data are corrected for thermal motion via statistical relationships between the intensities and the atomic scattering factors. The temperature factor and the scale factor are obtained by either a Wilson plot [31] or a K curve [32]. Normalized structure factors are used in the phase prediction formulae because they are corrected for the decrease in intensity of the scattering with  $\sin \theta$  and for the effect of thermal motion. The  $|E(hk\ell)|$  are, therefore, more compatible with assumption 2 of the theory of the direct method.

The probability that Equation 4 will correctly predict a positive phase is:

$$P_+(hk\ell) = \frac{1}{2} + \frac{1}{2} \tanh[(\sigma_3/\sigma_2^{3/2})\alpha'] \quad (6)$$

where  $\alpha'$  is given by:

$$\alpha' = |E(hk\ell)| \sum_{h'k'\ell'} E(h'k'\ell')E(h-h',k-k',\ell-\ell') \quad (7)$$

and  $\sigma$  is given by:

$$\sigma_n = \sum_j Z_j^n \quad (8)$$

and  $Z_j$  is the atomic number of the  $j$ th atom. Equations 6 and 7 show that the probability is directly proportional to the magnitudes of the absolute values of  $E(hk\ell)$ ; therefore, it is advantageous to use reflections which have large  $|E|$  values. If the signs of the strong

reflections are known, Equation 4 can be used to predict the sign of the third reflection with a high probability.

For the noncentrosymmetric case the equation used to determine the phases is of the form:

$$\phi(hk\ell) \approx \langle \phi(h'k'\ell') + \phi(h-h', k-k', \ell-\ell') \rangle_{(h'k'\ell')_r} \quad (9)$$

where  $\langle \rangle_r$  describes the weighted averages of  $\phi(h'k'\ell') + \phi(h-h', k-k', \ell-\ell')$  associated with large values  $|E|$ . Equation 9 applies only if all the  $|E|$  values are approximately of the same order of magnitude. To account for differing magnitudes of  $|E|$  the tangent formula is used:

$$\tan\phi(hk\ell) \approx \frac{E(h'k'\ell')E(h-h', k-k', \ell-\ell')}{E(h'k'\ell')E(h-h', k-k', \ell-\ell')} \frac{\sin\{\phi(h'k'\ell') + \phi(h-h', k-k', \ell-\ell')\}}{\cos\{\phi(h'k'\ell') + \phi(h-h', k-k', \ell-\ell')\}} \quad (10)$$

and equations 6, 7, and 8 are used to determine the probability of having the correct phase value.

Equations 4 and 10 require that the phases of some reflections be known in order to predict new phases. One origin in the unit cell is uniquely chosen by arbitrarily specifying the phases of three or fewer reflections having high  $|E|$  values and many interactions in the Sigma 2 equation. In non-centrosymmetric cases, the phase of an enantiomorph defining reflection is also assigned; this additional reflection defines the absolute configuration of the molecule. These reflections are then

used with a small number of additional strong reflections (the starting set) to derive new phases through the tangent formula. The phases of the starting set reflections are arbitrarily set, then permuted through all possible values, and refined iteratively by using the tangent formula.

Once all the possible phase sets are calculated, each one must be assessed to identify the most probable solution. This solution is used to calculate the electron density to identify the atomic positions. The program that was used in this work, MULTAN [33,34] assesses each solution via figures of merit which measure the degree of consistency of each phase set. Three figures of merit are calculated: the absolute figure of merit, (ABSFOM), which is a measure of the absolute consistency among the Sigma 2 relationships, psi zero, (PSIZERO), which compares the phase to that of a random structure, and the residual, (RESID), which is analogous to the crystallographic residual (see Section 2). These figures of merit are used to give a combined figure of merit, (CFOM), which is the most reliable indicator of the correct solution. The equation is of the form:

$$\begin{aligned}
 \text{CFOM} = & (0.6) \frac{\text{ABSFOM} - \text{ABSFOM}_{\min}}{\text{ABSFOM}_{\max} - \text{ABSFOM}_{\min}} \\
 & + (1.2) \frac{\text{PSIZERO}_{\max} - \text{PSIZERO}}{\text{PSIZERO}_{\max} - \text{PSIZERO}_{\min}} \\
 & + (1.2) \frac{\text{RESID}_{\max} - \text{RESID}}{\text{RESID}_{\max} - \text{RESID}_{\min}}
 \end{aligned} \tag{11}$$

The phase set with the highest combined figure of merit is the first to be used to calculate the electron density.

## 2. Structure Refinement

The solution of the crystal structure gives a set of initial values for the positional parameters the atoms in the cell. These initial coordinates, along with the estimates of the thermal parameters that were used to calculate  $E(hk\ell)$ , are refined to obtain the best agreement between the observed  $|F(hk\ell)|$  values and the calculated  $|F(hk\ell)|$ . The value of  $F_C(hk\ell)$  is calculated from the expression:

$$F_C(hk\ell) = K \sum_{i=1}^N f_i^0 e^{-B_i \sin^2 \theta / \lambda^2} e^{2\pi i(hx_i + ky_i + \ell z_i)} \quad (12)$$

where  $f_i^0$  is the atomic scattering factor at rest,  $B_i$  is the temperature factor, and  $x_i, y_i, z_i$  are the coordinates of atom  $i$ .

The crystallographic problem is overdetermined because there are more observations than parameters, therefore, a least squares calculation on a function representing the difference between the observed and calculated structure factor amplitudes is used to refine the structure. Since the structure factor expression is non-linear with respect to the parameters, it is expanded around the initial values of the parameters in a Taylor series. The expression is then solved for the difference between the initial value of a parameter,  $p_k$ , and its new value,  $p_k'$ , that is, it is solved for  $\Delta p_k$ . An anisotropic refinement of  $N$  atoms will have  $9N+1$  parameters: three coordinates and six thermal parameters for each atom plus an overall scale factor for the entire data set.

The function minimized is of the form:

$$R = \sum_{hk\ell} w(hk\ell) (|F(hk\ell)|_0 - |F(hk\ell)|_C)^2 \quad (13)$$

where  $w(hk\ell)$  is the weight applied to the reflection,  $hk\ell$ ,  $|F(hk\ell)|_0$  is the structure factor amplitude that is derived from the observed intensity of the reflection and  $|F(hk\ell)|_c$  is the structure factor amplitude that is calculated from the parameters. The weights applied to the  $hk\ell$  reflections are inversely proportional to the variance of the measured intensity, that is, strong, accurately measured reflections will be assigned a higher weight than weak, less accurately measured reflections.

The best value for each parameter is obtained by minimizing the function,  $R$ ; this is done by taking the derivative of  $R$  with respect to each parameter,  $p$ , and setting it to zero. This procedure will generate  $9N+1$  normal equations of the form:

$$\sum_{hk\ell} w(hk\ell) \frac{\partial (|F(hk\ell)|_0 - |F(hk\ell)|_c)}{\partial p_k} \Delta p_k \quad k = 1, 2, 3, \dots, 9N+1 \quad (14)$$

where  $\Delta p_k$  is the difference between the initial value and the new value of the parameter,  $p_k$ .

The procedure, therefore, solves for the changes in the value of  $p_k$ , not the value of  $p_k$  itself. Once the change in  $p$  is obtained, a new value,  $p'_k$ , can be calculated and the minimization repeated in an iterative fashion until the changes in the parameters are less than 10% of the value of their estimated errors. The method of least squares is described in more detail in Ibers [35] and Dunitz [36].

The precision of the model structure is assessed by calculating a crystallographic residual of the form:

$$R = \frac{\sum_{hkl} \left| |F(hkl)|_o - |F(hkl)|_c \right|}{\sum_{hkl} |F(hkl)|_o} \quad (15)$$

or for a weighted refinement:

$$R_w = \left[ \frac{\sum_{hkl} w(hkl) (|F(hkl)|_o - |F(hkl)|_c)^2}{\sum_{hkl} w(hkl) |F(hkl)|_o^2} \right]^{1/2} \quad (16)$$

For large structures or data sets obtained from crystals of poor quality, the ratio of observations to parameters may be small; there will not be sufficient observations to refine the number of parameters. This underdeterminacy may be overcome by adding restraints to the model structure that is being refined, thereby increasing the number of observations [37].

The program, RESLSQ [38], introduces restraints by including in the refinement a model that describes the ideal geometry. The positional parameters of the observed structure are restrained to the ideal geometry while the thermal parameters are restrained such that the motions of atoms do not exceed reasonable limits. The degree of restraint for each parameter is modified by the user during the course of the refinement.

This form of structure refinement uses the restraints as subsidiary conditions to increase the number of observations, thereby enabling refinements on limited data sets. The function minimized by this technique is of the form:

$$R' = \sum_{hk\ell} w(hk\ell) (|F(hk\ell)|_o - |F(hk\ell)|_c)^2 + \sum_i w_i (d_{\text{actual},i} - d_{\text{ideal},i})^2$$

(17)

where the  $hk\ell$  may range over different portions of the data set,  $i$  ranges over the distances to be restrained,  $d_{\text{actual},i}$  is the observed distance,  $d_{\text{ideal},i}$  is the ideal distance, and  $w(hk\ell)$  is the weight assigned to the observation. Angle restraints and planar restraints are added in a similar fashion and thermal restraints are added according to the methods described by Konnert and Hendrickson [39].

In RESLSQ, the minimization is carried out by the conjugate gradient technique [40] using an anisotropic sparse matrix with distance, angle, planar, and thermal variance restraints. The advantage of the conjugate gradient technique is that the sparse derivative matrix is retained between iterations so that the computer time needed to invert the matrix for each cycle of refinement is saved. RESLSQ was used to refine X-ray structures reported in this work because there were a small number of observed reflections in the data sets.

In two of the three structures to be discussed, an extinction correction was necessary. Extinction arises from reflection of the incident beam by the first planes it encounters thus causing the deeper planes to receive less power than would be expected and have lower observed intensities. An extinction correction is normally applied near the end of the refinement by redefining the calculated structure factor amplitude so it is corrected for extinction. This value is obtained through the equation:

$$F_0 F_C^* = k |F_C| (1 + 2g\delta |F_C|^2)^{-1/4} \quad (18)$$

where  $F_C^*$  is the calculated structure factor corrected for extinction and  $g$  is the extinction coefficient and is dependent on the mosaic spread distribution of a reflection assuming an isotropic Gaussian distribution function. The value  $\delta$  is obtained from the general theory of diffraction [41] and is given by:

$$\delta = \left( \frac{e^2}{mc^2 V} \right)^2 \frac{\lambda^3}{\sin 2\theta} \frac{p_2}{p_1} \frac{1}{T} \quad (19)$$

where  $e^2/mc^2$  is the classical radius of an electron,  $V$  is the volume of the unit cell,  $\lambda$  is the wavelength,  $p_2$  and  $p_1$  are the polarization terms and  $T$  is the average path length through the crystal. The theory of extinction corrections is given in more detail by Larson [42].

For the refinements where an extinction correction was applied, the final cycles of refinement were carried out using conventional least squares since the extinction correction was not included in RESLSQ.

### 3. Molecular Mechanics

The forces experienced by a molecule can be described by potential energy functions written in terms of structural features such as bond lengths, bond angles, torsional angles, and various types of non-bonded interactions. Molecular mechanics is an empirical calculation method which uses such potential energy functions for obtaining structural information. A Born Oppenheimer approximation is used which allows the Schrodinger equation describing the energy of a molecule to be separated into two parts: one describing the motions of the electrons and another

describing the motions of the nuclei. Each of these motions can be dealt with separately. Molecular mechanics studies the motions of the nuclei alone and assumes that the electrons distribute themselves in an optimal fashion around the nuclei. The force field is, then, the sum of the potential energies of the atomic interactions describing the above-mentioned structural features. This will give the classical potential energy function:

$$E_{\text{total}} = \sum_{\text{bond}} k_b (b_i - b_0)^2 + \sum_{\substack{\text{bond} \\ \text{angles}}} k_\theta (\theta_i - \theta_0)^2 + \sum_{\substack{\text{torsion} \\ \text{angles}}} k_\phi (\cos\{n[\phi_i - \phi_0]\}) \\ + \sum_{i>j} \{(B_{ij}/r_{ij}^{12}) - (A_{ij}/r_{ij}^6)\} + \sum_{i>j} q_i q_j / r_{ij}^2 E \quad (20)$$

The first three terms describe the energy difference in terms of intramolecular geometrical features. The fourth term describes the non-bonded van der Waals interactions as a 6-12 potential, the minimum of this term corresponds to the van der Waals contact distance. The last term describes the electrostatic interaction using Coulombs Law.

Other terms that can be used include a hydrogen bond potential. In an early force field, this was included as the sum of an electrostatic component and an empirical Lennard Jones component:

$$E_{\text{HB}} = A'/r^{12} - C'/r^6 + S(r) \quad (21)$$

where the electrostatic function,  $S(r)$ , was calculated from the partial charges [43,44]. More recently, however, a modified Lennard Jones

potential is used which is defined by a 10-12 potential function rather than a 6-12 function [51].

Pioneering work on the development of force fields was carried out by Hill [45] and Westheimer and Mayer [46]. More recently, force fields have been developed by Allinger [47], Schleyer [48], Bartell [49], and Lifson [50], however these force fields are, in general, parameterized for hydrocarbons only. Force fields which are parameterized to include heteratomic interactions and electrostatic and hydrogen bonding contributions are particularly useful for many problems of biological interest such as the study of protein and nucleic acid conformations and energies. Force field calculations on such large molecules are usually done with rigid bond lengths and angles which are fixed at ideal or crystallographically observed values. The atomic coordinates can then only be varied by torsional rotations of the residues. This assumption is made to conserve computer time in the calculation. Such a force field has been used in this work to obtain conformational energies of a number of protein inhibitor complexes.

A molecular mechanics program, YETI, was developed by Vedani and Dunitz [51] from the force field of Weiner and Kolman [52]. The program is designed to minimize the conformational energy of a protein-small molecule complex. It searches for the minimum energy conformation by performing torsional rotations of segments of the amino acid side chains of the protein combined with global translations, rotations and internal torsional motion of the small molecule. The bond lengths and angles are therefore not varied in the calculation. The program uses an "extended atom" potential approximation for all of the hydrogen atoms that are attached to carbon atoms to simplify the conformational energy

calculations and reduce the computer time required for the calculation. In this approximation the non-polar hydrogen atoms are included implicitly by representing the carbon atoms and their attached hydrogen atoms as single groups. Those hydrogen atoms, with the potential of forming hydrogen bonds, are treated explicitly. Due to the difficulties associated with the assignment of partial charges to atoms and with the choice of a value for the microscopic dielectric constant, the electrostatic terms of the potential energy expression are not explicitly included.

A special feature of this program is the incorporation of an extended hydrogen-bond potential function which accounts for the hydrogen-acceptor separation, the angle subtended at the hydrogen atom, the angle at the acceptor and the displacement of the hydrogen atom from a defined plane containing the lone-pair orbitals at the acceptor atom. The form of the hydrogen bond potential function is:

$$E_{HB} = \left( \frac{A'}{r_{H \cdots A}^i} - \frac{C'}{r_{H \cdots A}^j} \right) \cdot \cos^k(\theta_{D-H \cdots A}) \cdot \cos^m(\chi_{H \cdots A-AA} - \chi_0) \cdot \cos(w_{H \cdots A-AA-AB} - w_0) \quad (22)$$

A corresponds to the acceptor atom, D to the donor atom and AA and AB to selected atoms in the acceptor molecule. The first term corresponds to equation 21 where  $i = 12$  and  $j = 10$ . The second term accounts for the nonlinearity of the hydrogen bond. The third term accounts for deviations from the optimum angle at the acceptor atom. The values of  $\chi_0$  for different acceptor atoms have been derived from the Cambridge Crystallographic Data File [27]. The fourth term accounts for the

displacement of the hydrogen atom from the plane defined by A-AA-AB.

The program also includes a metal atom potential for a zinc atom. This potential function allows for variations from frequently occurring coordination types such as tetrahedral, pentacoordinate with D3h and C4v symmetry, and octahedral. The form of the metal potential is:

$$E_{\text{MET}} = \sum (A''/r_{\text{M}\dots\text{L}}^{12} - C''/r_{\text{M}\dots\text{L}}^{10}) \cdot \prod \cos^k(\psi_{\text{L}\dots\text{M}\dots\text{L}} - \psi_0) \quad (23)$$

The first term is the 10-12 potential function and allows each metal ligand distance to be varied separately. The second term considers the deviation of the angles subtended by the metal atom from their ideal value of  $\psi_0$ . These ideal values were assigned by a database search of metal ligand complexes [63].

YETI has been used in this work on a number of protein inhibitor complexes. An extended active site region of the protein is defined which includes the inhibitor molecule, a zinc metal atom and a water molecule. The minimum energy conformation of the complex is obtained by performing torsional rotations of predefined segments of the active site as well as translational and rotational motions of the inhibitor molecules, the zinc atom and the water molecule. The metal ion coordination for all the complexes minimized was tetracoordinate and, thus, the refinements were carried out imposing tetrahedral geometry.

### III. Crystal Structure Determination

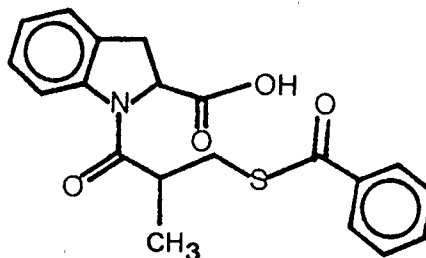
#### 1. Methods

For each of the crystal structures discussed the data were collected on an Enraf-Nonius CAD4F automated diffractometer. Twenty-five reflections were located by a photographic procedure and an automatic routine was used to center the reflections and determine an orientation matrix by calculating the angles between the scattering vectors. The symmetry and systematic absences of the intensities of the reflections were examined to determine the lattice and the space group. All three compounds crystallized in the orthorhombic space group,  $P2_12_12_1$ , with 4 molecules in the unit cell and systematic absences of  $(h00)$ ;  $h = 2n + 1$ ,  $(0k0)$ ;  $k = 2n + 1$ ,  $(00l)$ ,  $l = 2n + 1$ .

The data were collected using an  $\omega/2\theta$  scan with 96 steps for each scan. The middle 64 steps were considered to be the peak; the 16 steps on each side of the peak were considered to be background. Three standard reflections were measured every 1800 seconds of X-ray exposure to check for crystal decomposition.

A Lorentz factor was applied to each data set to correct for the unequal rates which different lattice points pass through the sphere of reflection. A polarization factor was applied to correct for the dependence of the reflection efficiency on the reflection angle. No absorption corrections were necessary.

## 2. Structure Solution of WY44088



(1)

S,S-1-[3-(benzoylthio)-2-methyl-1-oxopropyl]-indoline-2-carboxylic acid, (1, WY44088), is similar to the therapeutically used drug, captopril, because it contains a pyrrolidine ring, an amide bond, an  $\alpha$  methyl group, and a sulfhydryl group that chelates with the zinc atom in the enzyme. The aromatic ring attached to the pyrrolidine ring in WY44088 causes this compound to be more hydrophobic than captopril. The inhibitory action of WY44088;  $IC_{50} = 3.8 \times 10^{-8}$  M, is slightly less than that of captopril;  $IC_{50} = 1.1 \times 10^{-8}$  M [15], however, WY44088 is believed to be metabolized to the more potent mercapto-2-methyl-1-oxopropyl derivative;  $IC_{50} = 3.7 \times 10^{-9}$  M, to be discussed later. The X-ray structure of WY44088 was determined and compared to structures of other inhibitors and substrate analogues.

### 2.1 Experimental

Long, needle shaped crystals of WY44088, crystallized from a methanol and water mixture, were provided by Dr. D.H. Kim of Wyeth Pharmaceutical Laboratory, Pennsylvania. The end of a needle was cut, mounted on a glass fiber, and cooled to  $-100^{\circ}\text{C}$  using a continuous stream

of cold nitrogen gas. The quality of the crystal was not ideal; however, it was centered and the lattice parameters were determined. A quadrant of data was collected (+h, +k, +l) to  $\theta_{\max} = 22.5^\circ$ . The intensities of the three standard reflections: (4 0 2), (0 8 0), (3 3 -8), varied less than 4%. The crystal data are in Table 1.

After data reduction, normalized structure factor amplitudes were calculated by using a K curve and parity group rescaling. The 500 largest E values were used to solve the structure. An E map was calculated from the phase set with the highest combined figure of merit, (1.99). This solution identified the positions of 20 of the 26 nonhydrogen atoms in the structure. The remaining 6 atoms were identified in a difference Fourier synthesis. After isotropic refinement of the nonhydrogen atom parameters, the carboxylic hydrogen atom and the mercapto hydrogen atom could not be located in a difference Fourier synthesis. All other hydrogen atoms were included in calculated ideal positions. Due to the weak reflection intensities, possibly a result of the crystal drying out, refinement of the structure was difficult.

Further crystallization experiments with methanol and water mixtures produced a crystal of better quality. A single crystal was sealed in a 1.0 mm quartz capillary tube along with some mother liquor according to the method described by McPherson [53]. The presence of water in the capillary precluded reducing the temperature of the crystal to improve the diffraction pattern; instead, data were collected at room temperature. After centering the crystal and obtaining the lattice parameters, a quadrant of data was collected ( $\pm$ h, +k, +l) to  $\theta_{\max} = 66^\circ$ . The intensities of the three standard reflections,

(0 7 -6), (-4 0 1), (-3 3 8), varied less than 3%. The data collected on this crystal were of far better quality so there were more observed reflections than collected from the previous data set. The crystal data are in Table 1.

After data reduction, the structure was refined starting with the atomic coordinates of all of the 44 atoms located or calculated from the first data set. Although the number of observed reflections was larger than those obtained from the first data collection, the ratio of the number of observations to the number of parameters was still small. The structure was, therefore, refined by restrained least squares. A model was constructed using the bond distances and bond angles obtained from a data base search of 12 crystal structures having an indoline fragment. The bond distances and bond angles for the remaining atoms in the side chain and the carboxyl group were taken from the well refined crystal structure of captopril [54].

The nonhydrogen atoms were refined by decreasing the restraints on both the positional and thermal parameters of the atoms until they were refining solely on the observed structure factors. The hydrogen atoms were included in the structure with anisotropic thermal parameters set at 1.2 times the thermal parameters to which they were bonded and were not refined. After convergence with restrained least squares the final cycles of refinement were done using conventional least squares so that an extinction correction could be included. The statistics describing the refinement are in Table 1.

The conformation of the structure is shown in Figure 3. Tables 2 and 3 contain the atomic coordinates for the nonhydrogen and the hydrogen atoms, respectively, and Table 4 contains the anisotropic

thermal factors of the nonhydrogen atoms. The bond distances are in Table 5 and the bond angles are in Table 6. The torsion angles along the chain are in Table 7.

## 2.2 Results

The benzoylthio compound adopts a *cis* conformation about the peptide bond: C(2)-N(1)-C(10)-C(12) = -1(1)°. Similar conformations are found in the analogous N-propionylproline [55] and in the D-L peptide linkage of the N-t-butyloxycarbonyl-D-prolyl-D-prolyl-L-proline [56]. This *cis* conformation of the peptide bond is due to two factors: an intermolecular hydrogen bond (2.581(8) Å) between O(11) and O(20) of another molecule at (x + 1, y, z) and the aromatic ring attached to the pyrrolidine group that causes unfavorable steric interactions between the methyl group and the ring system. The aromatic ring not only influences the conformation of the peptide bond but also that of the pyrrolidine ring. The ring adopts an envelope conformation with C(3) 0.19(1) Å above the mean plane of atoms N(1), C(2), C(4), C(9). The aromatic ring in indoline appears to hold the pyrrolidine ring in this envelope form rather than the half chair conformation observed in the structure of captopril.

The final R factor for the structure is still rather high. This is mainly due to the large thermal motion in various parts of the molecule. Table 4 shows the largest thermal parameters to be in the atoms of both aromatic rings. Difference Fourier maps were examined for multiple discrete positions for these rings; however, the electron density was diffuse and could not be resolved into unique positions for the atoms. The maximum peak in the final difference Fourier map was

associated with S(15). This is a commonly observed phenomena and results from termination errors of the Fourier series. The structure of WY44088 was found to have a *cis* peptide bond in the crystal.

**Table 7**  
Torsion Angles for WY44088

Atoms	Angle (°)
N( 1)-C( 2)-C(18)-O(20)	154.4(7)
N( 1)-C( 2)-C(18)-O(19)	24.0(1)
C( 2)-N( 1)-C(10)-C(12)	-1.0(1)
N( 1)-C(10)-C(12)-C(14)	148.4(8)
C(10)-C(12)-C(14)-S(15)	-57.8(9)
C(12)-C(14)-S(15)-C(16)	-72.9(7)
C(14)-S(15)-C(16)-C(21)	179.8(5)
S(15)-C(16)-C(21)-C(22)	-173.7(8)

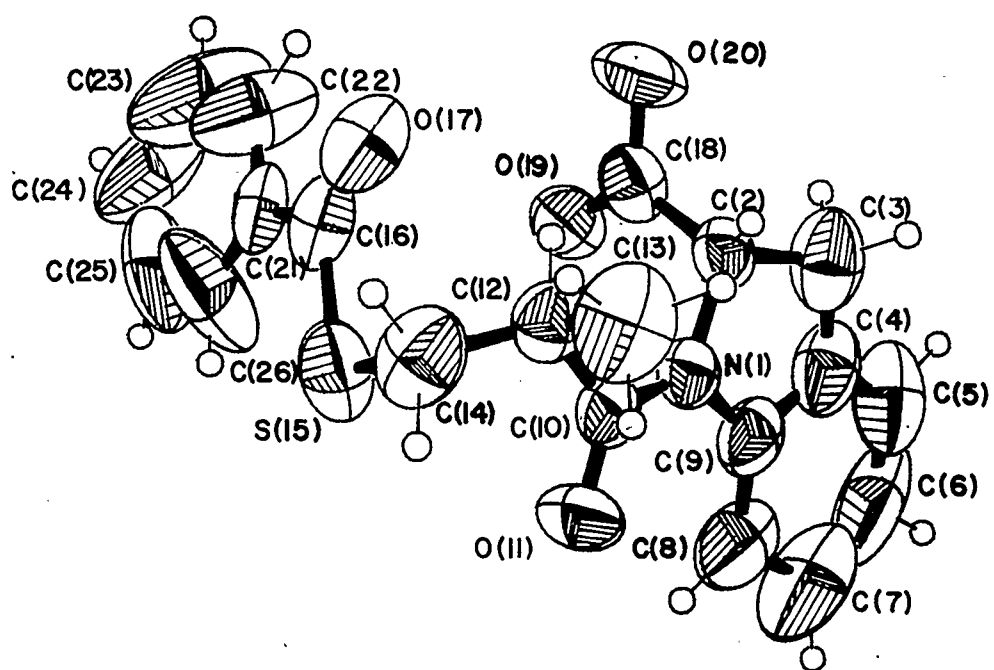


Figure 3

Molecular structure and atomic labelling  
scheme for WY44088

Table 1

Crystal Data for WY44088.  
 Values for the Initial Low Temperature  
 Data Set are in Parenthesis.

Molecular Formula	:	$C_{20}H_{19}O_4NS$
Molecular Weight	:	369.44 g mol <sup>-1</sup>
Space Group	:	$P2_12_12_1$
Cell Dimensions	:	a = 7.4867(4) Å (7.447(2)) Å b = 11.5461(6) Å (11.423(2)) Å c = 22.0064(2) Å (22.808(6)) Å
Volume	:	1902.3(2) Å <sup>3</sup> (1940.2(8) Å <sup>3</sup> )
Range of $\theta$ Values Used to Determine the Cell	:	24.4° - 50.2° (12.1° - 16.7°)
No. of Reflections Used for Cell Determination	:	50 (25)
Density (calculated)	:	1.29 g cm <sup>-3</sup> (1.32 g cm <sup>-3</sup> )
Radiation, Wavelength	:	Cu, K $\alpha$ $\lambda$ = 1.54178 Å (Mo, K $\alpha$ $\lambda$ = 0.71069 Å)
Monochromatization	:	Ni filter (graphite monochromator)
Temperature	:	25°C (-90°C)
Scan Range	:	1.5(0.87 + 0.142 tan $\theta$ ) (1.5(1.10 + 0.344 tan $\theta$ ))
Theta Maximum	:	66° (22.5°)
Scan Mode	:	$\omega/2\theta$
Absorption Coefficient	:	16.8 cm <sup>-1</sup>
Unique Reflections	:	1896 (1894)
Observed Reflections ( $I > 2\sigma(I)$ )	:	1537 (1122)
Weighting Function	:	$\omega^{-1} = \sigma^2(F_o) + 0.00005 F_o^2$
R	:	0.093
R <sub>w</sub>	:	0.073
Highest Residual Peak	:	0.37 e/Å <sup>3</sup> , associated with S(15)
Maximum Shift/Error	:	0.0132
Goodness of Fit	:	1.598
Extinction (isotropic)	:	2.17 x 10 <sup>-3</sup>

**Table 2**  
 Fractional Atomic Coordinates ( $\times 10^4$ ) and Equivalent  
 Isotropic Temperature Factors ( $\times 10$ ) for  
 the Nonhydrogen Atoms of WY44088  
 Beq is defined as one-third the trace of the Bij matrix

Atom	x/a	y/b	z/c	Beq
N(1)	8353( 9)	6007( 5)	1630( 3)	53( 3)
C(2)	6601(11)	6373( 6)	1859( 3)	56( 4)
C(3)	6416(15)	7626( 8)	1628( 4)	92( 6)
C(4)	7795(17)	7774( 9)	1185( 4)	83( 6)
C(5)	7903(21)	8704( 9)	794( 6)	110( 8)
C(6)	9436(35)	8581(16)	468( 8)	184(17)
C(7)	10768(27)	7784(17)	428( 8)	172(14)
C(8)	10450(16)	6796(10)	831( 5)	112( 8)
C(9)	8972(14)	6855( 9)	1189( 4)	70( 5)
C(10)	9176(11)	5046( 7)	1822( 4)	59( 4)
O(11)	10660( 7)	4778( 5)	1603( 3)	93( 4)
C(12)	8268(11)	4304( 7)	2304( 4)	63( 4)
C(13)	8964(13)	4746( 8)	2914( 4)	101( 6)
C(14)	8733(13)	3062( 8)	2219( 4)	88( 6)
S(15)	8164( 4)	2457( 2)	1483( 1)	88( 2)
C(16)	5785(13)	2367( 8)	1562( 4)	71( 5)
O(17)	5025(10)	2715( 6)	2002( 2)	85( 4)
C(18)	5075(13)	5629( 7)	1594( 4)	64( 5)
O(19)	5186( 8)	5114( 5)	1126( 2)	71( 3)
O(20)	3672( 7)	5619( 6)	1964( 3)	103( 4)
C(21)	4880(17)	1888( 6)	1011( 4)	73( 5)
C(22)	3156(18)	1881(12)	992( 4)	130( 9)
C(23)	2246(20)	1416(16)	524( 7)	172(15)
C(24)	3014(25)	921(15)	76( 8)	142(12)
C(25)	4759(29)	1001(10)	11( 5)	128(10)
C(26)	5736(18)	1423(10)	522( 7)	150(11)

**Table 3**  
Fractional Atomic Coordinates ( $\times 10^4$ ) and Equivalent  
Isotropic Temperature Factors ( $\times 10$ ) for  
the Hydrogen Atoms of WY44088

Atom	x/a	y/b	z/c	Biso
H(21)	6692	6397	2356	44
H(31)	5023	7747	1469	59
H(32)	6433	8272	2015	59
H(51)	6883	9382	753	75
H(61)	9728	9338	185	82
H(71)	11919	7906	171	77
H(81)	11406	6126	855	69
H(121)	6885	4397	2283	37
H(131)	8654	5588	3125	54
H(132)	8731	4093	3263	54
H(133)	10451	4741	2881	54
H(141)	10188	2942	2302	49
H(142)	8163	2522	2585	49
H(221)	2389	2272	1336	68
H(231)	904	1481	477	86
H(241)	2407	440	-248	82
H(251)	5526	831	-388	87
H(261)	6980	1409	504	84

Table 4

Anisotropic Temperature Factors ( $\times 10^3$ )

for the Nonhydrogen Atoms of WY44088

The temperature factor expression is of the form:

$$T = \exp - 2\pi^2(U_{11}(ha^*)^2 + \dots + \dots + U_{12}(hka^*b^*) + \dots)$$

Atom	U11	U22	U33	U12	U13	U23
N(1)	69( 4)	65( 4)	69( 4)	-3( 4)	-5( 4)	-14( 4)
C(2)	75( 5)	66( 5)	71( 5)	1( 5)	-2( 5)	-17( 4)
C(3)	1354( 92)	790( 63)	1349( 81)	37( 71)	-477( 71)	61( 67)
C(4)	1575(109)	849( 70)	714( 59)	-331( 76)	35( 67)	-69( 56)
C(5)	2224(144)	854( 71)	1115( 87)	-127( 94)	-112( 95)	18( 68)
C(6)	3693(338)	1796(177)	1503(136)	-1872(205)	1243(179)	-685(129)
C(7)	3068(248)	2354(208)	1120( 91)	-1663(189)	1293(136)	-697(138)
C(8)	1617(109)	1596(101)	1044( 78)	-748( 92)	531( 83)	-664( 78)
C(9)	1064( 76)	863( 64)	729( 60)	-316( 63)	122( 56)	-224( 54)
C(10)	639( 49)	680( 54)	903( 61)	-76( 49)	-128( 50)	-218( 50)
O(11)	569( 31)	1215( 50)	1749( 61)	91( 37)	106( 39)	-441( 48)
C(12)	767( 52)	768( 52)	863( 54)	-36( 56)	-124( 51)	-4( 47)
C(13)	1565( 91)	1380( 79)	892( 61)	-169( 79)	-406( 63)	14( 62)
C(14)	1157( 77)	984( 66)	1214( 74)	-65( 65)	-271( 63)	316( 59)
S(15)	1239( 21)	771( 14)	1315( 20)	162( 19)	-292( 19)	-121( 17)
C(16)	1129( 79)	612( 53)	957( 66)	-195( 58)	-310( 65)	88( 58)
O(17)	1422( 55)	1122( 50)	666( 33)	-439( 49)	-65( 41)	35( 37)
C(18)	857( 61)	727( 56)	836( 62)	115( 54)	-122( 62)	-79( 51)
O(19)	802( 36)	977( 41)	934( 37)	70( 36)	-35( 37)	-181( 35)
O(20)	651( 36)	1680( 61)	1582( 57)	-27( 43)	303( 40)	-761( 54)
C(21)	1271( 82)	470( 43)	1022( 72)	-230( 58)	-63( 76)	-21( 48)
C(22)	1354( 97)	2732(157)	835( 71)	-965(116)	142( 78)	-564( 86)
C(23)	1724(140)	3580(233)	1234(108)	-1520(154)	-19(110)	-609(132)
C(24)	2013(169)	2141(164)	1226(121)	-1339(148)	-89(127)	-285(107)
C(25)	2900(189)	963( 84)	994( 90)	220(121)	-23(138)	-432( 72)
C(26)	1929(139)	1662(114)	2122(137)	849(104)	-618(123)	-1155(108)

**Table 5**  
Bond Distances (Å) for WY44088

Atoms	Distance	Atoms	Distance
N( 1)-C( 2)	1.47(1)	C(21)-C( 26)	1.36(2)
N( 1)-C( 9)	1.45(1)	C(22)-C( 23)	1.35(2)
N( 1)-C(10)	1.34(1)	C(23)-C( 24)	1.28(2)
C( 2)-C( 3)	1.54(1)	C(24)-C( 25)	1.32(3)
C( 2)-C(18)	1.54(1)	C(25)-C( 26)	1.43(2)
C( 3)-C( 4)	1.43(2)	C( 2)-H( 21)	1.10
C( 4)-C( 5)	1.38(2)	C( 3)-H( 31)	1.11
C( 4)-C( 9)	1.38(2)	C( 3)-H( 32)	1.13
C( 5)-C( 6)	1.36(3)	C( 5)-H( 51)	1.10
C( 6)-C( 7)	1.36(3)	C( 6)-H( 61)	1.10
C( 7)-C( 8)	1.46(2)	C( 7)-H( 71)	1.04
C( 8)-C( 9)	1.36(2)	C( 8)-H( 81)	1.06
C(10)-O(11)	1.25(1)	C(12)-H(121)	1.04
C(10)-C(12)	1.52(1)	C(13)-H(131)	1.10
C(12)-C(13)	1.53(1)	C(13)-H(132)	1.09
C(12)-C(14)	1.49(1)	C(13)-H(133)	1.12
C(14)-S(15)	1.82(1)	C(14)-H(141)	1.11
S(15)-C(16)	1.79(1)	C(14)-H(142)	1.10
C(16)-O(17)	1.19(1)	C(22)-H(221)	1.05
C(16)-C(21)	1.49(1)	C(23)-H(231)	1.01
C(18)-O(19)	1.19(1)	C(24)-H(241)	1.01
C(18)-O(20)	1.33(1)	C(25)-H(251)	1.07
C(21)-C(22)	1.29(2)	C(26)-H(261)	0.93

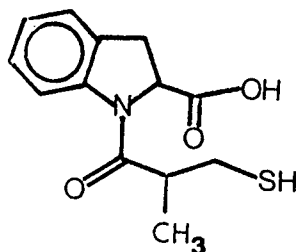
**Table 6**  
Bond Angles (°) for WY44088

Atoms	Angles	Atoms	Angles
C( 2)-N( 1)-C( 9)	108.7( 6)	C( 3)-C( 2)-H( 21)	108
C( 2)-N( 1)-C(10)	122.8( 6)	C( 18)-C( 2)-H( 21)	116
C( 9)-N( 1)-C(10)	128.5( 7)	C( 2)-C( 3)-H( 31)	108
N( 1)-C( 2)-C( 3)	103.7( 7)	C( 2)-C( 3)-H( 32)	112
N( 1)-C( 2)-C(18)	111.8( 6)	C( 4)-C( 3)-H( 31)	117
C( 3)-C( 2)-C(18)	109.4( 7)	C( 4)-C( 3)-H( 32)	115
C( 2)-C( 3)-C( 4)	105.9( 8)	H( 31)-C(30)-H( 32)	99
C( 3)-C( 4)-C( 5)	124.2(11)	C( 4)-C( 5)-H( 51)	124
C( 3)-C( 4)-C( 9)	111.3( 9)	C( 6)-C( 5)-H( 51)	128
C( 5)-C( 4)-C( 9)	124.5(11)	C( 5)-C( 6)-H( 61)	113
C( 4)-C( 5)-C( 6)	107.3(13)	C( 7)-C( 6)-H( 61)	111
C( 5)-C( 6)-C( 7)	136.3(17)	C( 6)-C( 7)-H( 71)	123
C( 6)-C( 7)-C( 8)	111.6(16)	C( 8)-C( 7)-H( 71)	125
C( 7)-C( 8)-C( 9)	116.4(12)	C( 7)-C( 8)-H( 81)	119
N( 1)-C( 9)-C( 4)	108.6( 8)	C( 9)-C( 8)-H( 81)	124
N( 1)-C( 9)-C( 8)	127.8( 9)	C( 10)-C(12)-H(121)	111
C( 4)-C( 9)-C( 8)	123.6(10)	C( 13)-C(12)-H(121)	110
N( 1)-C(10)-O(11)	119.6( 7)	C( 14)-C(12)-H(121)	109
N( 1)-C(10)-C(12)	118.7( 7)	C( 12)-C(13)-H(131)	126
O(11)-C(10)-C(12)	121.7( 7)	C( 12)-C(13)-H(132)	109
C(10)-C(12)-C(13)	105.8( 7)	C( 12)-C(13)-H(133)	106
C(10)-C(12)-C(14)	110.4( 7)	H(131)-C(13)-H(132)	106
C(13)-C(12)-C(14)	110.7( 7)	H(131)-C(13)-H(133)	104
C(12)-C(14)-S(15)	115.4( 6)	H(132)-C(13)-H(133)	102
C(14)-S(15)-C(16)	99.7( 4)	C( 12)-C(14)-H(141)	109
S(15)-C(16)-O(17)	122.2( 8)	C( 12)-C(14)-H(142)	111
S(15)-C(16)-C(21)	113.1( 7)	S( 15)-C(14)-H(141)	109
O(17)-C(16)-C(21)	124.5( 9)	S( 15)-C(14)-H(142)	110
C( 2)-C(18)-O(19)	123.6( 8)	H(141)-C(14)-H(142)	101
C( 2)-C(18)-O(20)	111.0( 7)	C( 21)-C(22)-H(221)	121
O(19)-C(18)-O(20)	125.4( 8)	C( 23)-C(22)-H(221)	116
C(16)-C(21)-C(22)	118.8( 9)	C( 22)-C(23)-H(231)	123

Table 6 continued:

C(16)-C(21)-C(26)	125.0(11)	C( 24)-C(23)-H(231)	114
C(22)-C(21)-C(26)	116.2(10)	C( 23)-C(24)-H(241)	126
C(21)-C(22)-C(23)	122.3(12)	C( 25)-C(24)-H(241)	114
C(22)-C(23)-C(24)	122.8(15)	C( 24)-C(25)-H(251)	128
C(23)-C(24)-C(25)	120.0(16)	C( 26)-C(25)-H(251)	116
C(24)-C(25)-C(26)	116.5(14)	C( 21)-C(26)-H(261)	121
C(21)-C(26)-C(25)	121.0(13)	C( 25)-C(26)-H(261)	118
N( 1)-C( 2)-H(21)	107		

### 3. Structure Solution of WY44221



(2)

S,S-1-[3-(mercapto)-2-methyloxopropyl]-indoline-2-carboxylic acid (2, WY44221), is an angiotensin converting enzyme inhibitor that is three times more potent than the therapeutically used drug, captopril. As with WY44088, WY44221 differs from captopril in that it has an aromatic ring attached to the pyrrolidine ring. Kim and coworkers [15] postulated that ACE has a hydrophobic pocket at the active site; the aromatic ring would enhance binding of WY44221 to the enzyme. The X-ray structure of WY44221 was determined and compared to other ligands of the enzyme.

#### 3.1 Experimental

Long, needle-shaped crystals of WY44221 were provided by Dr. D.H. Kim of Wyeth Pharmaceutical Laboratory, Pennsylvania. A single crystal was mounted on a glass fiber and cooled to  $-90^{\circ}\text{C}$  by using a continuous stream of cold nitrogen gas.

After centering the crystal and determining the lattice parameters, a quadrant of data were collected  $(+h, +k, \pm l)$  to  $\theta_{\text{max}} = 22.5^{\circ}$ . The intensities of the three standard reflections:  $(4 -1 3)$ ,  $(-3 5 -1)$ ,

(1 -1 6) varied less than 5%. The crystal data are in Table 8. After data reduction, normalized structure factor amplitudes were calculated by using a K curve and parity group rescaling. The 500 largest E values were used to solve the structure. An E map was calculated from the phase set with the highest combined figure of merit, (3.0). This solution identified the positions of all of the nonhydrogen atoms in the structure.

The structure was refined using restrained least squares so that the low number of observed reflections could be used to best advantage. To guide the refinement, a model of the structure was constructed as described for WY44088. A difference Fourier synthesis was calculated to locate the hydrogen atoms. All were located except the two hydrogen atoms on the methyl carbon atom, C(13), the hydrogen atom of the carboxylic acid group, and the hydrogen atom on S(15). The hydrogen atoms were included in the model in idealized positions with anisotropic temperature parameters defined to be 1.2 times the thermal parameters of the atom to which they were bonded. The parameters for the hydrogen atoms were not refined. The refinement was completed by lowering both the thermal constraints on the nonhydrogen atoms and the distance constraints until the structure was refining completely on the observed structure factors. The maximum peak in the final difference Fourier map was associated with the sulphur atom. As described for WY44088, this peak is a result of termination errors of the Fourier series.

The conformation of the structure is shown in Figure 4. Table 9 contains the atomic coordinates and Table 10 the anisotropic temperature factors for the nonhydrogen atoms with the atoms labelled as in Figure

4. The bond distances are in Table 11 and bond angles are in Table 12. The torsion angles along the chain are in Table 13.

### 3.2 Results

The structure of the WY44221 is similar to that of WY44088. The peptide bond is *cis* with the torsion angle: C(2)-N(1)-C(10)-C(12) =  $-13.4(9)^\circ$ . The carbonyl oxygen atom, O(11), forms two intermolecular hydrogen bonds with the carboxylate oxygen atoms; O(11)-O(17) = 2.742(8) Å and O(11)-O(18) = 2.98(1) Å, each carboxylate oxygen atom at  $(-x + 2.5, -y + 1, z + 1/2)$ . The hydrogen atom involved in these hydrogen bonds was not located in a difference Fourier synthesis. The carboxylate distances, C(16)-O(17) and C(16)-O(18), are equivalent, within the  $2\sigma$  limit, thus the hydrogen atom must be equidistant from the two oxygen atoms, O(17) and O(18). This suggests a three-center intermolecular hydrogen bond with the hydrogen atom donated from O(17) and O(18) to O(11). The hydrogen bond distances indicate a slightly stronger hydrogen bond between O(11) and O(17).

The pyrrolidine ring adopts an envelope conformation with C(3) 0.34(1) Å below the plane of atoms defined by N(1), C(2), C(4) and C(9). The aromatic ring of the indoline fragment holds the 5 membered ring in this envelope conformation as was observed for WY44088 and different from the half chair conformation observed for captopril.

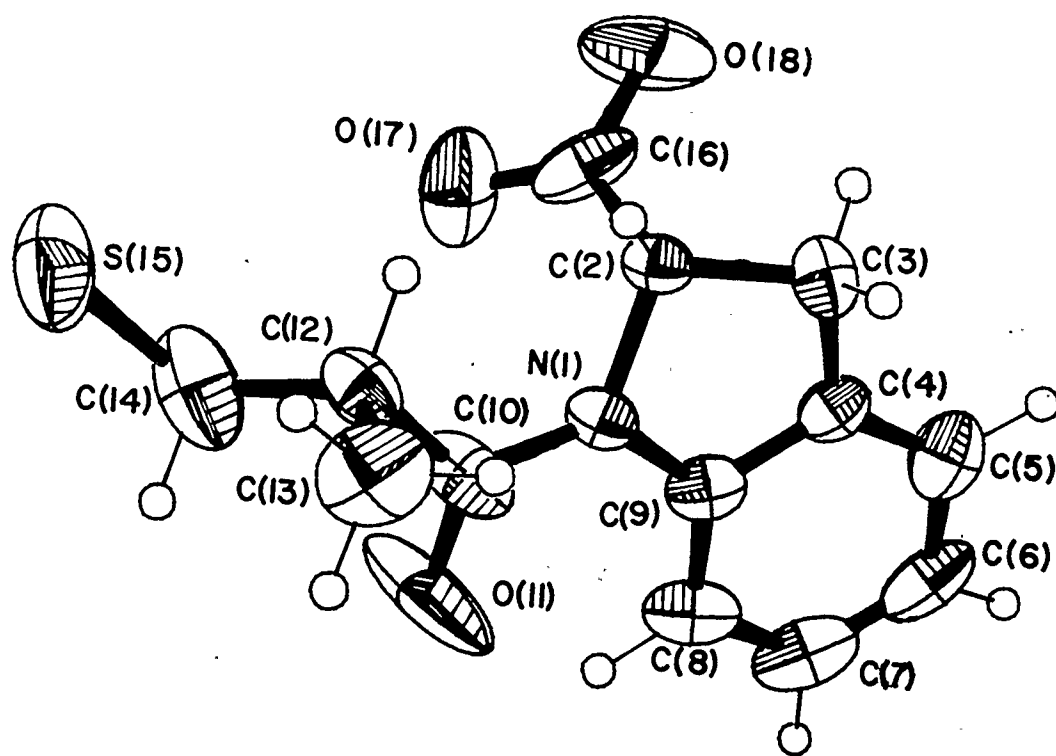


Figure 4  
Molecular structure and atomic  
labelling scheme for WY44221

**Table 8**  
Crystal Data for WY44221

Molecular Formula	:	$C_{13}H_{15}O_3NS$
Molecular Weight	:	265.33 g mol <sup>-1</sup>
Space Group	:	$P_{2_1 2_1 2_1}$
Cell Dimensions	:	$a = 9.981(3) \text{ \AA}$ $b = 10.323(3) \text{ \AA}$ $c = 12.801(6) \text{ \AA}$
Volume	:	1318.9(8) Å <sup>3</sup>
Range of $\theta$ Values Used to Determine the Cell	:	9.0° - 17.5°
No. of Reflections Used	:	25
Density (calculated)	:	1.34 g cm <sup>-3</sup>
Radiation, Wavelength	:	Mo, K $\alpha$ $\lambda = 0.71069 \text{ \AA}$
Monochromatization	:	graphite monochromator
Temperature	:	-90°C
Scan Range	:	1.5(0.67 + 0.344 tan $\theta$ )
Theta Maximum	:	22.5°
Scan Mode	:	$\omega/2\theta$
Absorption Coefficient	:	2.448 cm <sup>-1</sup>
Unique Reflections	:	1347
Observed Reflections	:	1042
(I 1.5 > (I))		
Weighting Function	:	$w^{-1} = \sigma^2(F_o) + 0.0001 F_o^2$
R	:	0.077
Rw	:	0.078
Highest Residual Peak	:	0.73 e/Å <sup>3</sup> (associated with S(15))
Maximum Shift/Error (Å)	:	0.230
Goodness of Fit	:	0.935

Table 9

Fractional Atomic Coordinates ( $\times 10^4$ ) and Equivalent  
Isotropic Temperature Factors ( $\times 10$ ) for WY44221

Beq is defined as one-third the trace of the Bij matrix

Atom	x/a	y/b	z/c	Beq
N(1)	11686( 4)	6783( 4)	997( 3)	30(2)
C(2)	11149( 5)	7183( 5)	-33( 4)	28(3)
C(3)	11213( 6)	8646( 5)	-9( 5)	37(3)
C(4)	12290( 5)	8901( 5)	778( 4)	31(3)
C(5)	12966( 6)	10035( 6)	995( 5)	45(4)
C(6)	13888( 6)	10034( 7)	1830( 5)	48(4)
C(7)	14124( 6)	8940( 8)	2390( 5)	52(4)
C(8)	13439( 6)	7793( 8)	2178( 4)	46(4)
C(9)	12526( 5)	7794( 6)	1360( 4)	33(3)
C(10)	11530( 7)	5614( 7)	1452( 5)	49(4)
O(11)	12187( 7)	5345( 6)	2228( 4)	110(4)
C(12)	10503( 6)	4677( 6)	1025( 5)	38(3)
C(13)	9271( 8)	4780( 9)	1742( 6)	61(5)
C(14)	11075( 8)	3314( 7)	985( 7)	66(5)
S(15)	9951( 2)	2149( 1)	384( 2)	69(1)
C(16)	12014( 6)	6600( 7)	-888( 5)	49(4)
O(17)	12502( 5)	5515( 4)	-765( 4)	70(3)
O(18)	12064( 6)	7142( 7)	-1748( 3)	80(4)
H(21)	10206(56)	6841(49)	-161(37)	33
H(31)	11513(59)	8935(54)	-732(46)	44
H(32)	10340(60)	9019(53)	284(45)	44
H(51)	12792(63)	10886(58)	601(50)	54
H(61)	14452(61)	10864(65)	1928(46)	58
H(71)	14827(66)	8949(70)	2988(44)	62
H(81)	13593(64)	6969(67)	2618(43)	55
H(121)	10253(61)	4967(56)	276(43)	45
H(131)	8917(74)	5720(76)	1771(54)	74
H(132)	8540(72)	4153(74)	1461(53)	74
H(133)	9570(67)	4461(72)	2479(56)	74
H(141)	11993(74)	3282(66)	605(63)	79
H(142)	11210(74)	3012(71)	1759(62)	79

**Table 10**Anisotropic Temperature Factors ( $\times 10^3$ )

for the Nonhydrogen Atoms of WY44221

The temperature factor expression is of the form:

$$T = \exp - 2\pi^2(U_{11}(ha^*)^2 + \dots + \dots + U_{12}(hka^*b^*) + \dots)$$

Atom	U11	U22	U33	U12	U13	U23
N(1)	27(2)	36(2)	26(2)	1(2)	-3(2)	4(2)
C(2)	26(2)	34(2)	24(2)	-3(2)	-4(2)	2(2)
C(3)	34(3)	30(2)	46(3)	0(2)	-1(3)	5(3)
C(4)	27(2)	37(2)	28(2)	0(2)	8(2)	-7(2)
C(5)	35(3)	43(3)	57(3)	1(3)	11(3)	-9(3)
C(6)	32(3)	62(3)	50(3)	-13(3)	8(3)	-31(3)
C(7)	28(3)	85(5)	43(3)	-8(3)	4(3)	-22(3)
C(8)	36(3)	71(4)	30(2)	-3(4)	-2(3)	1(3)
C(9)	24(2)	46(3)	29(2)	0(3)	4(2)	-4(2)
C(10)	40(3)	58(4)	50(3)	-8(3)	-9(3)	25(3)
O(11)	108(3)	113(3)	110(3)	-61(3)	-80(3)	85(2)
C(12)	34(3)	41(3)	40(3)	-5(3)	-1(3)	14(3)
C(13)	51(4)	76(5)	57(4)	-18(4)	20(3)	-5(4)
C(14)	51(4)	52(4)	95(5)	6(4)	1(4)	24(4)
S(15)	74(1)	36(1)	99(1)	9(1)	-12(1)	6(1)
C(16)	34(3)	72(4)	41(3)	-18(3)	4(3)	-26(3)
O(17)	89(3)	43(2)	76(3)	6(3)	54(2)	-4(2)
O(18)	79(3)	136(5)	25(2)	15(4)	16(2)	9(3)

**Table 11**  
Bond distances (Å) for WY44221

Atoms	Distances	Atoms	Distances
N( 1)-C( 2)	1.475( 7)	C(14)-S( 15)	1.805( 9)
N( 1)-C( 9)	1.410( 8)	C(16)-O( 17)	1.230( 9)
N( 1)-C(10)	1.351( 9)	C(16)-O( 18)	1.236( 9)
C( 2)-C( 3)	1.515( 8)	C( 2)-H( 21)	1.00
C( 2)-C(16)	1.506( 9)	C( 3)-H( 31)	1.02
C( 3)-C( 4)	1.475( 9)	C( 3)-H( 32)	1.01
C( 4)-C( 5)	1.376( 9)	C( 5)-H( 51)	1.03
C( 4)-C( 9)	1.385( 9)	C( 6)-H( 61)	1.03
C( 5)-C( 6)	1.400(10)	C( 7)-H( 71)	1.03
C( 6)-C( 7)	1.359(11)	C( 8)-H( 81)	1.03
C( 7)-C( 8)	1.390(12)	C(12)-H(121)	1.03
C( 8)-C( 9)	1.378( 8)	C(13)-H(131)	1.03
C(10)-O(11)	1.216( 9)	C(13)-H(132)	1.03
C(10)-C(12)	1.501(10)	C(13)-H(133)	1.04
C(12)-C(13)	1.521(10)	C(14)-H(141)	1.02
C(12)-C(14)	1.518(10)	C(14)-H(142)	1.05

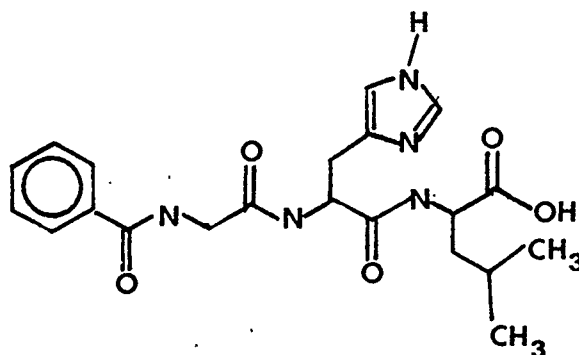
**Table 12**  
Bond Angles (°) for WY44221

Atoms	Angles	Atoms	Angles
C( 2)-N( 1)-C( 9)	107.1(4)	C( 16)-C( 2)-H( 21)	105
C( 2)-N( 1)-C(10)	126.5(5)	C( 2)-C( 3)-H( 31)	106
C( 9)-N( 1)-C(10)	126.0(5)	C( 2)-C( 3)-H( 32)	111
N( 1)-C( 2)-C( 3)	104.0(5)	C( 4)-C( 3)-H( 31)	111
N( 1)-C( 2)-C(16)	109.3(5)	C( 4)-C( 3)-H( 32)	107
C( 3)-C( 2)-C(16)	113.3(5)	H( 31)-C( 3)-H( 32)	118
C( 2)-C( 3)-C( 4)	103.0(5)	C( 4)-C( 5)-H( 51)	123
C( 3)-C( 4)-C( 5)	129.3(6)	C( 6)-C( 5)-H( 51)	119
C( 3)-C( 4)-C( 9)	109.6(5)	C( 5)-C( 6)-H( 61)	116
C( 5)-C( 4)-C( 9)	121.0(6)	C( 7)-C( 6)-H( 61)	123
C( 4)-C( 5)-C( 6)	117.7(6)	C( 6)-C( 7)-H( 71)	120
C( 5)-C( 6)-C( 7)	120.9(7)	C( 8)-C( 7)-H( 71)	118
C( 6)-C( 7)-C( 8)	121.7(6)	C( 7)-C( 8)-H( 81)	122
C( 7)-C( 8)-C( 9)	117.5(7)	C( 9)-C( 8)-H( 81)	121
N( 1)-C( 9)-C( 4)	109.8(5)	C( 10)-C(12)-H(121)	108
N( 1)-C( 9)-C( 8)	129.0(6)	C( 13)-C(12)-H(121)	111
C( 4)-C( 9)-C( 8)	121.2(6)	C( 14)-C(12)-H(121)	109
N( 1)-C(10)-O(11)	119.8(7)	C( 12)-C(13)-H(131)	111
N( 1)-C(10)-C(12)	119.8(6)	C( 12)-C(13)-H(132)	107
O(11)-C(10)-C(12)	120.3(7)	C( 12)-C(13)-H(133)	108
C(10)-C(12)-C(13)	105.5(6)	H(131)-C(13)-H(132)	112
C(10)-C(12)-C(14)	111.3(6)	H(131)-C(13)-H(133)	111
C(13)-C(12)-C(14)	112.3(6)	H(132)-C(13)-H(133)	108
C(12)-C(14)-S(15)	114.1(6)	C( 12)-C(14)-H(141)	112
C( 2)-C(16)-O(17)	119.6(6)	C( 12)-C(14)-H(142)	107
C( 2)-C(16)-O(18)	119.0(7)	S( 15)-C(14)-H(141)	108
O(17)-C(16)-O(18)	120.6(7)	S( 15)-C(14)-H(142)	106
N( 1)-C( 2)-H(21)	112	H(141)-C(14)-H(142)	109
C( 3)-C( 2)-H(21)	113		

**Table 13**  
Torsion Angles for WY44221

Atoms	Angle (°)
N( 1)-C( 2)-C(16)-O(17)	35.3(8)
N( 1)-C( 2)-C(16)-O(18)	-154.7(6)
C( 2)-N( 1)-C(10)-C(12)	-13.4(9)
N( 1)-C(10)-C(12)-C(14)	137.3(7)
C(10)-C(12)-C(14)-S(15)	-175.3(5)

#### 4. Structural Solution of Hippuryl-L-histidyl-L-leucine



(3)

Hippuryl-L-histidyl-L-leucine (3), is a substrate analogue of angiotensin converting enzyme. The dipeptide, L-histidyl-L-leucine, is cleaved from angiotensin I forming the octapeptide, angiotensin II.

The tripeptide has a relative binding affinity of  $1/K_m = 4.54 \times 10^{-4} \mu\text{M}^{-1}$  and is hydrolyzed by angiotensin converting enzyme [57], thus, it acts as a substrate analogue. Kinetic studies of the inhibition of angiotensin converting enzyme are often carried out using hip-L-his-L-leu as the substrate [9,12,57,58] measuring the absorbance at 228 nm of the hippuric acid released by the action of the enzyme.

The X-ray crystal structure for hip-L-his-L-leu was determined for comparison to the structure of ACE inhibitors.

##### 4.1 Experimental

Hip-L-his-L-leu was purchased from Peninsula Laboratories in Belmont, California and crystallized by slow evaporation from a methanol and water mixture to give sticky colorless crystals. A single crystal was sealed in a 1.0 mm quartz capillary tube along with some mother liquor according to the method described by McPherson [53].

The presence of water in the capillary precluded reducing the temperature of the crystal to improve the diffraction pattern; instead, data were collected at room temperature.

After centering the crystal and obtaining the lattice parameters, a full sphere of data was collected to  $\theta = 10^\circ$  to check the symmetry of the lattice. A quadrant of data was collected (+h, +k, +l) from  $10^\circ$  to  $22.5^\circ$ . The intensities of the three standard reflections, (5 7 0), (0 4 8), (4 -2 1) varied less than 4%. The crystal data are in Table 14.

After data reduction, normalized structure factor amplitudes were calculated by using a Wilson plot and parity group rescaling. The 500 largest E values were used to solve the structure. An E map was calculated from the phase set with the highest combined figure of merit, (2.84). This solution identified the positions of all of the nonhydrogen atoms of the tripeptide except for a terminal methyl carbon atom of the leucine side chain. The last atom of the tripeptide as well as 5 peaks corresponding to the oxygen atoms of 5 water molecules were identified in a difference Fourier synthesis.

The structure was initially refined using restrained least squares so that the low number of observed reflections could be used to best advantage. To guide the refinement, a model of the tripeptide was constructed from the bond distances and bond angles of the X-ray structure determinations of leucine, histidine and hippuric acid [59].

The nonhydrogen atoms were refined by maintaining full constraints on the positional parameters and decreasing the thermal parameter constraints to 60%. A difference Fourier synthesis was calculated to locate the hydrogen atoms. Seven of the ten hydrogen atoms from the water molecules, one hydrogen on each methyl group of the leucine side

chain and the hydrogen atoms bound to both ring nitrogen atoms of the histidine side chain were located. The remaining hydrogen atoms on the tripeptide were placed in calculated ideal positions. The hydrogen atoms were included in the model with anisotropic thermal parameters defined as 1.2 times the thermal parameter of the atom to which they were bonded. The parameters for the hydrogen atoms were not refined. After convergence with the restrained least squares procedure, with the restraints removed, conventional least squares were used for the final cycles of refinement so that an extinction correction could be included. The statistics describing the refinement are in Table 14.

The conformation of the tripeptide with the solvent molecules is shown in Figure 5. Tables 15 and 16 contains the atomic coordinates for the nonhydrogen and hydrogen atoms, respectively, with the atoms labelled as in Figure 5, Table 17 contains the anisotropic temperature factors of the nonhydrogen atoms. The bond distances are in Table 18 and bond angles are in Table 19.

#### 4.2 Results

The tripeptide adopts an extended conformation except that the terminal carboxylate group folds back, as indicated by the torsion angle:  $C(2)-C(4)-N(5)-C(6) = -96.7(7)^\circ$ , to form an intramolecular hydrogen bond between the carboxylate oxygen atom, O(1), and the histidine ring nitrogen atom, N(24). The three peptide bonds, N(5)-C(6), N(9)-C(10), and N(13)-C(14) are all *trans*; their torsion angles are  $174.8(5)^\circ$ ,  $171.3(5)^\circ$  and  $173.1(5)^\circ$ , respectively.

The tripeptide is surrounded by a hydrated sheath of solvent molecules. The hydrogen bonding network is shown in Figure 5 and the

geometric parameters of the hydrogen bonds are tabulated in Table 6. All of the nitrogen atoms and oxygen atoms of the peptide are involved in hydrogen bonding. Both of the carboxylate oxygen atoms, O(1) and O(3), form two hydrogen bonds; O(1) forms an intramolecular hydrogen bond to N(24), as mentioned above, and an intermolecular hydrogen bond to N(26) of an adjacent molecule; O(3) forms hydrogen bonds to two different water molecules, W4 and W5.

A stereo view of the crystal packing of the tripeptide is shown in Figure 6. The molecules do not pack in linear chains, rather, the tail end of one molecule overlaps slightly with the head of an adjacent molecule so that a hydrophobic region consisting of the phenyl ring and the leucine side chain is formed. The water molecules are interspersed between the tripeptides which are linked through the hydrogen bond network described in Table 19.

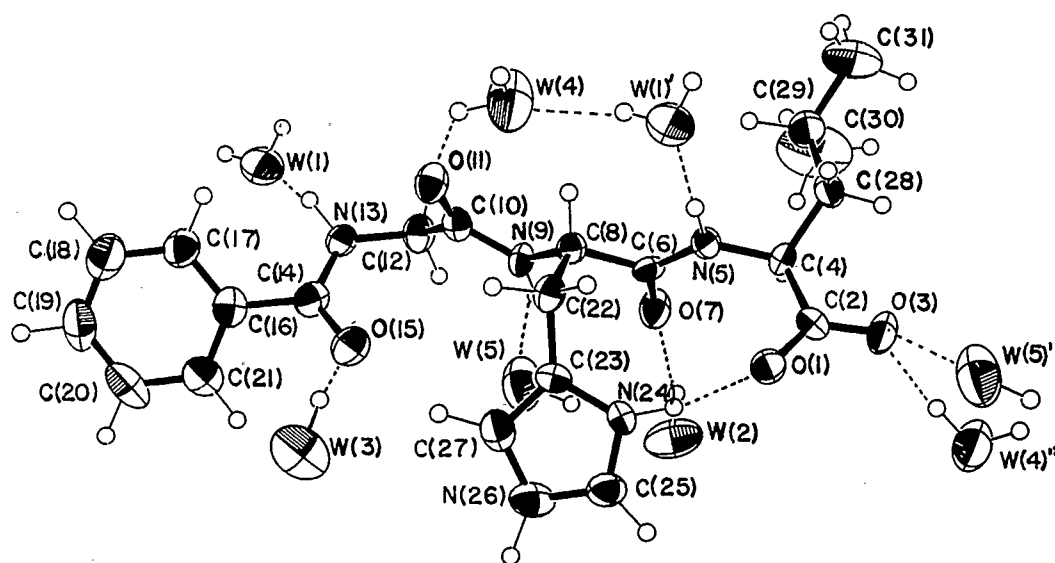


Figure 5

Molecular structure and atomic labelling scheme for  
hip-L-his-L-leu

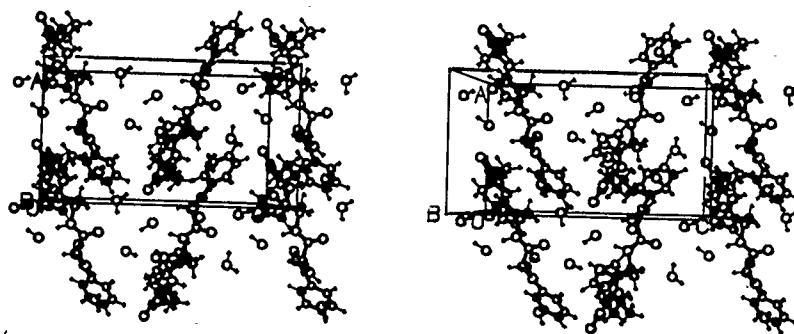


Figure 6

Stereo view of the crystal packing of  
hip-L-his-L-leu showing the water  
sheath around the molecule

**Table 14**  
Crystal Data for Hip-L-his-L-leu

Molecular Formula	:	$C_{21}H_{27}N_5O_4 \cdot 5H_2O$
Molecular Weight	:	519.557 g mol <sup>-1</sup>
Crystal Size	:	0.4 x 0.3 x 0.1 mm
Space Group	:	$P_{2_1}^2$
Cell Dimensions	:	a = 10.055(2) Å b = 14.974(4) Å c = 17.825(5) Å
Volume	:	2683(1) Å <sup>3</sup>
Range of $\theta$ Values Used to Determine the Cell	:	8.7° - 16.4°
No. of Reflections Used	:	25
Density (calculated)	:	1.29 g cm <sup>-3</sup>
Radiation, Wavelength	:	Mo, K $\alpha$ $\lambda$ = 0.71069 Å
Monochromatization	:	graphite monochromator
Temperature	:	25°C
Scan Range	:	1.5(0.93 + 0.142 tan $\theta$ )
Theta Maximum	:	22.5°
Scan Mode	:	$\omega/2\theta$
Absorption Coefficient	:	1.110 cm <sup>-1</sup>
Unique Reflections	:	1990
Observed Reflections ( $I > 2\sigma(I)$ )	:	1452
Weighting Function	:	$\omega^{-1} = \sigma^2(F_o) + 0.0005 F_o^2$
R	:	0.054
R <sub>w</sub>	:	0.059
Highest Residual Peak	:	0.23 e/Å <sup>3</sup> (associated with C(30))
Maximum Shift/Error	:	0.0416
Goodness of Fit	:	1.32
Extinction (isotropic)	:	$2.589 \times 10^{-3}$

**Table 15**

Fractional Atomic Coordinates ( $\times 10^4$ ) and Equivalent  
Isotropic Temperature Factors ( $\times 10$ ) for  
the Nonhydrogen Atoms of Hip-L-his-L-leu

Beq is defined as one-third the trace of the Bij matrix.

Atom	x/a	y/b	z/c	Beq
O(1)	12831( 5)	-766( 3)	239( 3)	44(3)
C(2)	13153( 7)	22( 5)	93( 4)	32(3)
O(3)	14160( 5)	226( 3)	-272( 3)	53(3)
C(4)	12273( 6)	784( 4)	373( 3)	28(3)
N(5)	11346( 5)	489( 3)	938( 3)	27(2)
C(6)	10078( 6)	259( 4)	802( 3)	25(3)
O(7)	9559( 4)	270( 3)	185( 2)	39(2)
C(8)	9352( 6)	-112( 4)	1500( 3)	25(3)
N(9)	7934( 5)	-67( 3)	1344( 2)	24(2)
C(10)	7055( 6)	-48( 4)	1911( 4)	26(3)
O(11)	7367( 4)	-117( 3)	2580( 2)	35(2)
C(12)	5614( 7)	141( 5)	1662( 4)	35(3)
N(13)	4649( 5)	-378( 4)	2074( 3)	32(3)
C(14)	4591( 6)	-1266( 4)	1992( 3)	35(3)
O(15)	5435( 5)	-1672( 3)	1611( 3)	46(3)
C(16)	3466( 6)	-1742( 4)	2369( 3)	35(3)
C(17)	2933( 7)	-1461( 5)	3046( 4)	41(4)
C(18)	1873( 8)	-1903( 5)	3366( 4)	52(4)
C(19)	1363( 8)	-2625( 6)	3008( 5)	54(4)
C(20)	1845( 8)	-2916( 5)	2314( 5)	51(4)
C(21)	2917( 7)	-2477( 5)	1998( 4)	42(4)
C(22)	9818( 6)	-1054( 4)	1702( 3)	28(3)
C(23)	9725( 6)	-1728( 4)	1092( 3)	27(3)
N(24)	10623( 5)	-1774( 3)	511( 3)	31(2)
C(25)	10302( 7)	-2447( 5)	73( 4)	39(3)
N(26)	9236( 6)	-2847( 4)	342( 3)	39(3)
C(27)	8857( 7)	-2404( 5)	983( 4)	39(3)
C(28)	13073( 6)	1568( 4)	659( 3)	33(3)
C(29)	12309( 8)	2389( 5)	888( 5)	51(4)

Table 15 continued:

C(30)	11618(11)	2816( 7)	236( 7)	107(8)
C(31)	13251(11)	3066( 6)	1275( 5)	84(6)
O(W1)	2125( 5)	617( 4)	2491( 3)	57(3)
O(W2)	9051( 6)	-505( 4)	-1199( 3)	66(3)
O(W3)	6068( 5)	-3436( 4)	1752( 4)	68(3)
O(W4)	9935( 5)	173( 5)	3332( 3)	69(3)
O(W5)	6737( 6)	-657( 5)	-68( 3)	72(3)

**Table 16**  
 Fractional Atomic Coordinates ( $\times 10^4$ ) and  
 Isotropic Temperature Factors ( $\times 10$ ) for  
 the Hydrogen Atoms of Hip-L-his-L-leu

Atom	x/a	y/b	z/c	Biso
H(241)	11162	-1351	223	38
H(41)	11710	1049	-73	29
H(51)	11708	448	1483	28
H(81)	9560	265	1973	22
H(91)	7628	-70	793	27
H(121)	5413	825	1756	34
H(122)	5511	6	1099	34
H(131)	4000	-56	2450	37
H(171)	3363	-910	3310	46
H(181)	1471	-1692	3884	56
H(191)	513	-2970	3242	59
H(201)	1393	-3458	2042	59
H(211)	3290	-2695	1492	45
H(221)	10795	-1061	1807	30
H(222)	9237	-1333	2091	9
H(251)	10846	-2659	-383	39
H(261)	8760	-3386	0	45
H(271)	8067	-2517	1373	44
H(281)	13630	1337	1127	37
H(282)	13746	1751	242	37
H(291)	11538	2159	1258	54
H(301)	12380	3190	-73	119
H(302)	10878	3246	430	119
H(303)	11187	2332	-107	119
H(311)	14100	3068	893	94
H(312)	12717	3688	1336	94
H(313)	13413	2847	1839	94
H(W11)	2483	1061	2679	62
H(W12)	1311	651	2682	62
H(W21)	9371	-186	-751	72

Table 16 continued:

H(W31)	5932	-2701	1805	74
H(W41)	10396	0	3768	74
H(W42)	8988	0	3393	74
H(W51)	7306	-548	-536	81

**Table 17**  
 Anisotropic Temperature Factors ( $\times 10^3$ )  
 for the Nonhydrogen Atoms  
 of Hip-L-his-L-leu

The temperature factor expression is of the form:  
 $T = \exp - 2\pi^2(U_{11}(ha^*)^2 + \dots + \dots + U_{12}(hka^*b^*) + \dots)$

Atom	U11	U22	U33	U12	U13	U23
O(1)	46(3)	35(3)	87( 4)	1(3)	26(3)	-18(3)
C(2)	42(4)	34(4)	46( 4)	-11(4)	2(4)	-5(4)
O(3)	62(4)	56(3)	84( 4)	-11(3)	46(3)	-10(3)
C(4)	31(4)	42(4)	33( 4)	-3(4)	11(3)	-3(3)
N(5)	26(3)	41(3)	34( 3)	-3(3)	-2(3)	-4(3)
C(6)	31(4)	32(4)	31( 4)	6(3)	1(3)	-10(3)
O(7)	33(3)	77(4)	37( 3)	-12(3)	-2(2)	-1(3)
C(8)	24(4)	35(4)	34( 4)	1(3)	0(3)	-3(3)
N(9)	22(3)	48(3)	24( 3)	-3(3)	0(2)	5(3)
C(10)	31(4)	27(4)	42( 4)	3(3)	3(4)	6(3)
O(11)	35(3)	60(3)	40( 3)	1(2)	0(2)	7(3)
C(12)	33(4)	50(4)	48( 4)	3(4)	2(4)	7(4)
N(13)	28(3)	44(4)	51( 3)	1(3)	13(3)	-11(3)
C(14)	21(3)	62(4)	49( 4)	0(4)	0(3)	-11(4)
O(15)	41(3)	58(3)	75( 3)	8(3)	19(3)	-13(3)
C(16)	33(4)	54(4)	45( 4)	2(4)	-3(3)	9(4)
C(17)	49(5)	70(5)	38( 4)	-12(4)	-1(4)	-2(4)
C(18)	71(6)	70(6)	58( 5)	3(5)	17(5)	10(5)
C(19)	56(5)	59(5)	91( 6)	-2(5)	27(5)	24(5)
C(20)	52(5)	39(4)	105( 7)	-10(4)	-10(5)	9(4)
C(21)	39(4)	44(4)	75( 5)	8(4)	-10(4)	-1(4)
C(22)	34(4)	40(4)	34( 3)	4(3)	2(3)	8(3)
C(23)	39(4)	28(3)	36( 3)	1(3)	-5(3)	-3(3)
N(24)	38(3)	34(3)	47( 3)	-12(3)	9(3)	-3(3)
C(25)	38(4)	48(4)	61( 4)	3(4)	0(4)	-17(4)
N(26)	39(4)	53(4)	58( 4)	4(3)	-18(3)	-16(3)
C(27)	41(4)	46(4)	61( 5)	-4(4)	4(4)	5(4)
C(28)	31(4)	38(4)	58( 4)	-6(3)	7(3)	-6(3)

Table 17 continued:

C(29)	62(5)	44(4)	87( 5)	-6(4)	28(5)	-19(4)
C(30)	125(9)	83(7)	197(12)	67(7)	-53(9)	-31(7)
C(31)	137(9)	64(6)	119( 8)	-13(7)	7(7)	-42(5)
O(W1)	65(4)	87(4)	64( 3)	-17(3)	-8(3)	-16(3)
O(W2)	113(5)	88(4)	48( 3)	22(4)	-22(3)	-15(3)
O(W3)	60(4)	67(4)	131( 5)	13(3)	-22(4)	4(4)
O(W4)	59(4)	141(6)	63( 3)	-17(4)	-11(3)	21(4)
O(W5)	73(4)	134(5)	68( 4)	-38(4)	-4(3)	8(4)

**Table 18**  
Table of Bond Distances (Å)  
for Hip-L-his-L-leu

Atoms	Distance	Atoms	Distance
O( 1)-C( 2)	1.251( 8)	N( 5)-H( 51)	1.039
C( 2)-O( 3)	1.242( 9)	C( 8)-H( 81)	1.037
C( 2)-C( 4)	1.528( 9)	N( 9)-H( 91)	1.029
C( 4)-N( 5)	1.442( 8)	C(12)-H(121)	1.057
C( 4)-C(28)	1.511( 9)	C(12)-H(122)	1.028
N( 5)-C( 6)	1.342( 8)	N(13)-H(131)	1.052
C( 6)-O( 7)	1.218( 7)	C(17)-H(171)	1.044
C( 6)-C( 8)	1.545( 8)	C(18)-H(181)	1.056
C( 8)-N( 9)	1.454( 8)	C(19)-H(191)	1.082
C( 8)-C(22)	1.530( 8)	C(20)-H(201)	1.049
N( 9)-C(10)	1.344( 8)	C(21)-H(211)	1.030
C(10)-O(11)	1.236( 8)	C(22)-H(221)	1.000
C(10)-C(12)	1.541( 9)	C(22)-H(222)	0.998
C(12)-N(13)	1.445( 8)	N(24)-H(241)	0.979
N(13)-C(14)	1.340( 9)	C(25)-H(251)	1.030
C(14)-O(15)	1.245( 8)	N(26)-H(261)	1.119
C(14)-C(16)	1.496( 9)	C(27)-H(271)	1.069
C(16)-C(17)	1.386( 9)	C(28)-H(281)	1.063
C(16)-C(21)	1.397( 9)	C(28)-H(282)	1.041
C(17)-C(18)	1.379(11)	C(29)-H(291)	1.075
C(18)-C(19)	1.356(12)	C(30)-H(301)	1.097
C(19)-C(20)	1.399(12)	C(30)-H(302)	1.043
C(20)-C(21)	1.382(10)	C(30)-H(303)	1.042
C(22)-C(23)	1.486( 8)	C(31)-H(311)	1.092
C(23)-N(24)	1.376( 8)	C(31)-H(312)	1.081
C(23)-C(27)	1.351( 9)	C(31)-H(313)	1.071
N(24)-C(25)	1.315( 9)	O(W1)-H(W11)	0.828
C(25)-N(26)	1.318( 9)	O(W1)-H(W12)	0.888
N(26)-C(27)	1.375( 9)	O(W2)-H(W21)	0.984
C(28)-C(29)	1.506(10)	O(W3)-H(W31)	1.112
C(29)-C(30)	1.498(14)	O(W4)-H(W41)	0.941

Table 18 continued:

C(29)-C(31)	1.548(12)	O(W4)-H(W42)	0.992
C( 4)-H(41)	1.053	O(W5)-H(W51)	1.025

**Table 19**  
Bond Angles ( $^{\circ}$ ) for Hip-L-his-L-leu

Atoms	Angles ( $^{\circ}$ )	Atoms	Angles ( $^{\circ}$ )
O( 1)-C( 2)-O( 3)	123.5(6)	N( 13)-C(12)-H(121)	108.1
O( 1)-C( 2)-C( 4)	119.1(6)	N( 13)-C(12)-H(122)	108.8
O( 3)-C( 2)-C( 4)	117.4(6)	H(121)-C(12)-H(122)	109.0
C( 2)-C( 4)-N( 5)	111.9(5)	C( 12)-N(13)-H(131)	119.6
C( 2)-C( 4)-C( 28)	112.4(5)	C( 14)-N(13)-H(131)	119.9
N( 5)-C( 4)-C( 28)	110.3(5)	C( 16)-C(17)-H(171)	118.2
C( 4)-N( 5)-C( 6)	124.5(5)	C( 18)-C(17)-H(171)	120.9
N( 5)-C( 6)-O( 7)	124.5(6)	C( 17)-C(18)-H(181)	120.9
N( 5)-C( 6)-C( 8)	113.3(5)	C( 19)-C(18)-H(181)	120.4
O( 7)-C( 6)-C( 8)	122.0(5)	C( 18)-C(19)-H(191)	119.9
C( 6)-C( 8)-N( 9)	107.0(4)	C( 20)-C(19)-H(191)	117.7
C( 6)-C( 8)-C( 22)	112.1(5)	C( 19)-C(20)-H(201)	120.0
N( 9)-C( 8)-C( 22)	112.8(5)	C( 21)-C(20)-H(201)	121.2
N( 9)-C(10)-O( 11)	123.8(6)	C( 16)-C(21)-H(211)	121.3
N( 9)-C(10)-C( 12)	113.9(5)	C( 20)-C(21)-H(211)	119.4
O(11)-C(10)-C( 12)	122.1(6)	C( 8)-C(22)-H(221)	110.7
C(10)-C(12)-N( 13)	112.7(5)	C( 8)-C(22)-H(222)	111.7
C(12)-N(13)-C( 14)	120.5(5)	C( 23)-C(22)-H(221)	101.0
N(13)-C(14)-O( 15)	121.0(6)	C( 23)-C(22)-H(222)	100.8
N(13)-C(14)-C( 16)	117.1(5)	H(221)-C(22)-H(222)	116.1
O(15)-C(14)-C( 16)	121.9(6)	C( 23)-N(24)-H(241)	136.5
C(14)-C(16)-C( 17)	122.6(6)	C( 23)-N(24)-H(251)	132.7
C(14)-C(16)-C( 21)	117.5(6)	C( 25)-N(24)-H(241)	108.7
C(17)-C(16)-C( 21)	119.9(6)	N( 24)-C(25)-H(251)	125.1
C(16)-C(17)-C( 18)	120.9(7)	N( 26)-C(25)-H(251)	125.4
C(17)-C(18)-C( 19)	118.7(7)	C( 25)-N(26)-H(261)	118.5
C(18)-C(19)-C( 20)	122.2(8)	C( 27)-N(26)-H(261)	133.0
C(19)-C(20)-C( 21)	118.9(7)	C( 23)-C(27)-H(271)	120.4
C(16)-C(21)-C( 20)	119.4(7)	N( 26)-C(27)-H(271)	132.1
C( 8)-C(22)-C( 23)	115.8(5)	C( 4)-C(28)-H(281)	107.0
C(22)-C(23)-N( 24)	122.9(5)	C( 4)-C(28)-H(282)	108.1
C(22)-C(23)-C( 27)	130.9(6)	C( 29)-C(28)-H(281)	108.7

Table 19 continued:

N(24)-C(23)-C( 27)	106.2(5)	C( 29)-C(28)-H(282)	108.1
C(23)-N(24)-C( 25)	108.9(5)	H(281)-C(28)-H(282)	107.7
N(24)-C(25)-N( 26)	109.3(6)	C( 28)-C(29)-H(291)	105.8
C(23)-C(27)-N( 26)	107.5(6)	C( 30)-C(29)-H(291)	106.2
C( 4)-C(28)-C( 29)	117.0(6)	C( 31)-C(29)-H(291)	112.2
C(28)-C(29)-C( 30)	112.0(7)	C( 29)-C(30)-H(301)	106.4
C(28)-C(29)-C( 31)	110.1(7)	C( 29)-C(30)-H(302)	109.7
C(30)-C(29)-C( 31)	110.5(7)	C( 29)-C(30)-H(303)	110.6
C( 2)-C( 4)-H( 41)	110.2	H(301)-C(30)-H(302)	110.4
N( 5)-C( 4)-H( 41)	107.2	H(301)-C(30)-H(303)	110.6
C(28)-C( 4)-H( 41)	104.4	H(302)-C(30)-H(303)	109.1
C( 4)-N( 5)-H( 51)	116.4	C( 29)-C(31)-H(311)	101.7
C( 6)-N( 5)-H( 51)	119.1	C( 29)-C(31)-H(312)	107.8
C( 6)-C( 8)-H( 81)	111.3	C( 29)-C(31)-H(313)	108.1
N( 9)-C( 8)-H( 81)	109.2	H(311)-C(31)-H(312)	116.7
C(22)-C( 8)-H( 81)	104.4	H(311)-C(31)-H(313)	117.9
C( 8)-N( 9)-H( 91)	118.4	H(312)-C(31)-H(313)	104.1
C(10)-N( 9)-H( 91)	121.4	H(W11)-O(W1)-H(W12)	101.4
C(10)-C(12)-H(121)	108.2	H(W41)-O(W4)-H(W42)	108.1
C(10)-C(12)-H(122)	109.9		

**Table 20**  
 Hydrogen Bond Parameters (Y...H-X)  
 for Hip-L-his-L-leu

Bond	Y...X (Å)	Y...H (Å)	X-H (Å)	Angle Y...H-X (°)
O(1)...H(241)-N(24)	2.728(7)	1.893(5)	0.979	141.5(3)
O(W1)...H(131)-N(13)	3.035(8)	2.139(5)	1.052	141.6(3)
O(7)...H(W21)-O(W2)	2.772(7)	1.812(5)	0.984	164.5(4)
O(W2)...H(W51)-O(W5)	3.087(8)	2.116(6)	1.025	157.3(3)
O(W1)'...H(51)-N(5)	2.882(7)	1.861(5)	1.039	166.6(3)
O(15)...H-O(W3)*	2.728(7)	-	-	-
O(11)...H(W42)-O(W4)	2.942(7)	2.189(4)	0.992	131.5(3)
O(W5)...H(91)-N(9)	2.926(7)	1.982(6)	1.029	151.1(3)
O(3)...H-O(W5)'	2.932(8)	-	-	-
O(W4)...H(W12)' <sup>-</sup> -O(W1)'	2.747(8)	1.942(6)	0.888	149.8(4)
O(3)...H(W41)' <sup>-</sup> -O(W4) <sup>#</sup>	2.716(7)	1.801(5)	0.941	163.4(4)
O(1)...H(261) <sup>†</sup> -N(26) <sup>†</sup>	2.718(7)	1.633(5)	1.119	161.4(3)

' = (x+1,y,z)    # = (-x+2.5,-y,z-1/2)    † = (x+1/2,-y-1/2,-z)

\* The hydrogen atom was not located in the  
 difference Fourier synthesis

#### IV. Molecular Mechanics Experimental

##### 1. Methods

Before calculating the low energy binding conformations of ACE inhibitors bound to thermolysin, low energy conformations were calculated for complexes of thermolysin specific inhibitors and thermolysin. The inhibitors chosen were (2-benzyl-3-mercaptopropanyl)-L-alanylglycinamide (BAG) ( $K_i = 7.5 \times 10^{-7}$  M) [22] and  $\beta$ -phenylpropionyl-L-phenylalanine, (PPP) ( $K_i = 1.6 \times 10^{-3}$  M) [5].

For each of the calculations, the coordinates of the inhibitor molecule from the structure of the complex along with those of the 1.6 Å resolution refined structure of thermolysin [20] and the coordinates of all of the hydrogen atoms that could be involved in hydrogen bonds were used. The hydrogen atoms attached to the carbon atoms were included as the extended atom types. One water molecule was included in the minimizations; this water molecule forms a hydrogen bond to the main chain nitrogen atom of Trp 115 and is found in the crystal structures of the inhibitor-enzyme complexes. The enzyme residues included in the calculation of the energy were all those within 10 Å of the inhibitor. Only those hydrogen atoms capable of hydrogen bonding were specifically included in the inhibitor molecule; the other hydrogen atoms were accounted for by the extended-atom types.

The refinements were carried out by varying the torsional rotations of the inhibitor molecule and of the side chains of the enzyme residues (see Appendix 1 for the definitions of the amino acid torsion angles) that line the active site and those that form a sheath about the inhibitor molecule. The enzyme residues that were allowed to undergo torsional rotations did not, therefore, include all the residues within

10 Å of the inhibitor but only those that were closest to the inhibitor and had a complete environment of enzyme residues surrounding them. In the minimization, the zinc atom was allowed to translate and the water molecule and the inhibitor molecule were allowed to translate and rotate. The enzyme residues that coordinate to the zinc atom were also allowed to undergo torsional rotations in the minimization. The metal center geometry was selected as tetrahedral since this was the coordination geometry found in the crystal structures of each inhibitor complex. The energy minimization included contributions from the van der Waals interactions, hydrogen bond interactions, and the metal potential. Also assessed was the fit of the defined metal coordination type to that of an ideal fit with a value of 1.00.

Each of the refinements were carried out in three steps. Initially the refinement parameters were set for poor geometries. These refinement parameters included on/off switches for the van der Waals distances and the hydrogen bond distances as described by Brookes et al. [60]. Also included are the torsional, rotational, and translational step width parameters used in the first cycle. These were automatically optimized in the higher cycles. As the refinement progressed these parameters were tightened by increasing the on/off switch distances and the step width values. In the final stages of refinement the most stringent refinement parameters were applied. The parameters used in each step are tabulated in Table 21.

A convergence criterion for the refinements was set at 0.1 kcal/mole; changes in energy of less than this value indicated that the true local minimum had been reached.

The molecular mechanics calculations carried out deal only with the

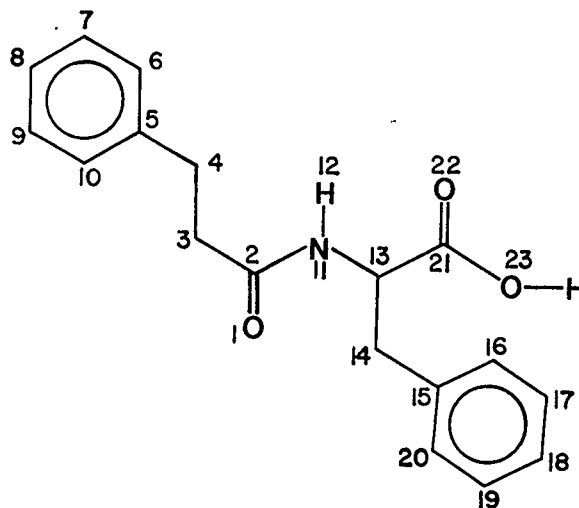
enthalpy of the enzyme-inhibitor complex. The entropy involved in the binding process, that is, the entropy due to the removal of the solvent from the active site of the enzyme and from the inhibitor molecule is not included in these calculations. However, since the structure of thermolysin changes very little in binding of the inhibitor molecule it may be assumed that the entropy contribution to the free energy is small and that the major contribution to the free energy is the enthalpy.

**Table 21**  
Refinement Parameters Used in the Molecular  
Mechanics Calculations

	Very Poor Geometries	Poor Geometries	Good Geometries
On/Off Switches			
van der Waals (Å)	3.5/4.0	5.5/6.0	7.5/8.0
hydrogen bond (Å)	3.5/4.0	4.0/4.5	4.5/5.0
Step Widths			
torsional (°)	0.01	1.0	5.0
rotational (°)	0.002	0.2	1.0
translational (°)	$2 \times 10^{-6}$	$2 \times 10^{-4}$	0.001

## 2. Minimization of the Complex of Thermolysin and PPP

### 2.1 Experimental



(4)

The coordinates of the inhibitor, PPP (4), were obtained from the X-ray structure of the complex with thermolysin [5]. The terminal carboxyl group was left in the anionic form since it was believed to be involved in hydrogen bonding to Arg 203. The 10 Å range around the PPP inhibitor included 70 enzyme residues. Also considered were the water molecule, the zinc atom, and, of course, the inhibitor molecule. The fit of the observed zinc coordination to ideal tetrahedral geometry was 0.801. The ligands involved in coordination to the metal ion were OE1 of Glu 166, NE2 of His 142 and NE2 of His 146 of the enzyme (see Table 24) and O(1) of the inhibitor molecule. The enzyme residues allowed to undergo torsional rotations included  $\tau_1$ ,  $\tau_2$  and  $\tau_3$  of Tyr 110,  $\tau_1$  and  $\tau_2$  of Asn 112,  $\tau_1$  and  $\tau_2$  of Phe 114,  $\tau_1$  and  $\tau_2$  of His

142,  $\tau_1$ ,  $\tau_2$  and  $\tau_3$  of Glu 143,  $\tau_1$  and  $\tau_2$  of His 146,  $\tau_1$ ,  $\tau_2$  and  $\tau_3$  of Tyr 157,  $\tau_1$ ,  $\tau_2$  and  $\tau_3$  of Glu 166 and  $\tau_1$ ,  $\tau_2$ ,  $\tau_3$  and  $\tau_4$  of Arg 203 (see Appendix I). The refinement results are given in Table 22. The values of the torsion angles before and after minimization are in Table 23. The maximum root mean square shift for the atoms was 0.69 for C(18) of the inhibitor. The average root mean square shift was 0.02 Å. The phenylalanine ring of the inhibitor had an average root mean square shift of 0.56 Å. The geometry of the metal ion is in Table 24. Stereoscopic views of the X-ray and minimized structures are shown in Figure 7.

## 2.2 Results

The total improvement in the energy of 38.6 kcal/mole was due mainly to improvements in the hydrogen bond interactions (23.2 kcal/mole). The minimized structure has only one true hydrogen bond between O(23) of the inhibitor and a terminal guanidine nitrogen atom of Arg 203. The distance O(23)-N(Arg 203) was improved only slightly, however, the angle subtended by the hydrogen atom was increased by 14.3° from its initial value of 151.5°. This hydrogen bond interaction was improved by a rotation of -4.9° for  $\tau_4$  of Arg 203 which placed the hydrogen atom of the guanidine group slightly closer to O(23) and, more importantly, increased the angle subtended at the hydrogen atom towards its optimal value of 180°. The second nitrogen atom of the guanidine group of Arg 203 did not participate in hydrogen bonding to the inhibitor. The distance between this nitrogen atom and O(23) is 3.53 Å in the minimized structure, too long for a hydrogen bond. A view of the hydrogen bond interaction after minimization is in Figure 8. The

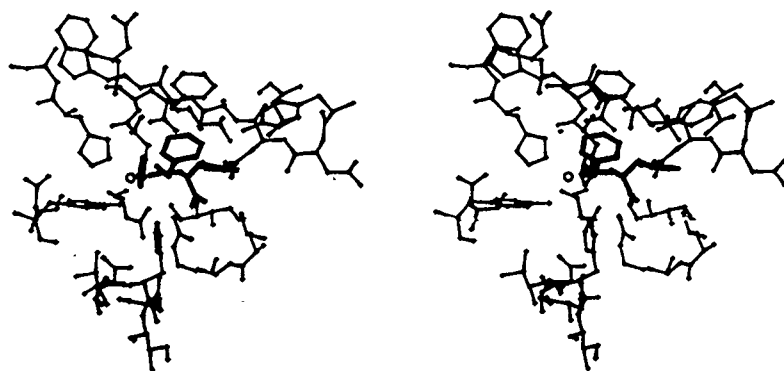
other two potential hydrogen bonding atoms of the inhibitor, N(11) and O(22) do not interact with any enzyme residues. The distances O(22)-N(Asn 112) = 3.65 Å and N(11)-O(Ala 113) = 3.39 Å are both too long for hydrogen bond formation. The terminal carboxyl group of the inhibitor molecule must span the active site cleft in order to form hydrogen bonds between the oxygen atoms O(22) and O(23) and the side chains of Asn 112 and Arg 203. The width of this cleft does not allow for two simultaneous hydrogen bonds to be formed, therefore, only one bond is formed to Arg 203. This single hydrogen bond indicates the importance of Arg 203 in binding of the inhibitor to thermolysin.

Another interaction stabilizing the binding of the inhibitor to the enzyme is the parallel stacking of the phenyl ring of the inhibitor with the phenyl ring of Phe 114. This stacking is shown in Figure 9, the stacking distance between the rings is approximately 3.4 Å. The refinement also reduced repulsions between poorly placed groups. Changes in the torsion angles of the inhibitor, C(3)-C(2)-N(11)-C(13) of  $7.1^\circ$  and N(11)-C(13)-C(14)-C(15) of  $-7.84^\circ$ , positioned the phenylalanine ring in the S<sub>1</sub> hydrophobic subsite and reduced unfavorable van der Waals interactions with the residues lining this pocket. Prior to the minimization, C(18) was only 2.88 Å from a terminal methyl carbon atom of Val 139. This distance increased to 3.07 Å with a concomitant decrease in the van der Waals repulsions between these groups. These rotations also increased the distance between C(14) and the main chain oxygen atom of Asn 112 from 2.91 Å to 3.14 Å decreasing the van der Waals repulsions.

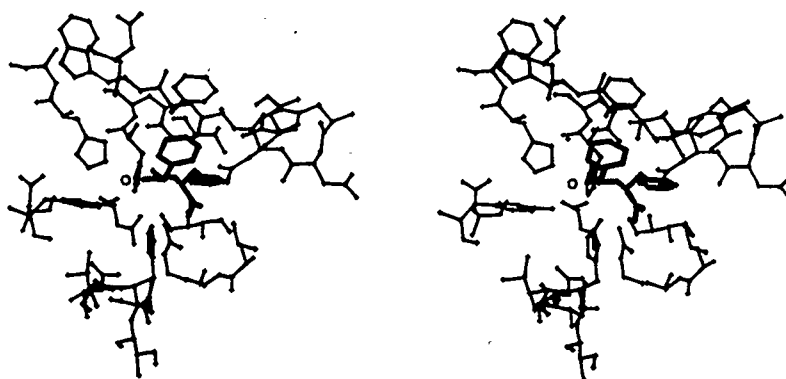
The minimization improved the fit of the coordination of the metal ion to the tetrahedral ideal geometry; the geometry given in Table 24

resulted in a decrease in energy of 4.07 kcal/mole. The distances between the metal atom and each of the four ligands decreased by approximately 0.1 Å, tightening the coordination sphere and approaching the ideal values of 2.00 Å for the Zn-N distances and 1.95 Å for the Zn-O distances. The angles subtended by the zinc also approached the ideal value of 109.5° with the exception of the angles O(1)-Zn-OE1(Glu 166) and O(1)-Zn-NE2(His 146); these two angles decreased by 1.66° and increased by 4.02°, respectively, from their initial values in the opposite direction from the ideal value. These changes were necessary, however, to accommodate the 10° change in the angle NE2(His 142)-Zn-OE1(Glu 166) and the 12° change in the angle OE1(Glu 166)-Zn-NE2(His 146) needed to improve the ideality of the coordination. A superposition of the metal coordination before and after minimization is shown in Figure 10.

The minimized structure shows improvements in the zinc coordination, in the position of the inhibitor phenylalanine ring in the S<sub>1</sub> subsite, and in the hydrogen bonding interactions between O(23) and the guanidine group of Arg 203. No hydrogen bonds are formed between N(11) or O(22) and the enzyme. Of the three potential hydrogen bonding atoms on the inhibitor, only one is actually used in a hydrogen bond, thus, there are a few strong interactions between the inhibitor and the active site.



(a)



(b)

**Figure 7**

Stereoscopic drawings of the (a) X-ray and  
(b) minimized complex of thermolysin and PPP.

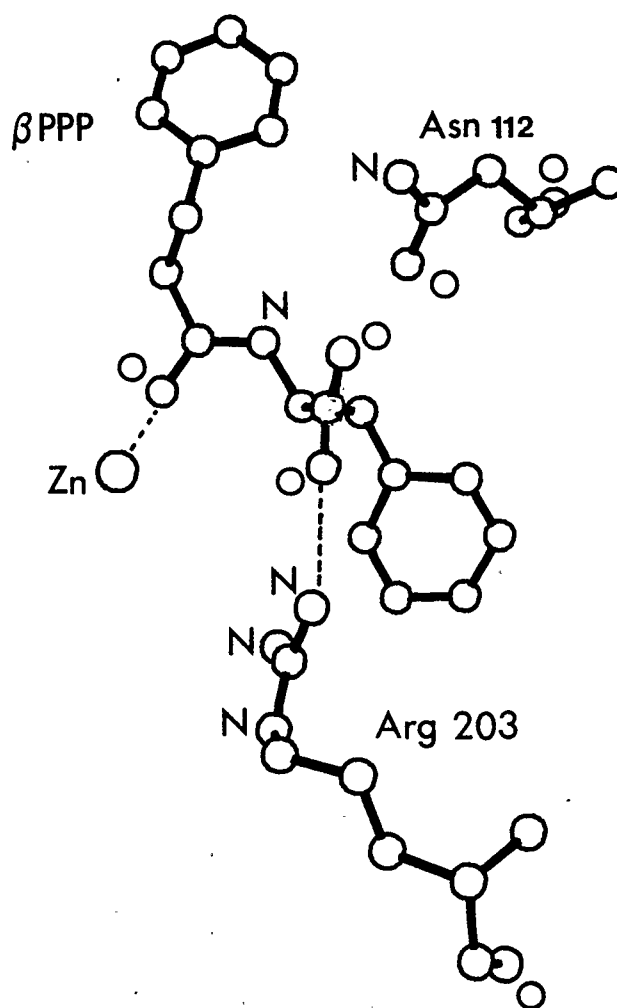


Figure 8

Hydrogen bond interaction between PPP and Arg 203  
after minimization

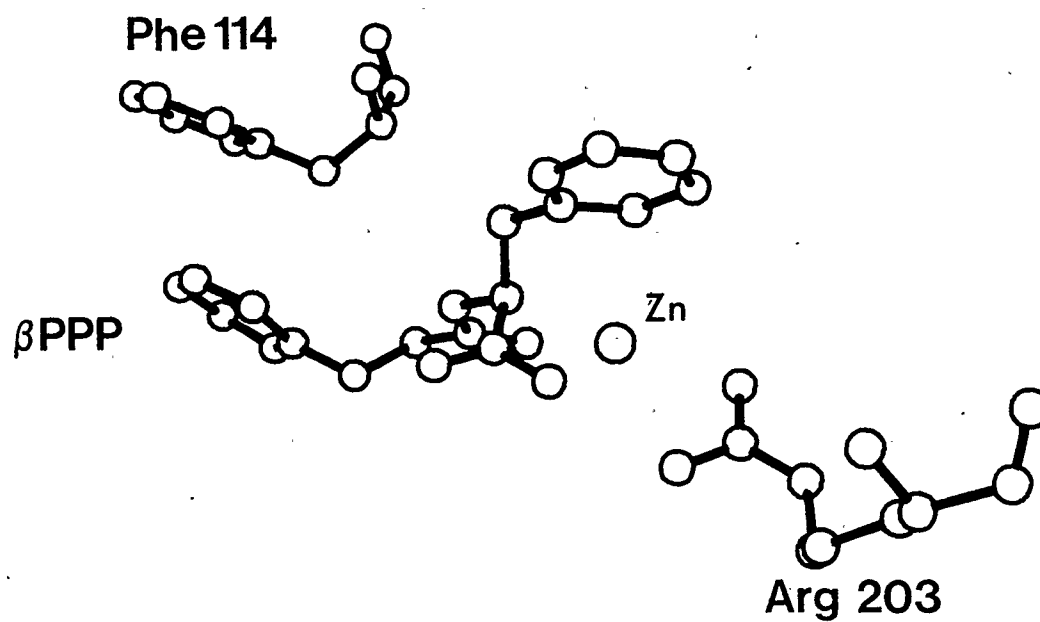


Figure 9

Stacking interaction between the  $\beta$  phenyl ring of PPP and Phe 114 of the enzyme after minimization.

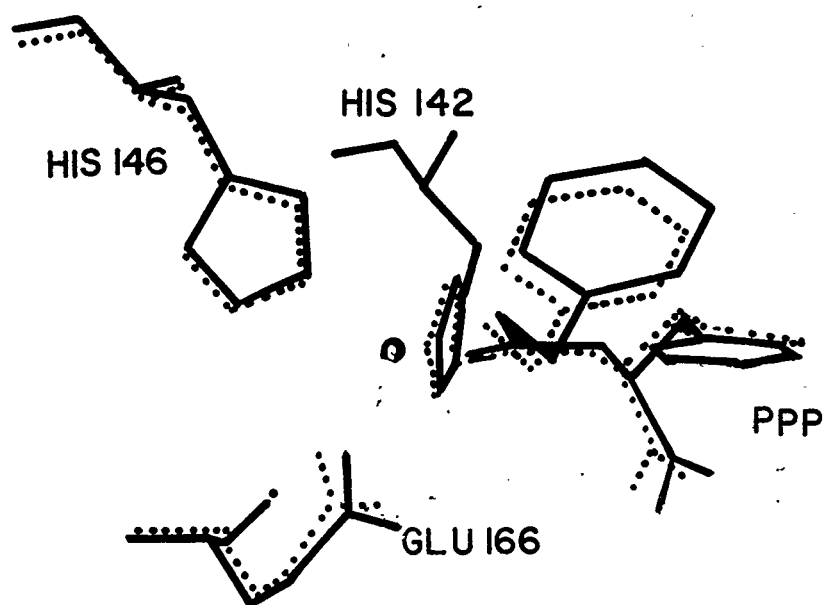


Figure 10

Superposition of the metal coordination geometry before and after refinement of the complex of thermolysin and PPP.

The solid lines correspond to the minimized structure and the dashed lines correspond to the unminimized structure.

**Table 22**  
 Minimization Data for the Complex  
 of Thermolysin and PPP

Number of Atoms	:	670	
Number of Residues	:	73	
Number of Dihedral			
Degrees of Freedom	:	31	
Number of Translational			
Degrees of Freedom	:	9	
Number of Rotational			
Degrees of Freedom	:	6	
Convergence Criterion	:	0.1 kcal/mole	
		Starting	Final
Coordination Fit to Ideal	:	0.801	0.901
Energies (kcal/mole)			
van der Waals	:	-466.5	-477.9
hydrogen bond	:	-52.5	-75.7
metal	:	-16.9	-21.0
total	:	-535.9	-574.5
Total Improvement	:	38.7	

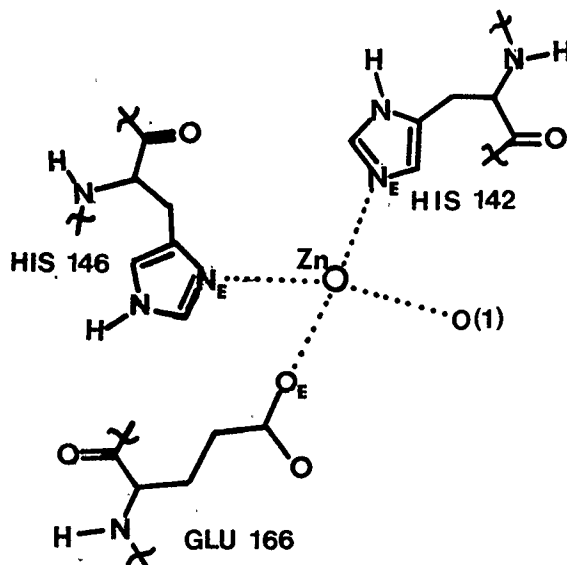
**Table 23**  
 Comparison of Torsion Angles Before and After Minimization  
 for the Complex of Thermolysin and PPP

	Before (°)	After (°)	$\Delta$ (°)
Tyr 110			
$\tau_1$	-169.1	-169.1	-0.1
$\tau_2$	69.7	69.6	-0.1
$\tau_3$	179.2	179.1	-0.0
Asn 112			
$\tau_1$	-142.0	-146.4	-4.4
$\tau_2$	155.9	153.2	-2.7
Phe 114			
$\tau_1$	52.2	52.1	-0.1
$\tau_2$	102.8	103.2	0.4
His 142			
$\tau_1$	170.4	165.8	-4.6
$\tau_2$	117.7	116.2	-1.6
Glu 143			
$\tau_1$	-62.3	-62.2	0.0
$\tau_2$	-44.2	-44.2	0.0
$\tau_3$	-27.0	-29.5	-2.4
His 146			
$\tau_1$	-81.2	-78.8	2.4
$\tau_2$	-57.4	-56.1	1.3
Tyr 157			
$\tau_1$	-151.0	-149.2	1.8
$\tau_2$	-112.9	-112.5	0.4
$\tau_3$	-179.6	-179.7	-0.1
Glu 166			
$\tau_1$	-84.6	-91.4	-6.8
$\tau_2$	-53.2	-57.8	-4.6
$\tau_3$	122.0	119.4	-2.6
Arg 203			
$\tau_1$	-65.6	-65.6	0.0
$\tau_2$	-179.2	-179.2	-0.0

Table 23 continued:

$\tau_3$	-74.3	-74.5	-0.2
$\tau_4$	-75.8	-80.7	-4.9
His 231			
$\tau_1$	-58.5	-63.4	-4.9
$\tau_2$	85.6	84.3	-1.3
Inhibitor			
C(6)-C(5)-C(4)-C(3)	-110.4	-108.9	1.5
C(5)-C(4)-C(3)-C(2)	133.6	135.0	1.4
C(4)-C(3)-C(2)-N(11)	-48.4	-48.5	-0.1
C(3)-C(2)-N(11)-C(13)	-176.9	176.0	7.1
C(2)-N(11)-C(13)-C(21)	-103.9	-108.0	-4.1
N(11)-C(13)-C(21)-O(23)	137.6	138.6	1.0
N(11)-C(13)-C(14)-C(15)	179.4	-172.9	-7.8
C(13)-C(14)-C(15)-C(16)	61.7	59.4	-2.3

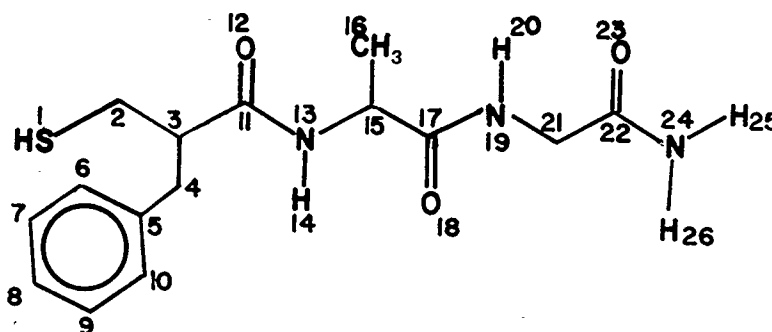
**Table 24**  
Distances (Å) and Angles (°) for the Zinc Atom Coordination  
Sphere for the Complex of Thermolysin and PPP



	Before	After	$\Delta$
<b>Distances</b>			
Zn-NE2(His 142)	2.11	2.00	-0.11
Zn-NE2(His 146)	2.08	1.98	-0.10
Zn-OE1(Glu 166)	2.08	1.90	-0.18
Zn-O(1)	2.03	1.93	-0.10
<b>Angles</b>			
NE2(His 142)-Zn-O(1)	119.9	116.1	-3.8
NE2(His 142)-Zn-OE1(Glu 166)	127.6	117.9	-9.7
NE2(His 142)-Zn-NE2(His 146)	102.4	104.1	1.7
O(1)-Zn-OE1(Glu 166)	97.2	95.6	-1.6
O(1)-Zn-NE2(His 146)	112.4	116.4	4.0
OE1(Glu 166)-Zn-NE2(His 146)	94.7	107.0	12.3

### 3. Minimization of the Complex of Thermolysin and BAG

#### 3.1 Experimental



(5)

The coordinates of the inhibitor, BAG (5), were obtained from the X-ray structure of the complex with thermolysin [22]. The S(1) atom of the inhibitor was left in the anionic form since it is involved in coordination to the zinc metal ion. The 10 Å range about the inhibitor included 71 enzyme residues, the zinc atom, the water molecule and the inhibitor molecule.

The fit of the observed zinc coordination to ideal tetrahedral geometry was 0.811. The metal ion ligands involved in coordination to the metal ion were NE2 of His 146 of the enzyme (see Table 27) and S(1) of the inhibitor molecule. The enzyme residues that were allowed to undergo torsional rotations included  $\tau_1$  and  $\tau_2$  of Asn 112,  $\tau_1$  and  $\tau_2$  of Phe 114,  $\tau_1$  and  $\tau_2$  of Phe 139,  $\tau_1$  and  $\tau_2$  of His 142,  $\tau_1$ ,  $\tau_2$  and  $\tau_3$  of Glu 143,  $\tau_1$  and  $\tau_2$  of His 146,  $\tau_1$ ,  $\tau_2$  and  $\tau_3$  of Tyr 157,  $\tau_1$ ,  $\tau_2$  and  $\tau_3$  of Glu 166,  $\tau_1$  and  $\tau_2$  of Leu 202

and  $\tau_1$ ,  $\tau_2$ ,  $\tau_3$  and  $\tau_4$  of Arg 203. The refinement results are given in Table 25. The values of the torsion angles before and after minimization are in Table 26. The maximum root mean square shift for the atoms was 1.41 Å for O(21) of the inhibitor. The average rms shift was 0.04 Å. Other large shifts were observed for the terminal amine group of the inhibitor (1.30 Å), the water molecule (0.19 Å), and the side chains of Glu 166 (0.04 Å), Arg 203 (0.21 Å) and His 131 (0.28 Å). The coordination geometry of the metal ion is in Table 27. Hydrogen bond parameters between the inhibitor and residues of the active site are summarized in Table 28. Stereoscopic drawings of the X-ray and the minimized structures are shown in Figure 11.

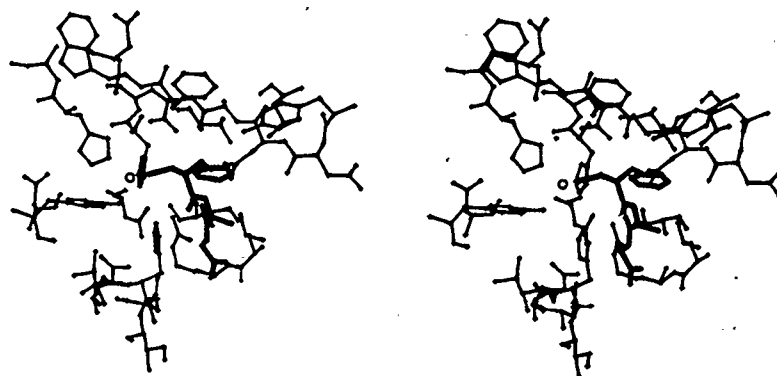
### 3.2 Results

The total improvement in the energy of 154.6 kcal/mole was considerably larger than that observed for the minimization of PPP. The contribution to the energy decrease from the metal atom potential was 10.6 kcal/mole. The fit to the ideal tetrahedral geometry was increased from 0.811 to 0.923; this was due to the improvement in all of the ligand-ligand angles. Most angles refined to values near the 109.5° ideal value with the exception of the angle S(1)-Zn-OE1(Glu 166) which moved further from ideal in the minimized structure. The distances between the three protein residue ligands and the zinc ion decreased towards their ideal values as was observed for PPP whereas the distance Zn-S(1) was increased by 0.398 Å; the ideal Zn-S distance is 2.10 Å. A superposition of the geometry of the metal ion coordination, before and after minimization, is in Figure 13.

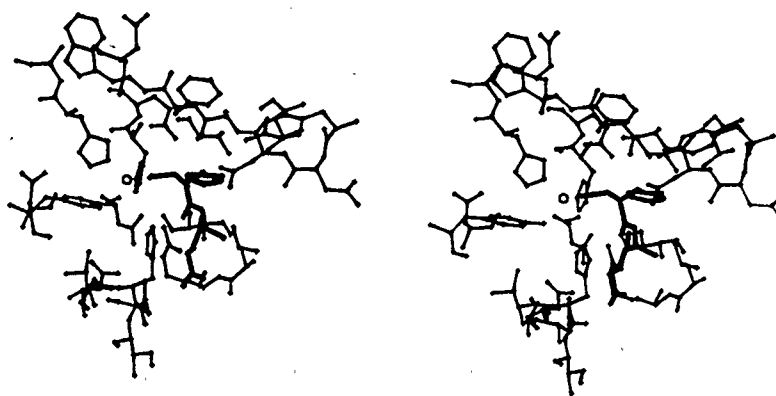
The decrease in energy was due to improvements in the van der Waals interactions (112.8 kcal/mole) and the hydrogen bond interactions (28.4 kcal/mole). The major structural changes that resulted from the minimization occurred in the torsion angles of the inhibitor (see Table 26). The major torsional shifts were  $+11.44^\circ$  for C(2)-C(3)-C(4)-C(5) and  $-15.76^\circ$  for N(13)-C(15)-N(17)-N(19). The former rotation repositioned the phenylalanine side chain of the inhibitor, so that the separation between C(4) and the carboxyl oxygen atom of the Glu 143 side chain increased from 2.94 Å to 3.15 Å and the separation between C(9) and the terminal guanidine hydrogen atom of Arg 203 increased from 2.89 Å to 3.48 Å. The second torsion angle rotation, coupled with the  $+6.30^\circ$  rotation of C(2)-C(3)-C(11)-N(13), repositioned O(12) to optimize the hydrogen bond interactions with both imide nitrogen atoms of the side chain of Arg 203, thus making this hydrogen bond more symmetrical, while maintaining the hydrogen bond between O(18) and the amine group of the side chain of Asn 112. The hydrogen bonding is also improved by the adjustment of the Arg 203 side chain; the two hydrogen atoms involved in hydrogen bonding to O(12) were shifted by 0.31 Å and 0.40 Å. The  $15.76^\circ$  rotation of the inhibitor torsion angle N(13)-C(15)-C(17)-N(19), therefore, optimizes the hydrogen bond interactions. A view of the residues involved in hydrogen bond interactions after minimization is shown in Figure 12.

The improvements in the structure that were achieved by the refinement include: the symmetrical hydrogen bond to Arg 203, the position of the phenyl ring in the S<sub>1</sub> subsite, and the regularization of the zinc coordination. In contrast to the PPP complex, there are more hydrogen bonds between BAG and thermolysin. These hydrogen bonds cause

the large torsional changes in the inhibitor and enzyme structures.



(a)



(b)

**Figure 11**

Stereoscopic drawings of (a) the X-ray and (b) the minimized complex of thermolysin and BAG

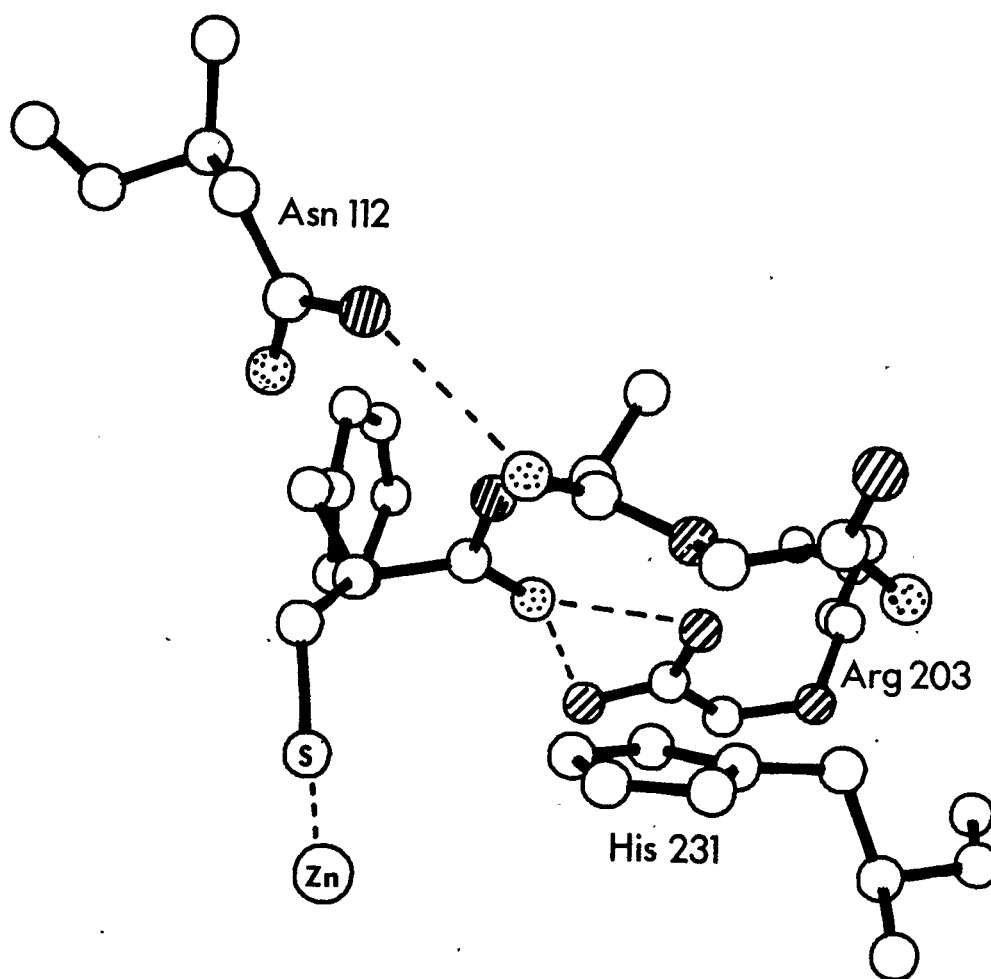
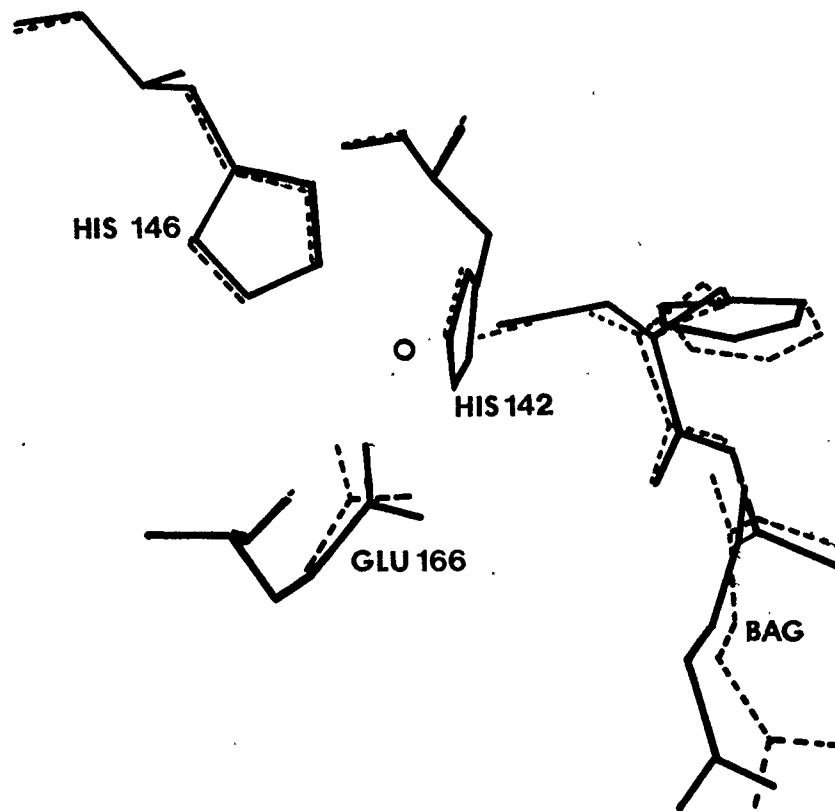


Figure 12

Hydrogen bonding residues for the complex of thermolysin  
and BAG after minimization.

● are the nitrogen atoms and ● are the oxygen atoms



**Figure 13**

Superposition of the metal coordination geometry before and after refinement of the complex of thermolysin and BAG.

The solid lines correspond to the minimized structure and the dashed lines correspond to the unminimized structure.

**Table 25**  
 Minimization Data for the Complex  
 of Thermolysin and BAG

Number of Atoms	:	682	
Number of Residues	:	74	
Number of Dihedral			
Degrees of Freedom	:	34	
Number of Translational			
Degrees of Freedom	:	9	
Number of Rotational			
Degrees of Freedom	:	6	
Convergence Criterion	:	0.1 kcal/mole	
		Starting	Final
Coordination Fit to Ideal	:	0.811	0.923
Energies (kcal/mole)			
van der Waals	:	-412.7	-525.5
hydrogen bond	:	-60.7	-92.0
metal	:	-4.2	-14.8
total	:	-477.7	-632.3
Total Improvement	:	145.6	

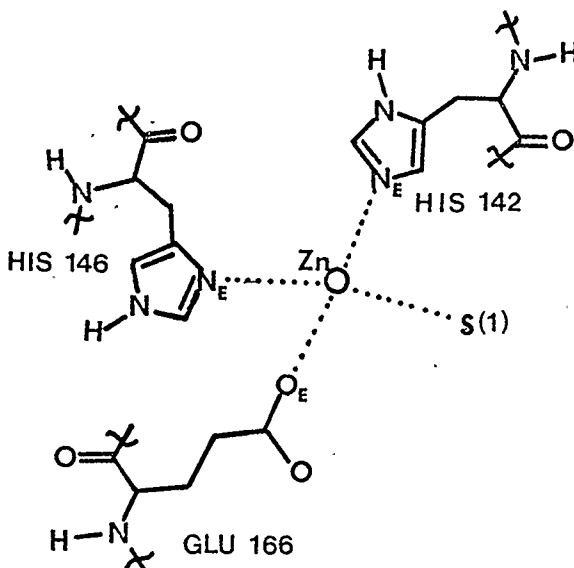
**Table 26**  
 Comparison of Torsion Angles Before and After Minimization  
 for the Complex of Thermolysin and BAG

	Before (°)	After (°)	$\Delta$ (°)
Asn 112			
$\tau_1$	-142.0	-147.3	-5.3
$\tau_2$	155.9	144.8	-11.1
Phe 114			
$\tau_1$	52.2	52.3	0.1
$\tau_2$	102.8	102.8	-0.0
His 142			
$\tau_1$	170.4	169.0	-1.4
$\tau_2$	117.7	116.3	-1.4
Glu 143			
$\tau_1$	-62.3	-62.7	-0.5
$\tau_2$	-44.2	-46.1	-1.9
$\tau_3$	-27.0	-27.3	-0.2
His 146			
$\tau_1$	-81.2	-79.1	2.1
$\tau_2$	-57.4	-56.4	1.0
Tyr 157			
$\tau_1$	-151.0	-149.8	1.2
$\tau_2$	-112.9	-109.5	3.4
$\tau_3$	-179.6	-179.8	-0.1
Glu 166			
$\tau_1$	-84.6	-90.6	-6.0
$\tau_2$	-53.2	-58.6	-5.5
$\tau_3$	122.0	120.2	-1.8
Leu 202			
$\tau_1$	-164.1	-162.7	1.4
$\tau_2$	61.0	65.3	4.2
Arg 203			
$\tau_1$	-65.6	-67.1	-1.5
$\tau_2$	-179.2	-176.1	3.1
$\tau_3$	-74.3	-76.5	-2.2

Table 26 continued:

$\tau_4$	-75.8	-78.0	-2.3
His 231			
$\tau_1$	-58.5	-63.7	-5.2
$\tau_2$	85.6	80.0	-5.6
Inhibitor			
S(1)-C(2)-C(3)-C(4)	159.6	160.2	0.7
C(2)-C(3)-C(4)-C(5)	-163.7	-152.2	11.4
C(3)-C(4)-C(5)-C(6)	-144.4	-144.5	0.0
C(2)-C(3)-C(11)-N(13)	-69.9	-63.6	6.3
C(3)-C(11)-N(13)-C(15)	164.3	164.3	0.0
C(11)-N(13)-C(15)-C(17)	-115.8	-119.4	-3.7
N(13)-C(15)-C(17)-N(19)	158.0	142.2	-15.8
C(15)-C(17)-N(19)-C(21)	177.2	177.2	0.0
C(17)-N(19)-C(21)-C(22)	-146.7	-143.7	3.0
N(19)-C(21)-C(22)-O(23)	-62.5	-60.1	2.4

**Table 27**  
Distances (Å) and Angles (°) for the Zinc Atom Coordination Sphere for the Complex of Thermolysin and BAG



	Before	After	$\Delta$
<b>Distances</b>			
Zn-NE2(His 142)	2.11	1.99	-0.12
Zn-NE2(His 146)	2.08	1.96	-0.12
Zn-OE1(Glu 166)	2.08	1.91	-0.17
Zn-S(1)	1.97	2.37	0.40
<b>Angles</b>			
NE2(His 142)-Zn-S(1)	119.7	117.0	-2.7
NE2(His 142)-Zn-OE1(Glu 166)	127.6	117.4	-10.2
NE2(His 142)-Zn-NE2(His 146)	102.4	107.2	4.8
S(1)-Zn-OE1(Glu 166)	98.8	96.0	-2.8
S(1)-Zn-NE2(His 146)	110.5	111.0	0.5
OE1(Glu 166)-Zn-NE2(His 146)	94.7	107.8	13.1

**Table 28**  
 Hydrogen Bond Interactions Before and After  
 Minimization for the Complex of Thermolysin and BAG

	Before				After			
	H-X (Å)	H...Y (Å)	X...Y (Å)	Angle (°)	H-X (Å)	H...Y (Å)	X...Y (Å)	Angle (°)
N(Asn 112)-H...O(18)	0.99	1.92	2.90	167.6	0.99	1.91	2.86	146.8
O(Water)-H...N(Trp 115)	0.98	2.14	3.19	170.3	0.98	1.94	2.99	169.7
N1(Arg 203)-H...O(12)	1.02	1.92	2.79	143.5	1.02	1.92	2.78	143.3
N2(Arg 203)-H...O(12)	0.99	2.18	2.96	135.0	0.99	1.97	2.82	141.5

#### 4. Minimization of the Complex of Thermolysin and WY44221

##### 4.1 Kinetic Study of the Inhibition of Thermolysin by WY44221

Since one of the criteria in Chapter I for choosing an enzyme model of ACE was that it had to be inhibited by ACE inhibitors, the inhibition constant for WY44221 in thermolysin was determined. The rate of hydrolysis of a synthetic substrate, 3(2-furylacroyloyl)glycyl-L-leucine amide (FAGLA) was measured. The preparation of the assay solutions and the experimental procedure are outlined by Corbett [61]. Varying concentrations of the inhibitor were added to the enzyme solution followed by the addition of a constant amount of substrate; the decrease in absorbance was measured at 345 nm. This absorbance change corresponds to the hydrolysis of the peptide bond of FAGLA ( $\Delta\epsilon_{345} = -348 \text{ M}^{-1} \text{ cm}^{-1}$ ). The values for  $k_{\text{cat}}/K_m$  were calculated from the change in absorbance (A) according to the equation:

$$\ln \left[ \frac{A_0 - A_\infty}{A_t - A_0} \right] = \frac{k_{\text{cat}}}{K_m} [E]t \quad (24)$$

where  $A_0$  is the absorbance at time zero,  $A_\infty$  is the absorbance of the hydrolysed substrate,  $A_t$  is the absorbance of the substrate plus product at time  $t$  and  $[E]$  is the enzyme concentration. The value for  $k_{\text{cat}}/K_m$  can be obtained from the slope of the plot of the above equation. A plot of  $k_{\text{cat}}/K_m$  versus the negative logarithm of the inhibitor concentration is shown in Figure 14; from this plot the value of  $K_i$  is found to be  $2.92 \times 10^{-4} \text{ M}$ . A preliminary assay was run in which the enzyme and WY44221 were incubated for one hour before adding the substrate. In this case, the  $k_{\text{cat}}/K_m$  value was found to be lower, indicating that the inhibition is dependent on the rate at which the

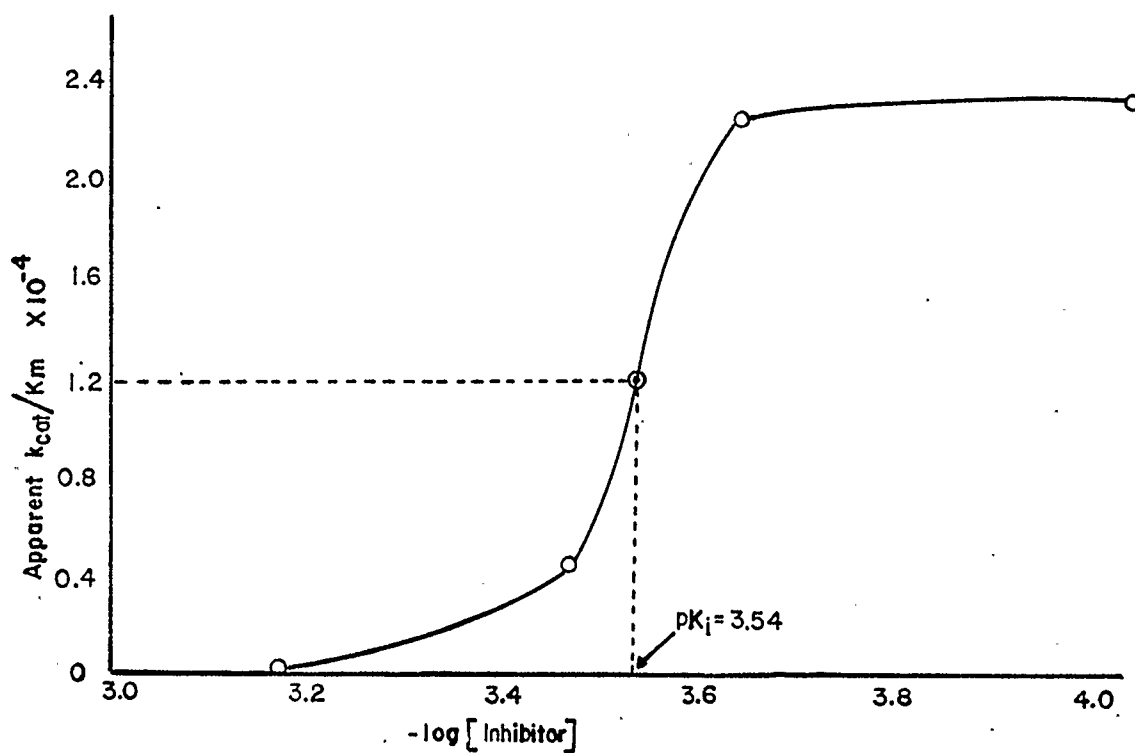


Figure 14

Plot of  $k_{cat}/K_m$  versus the negative logarithm of the inhibitor concentration.

The substrate concentration was constant at  $1.25 \times 10^{-3}$  M.

inhibitor binds to the enzyme. The inhibition constant found is, therefore, only an apparent  $K_i$ ; the true value is expected to be somewhat less than this. It was observed, however, that thermolysin is inhibited by WY44221 making this enzyme a good model for studies of ACE inhibitors.

## 4.2 Experimental

The coordinates of WY44221 used for the molecular mechanics calculation were obtained by computer graphically 'docking' the crystal structure into the active site of the refined structure of thermolysin, at 1.6 Å resolution. The thermolysin structure was modified to include all of the hydrogen atoms that were capable of hydrogen bonding. The structure of the inhibitor was adjusted to obtain the best fit in the active site of the enzyme. The modelled structure has a *cis* peptide bond C(2)-N(1)-C(10)-C(12) = 2.0°. The 10 Å range about the inhibitor included 63 residues of the enzyme, the zinc atom and the inhibitor molecule. The water molecule that was hydrogen bonded to the main chain nitrogen atom of Trp 115 was, initially, not included.

The refinement program used to minimize this molecule was an older version from that used on the previous complexes. The partial charges for the substrate atoms and the metal atom were not implicitly included in the program; those for the substrate were obtained by a CNDO calculation [62]. A coulombic energy contribution to the final energy was included in the calculation. There was also no metal atom potential included in the program, therefore, there were no specific atoms defined as coordinating to the zinc atom in a tetrahedral geometry.

The enzyme residues that were allowed to undergo torsional

rotations included  $\tau_1$  and  $\tau_2$  of Asn 112,  $\tau_1$  and  $\tau_2$  of Leu 133,  $\tau_1$  and  $\tau_2$  of Asp 138,  $\tau_1$  of Val 139,  $\tau_1$ ,  $\tau_2$  and  $\tau_3$  of Glu 143,  $\tau_1$  and  $\tau_2$  of Ile 188,  $\tau_1$  and  $\tau_2$  of Leu 202,  $\tau_3$  and  $\tau_4$  of Arg 203. The inhibitor molecule was initially frozen in the active site. As the refinement progressed, the constraints of the inhibitor molecule were relaxed and the molecule was allowed to move freely. The refinement parameters were initially set for poor geometries and, in the final stages of refinement, were changed for better geometries.

The converged complex was then further minimized using the new version of YETI which had also been used on the previous calculations. This version does not include electrostatic terms since reliable values of the atomic partial charges and a microscopic dielectric constant are so difficult to assign. The water molecule hydrogen bonded to the Trp 115 residue was included in subsequent calculations. The enzyme residues that were allowed to undergo torsional rotations included those mentioned above and  $\tau_1$  and  $\tau_2$  of Phe 130,  $\tau_1$  and  $\tau_2$  of Arg 203, and  $\tau_1$  and  $\tau_2$  of His 231. The calculation was carried out in the same manner as the PPP and BAG refinements.

The refinement statistics are given in Table 29. The values of the torsion angles before and after minimization are in Table 30. The maximum root mean square shift for the atoms was 2.40 Å for C(6) of the inhibitor. Atoms C(4), C(5), C(6) and C(7) had shifts greater than 2 Å. Of the enzyme residues, Leu 202 had the largest shift, one of the terminal methyl groups shifting by 2.17 Å. The average RMS shift was 0.08 Å. Stereoscopic drawings of the X-ray and minimized structures are in Figure 15.

### 4.3 Results

The major structural changes resulting from the minimization calculation were in the inhibitor and the side chains of Leu 202 and Glu 143. Before minimization, the CH group of the Leu 202 side chain was directed towards the inhibitor, giving a number of unfavorable contacts with the aromatic ring and the carboxyl group. The minimization increases all these distances to over 3.7 Å by rotating the Leu side chain such that the CH group points away from the inhibitor and forms a pocket for the indoline group. Glu 143 also shifted considerably. Before the refinement, the methyl group of the inhibitor was only 2.59 Å from one of the carboxyl oxygen atoms of the Glu 143 side chain. The rotation of the side chain as well as the  $-24.7^\circ$  rotation of S(15)-C(14)-C(12)-C(10) moved these two groups away from each other; C(13)-O(Glu 143) = 3.11 Å.

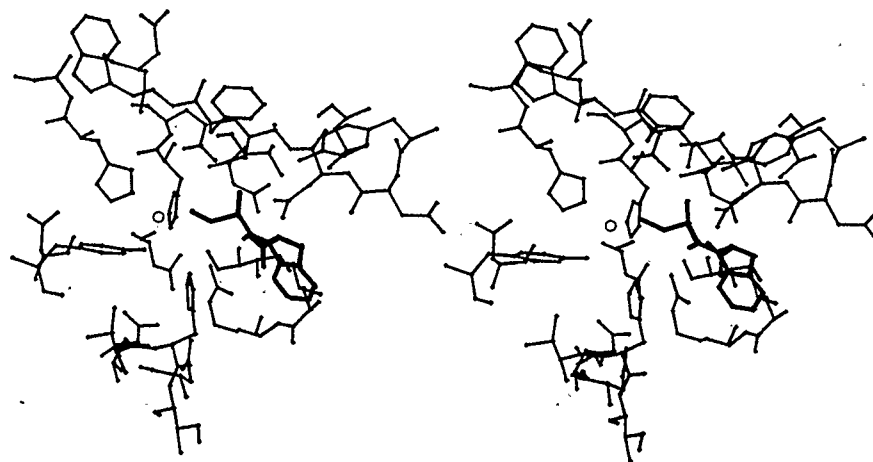
Other unfavorable interactions with the methyl group of the inhibitor were made with the main chain oxygen atom of Ala 113 and the side chain carbonyl oxygen atom of Asn 112: C(13)-O(Ala 113) = 2.87 Å and C(13)-O(Asn 112) = 2.89 Å. The rotations of  $\tau_1$  and  $\tau_2$  of Asn 112 of  $-5.8^\circ$  and  $-13.7^\circ$  as well as the rotation of the side chain of the inhibitor increased these distances to 3.06 Å and 3.26 Å respectively. In the refined structure, the methyl group is positioned so that it points toward the top of the active site cleft, in approximately the same position as the CH of the benzyl side chain of BAG. The S<sub>1</sub> hydrophobic pocket of thermolysin is empty since the substituent on C(12) is only a methyl group; a larger hydrophobic substituent, such as the benzyl group of BAG, would be needed to fill the hydrophobic pocket.

The 15.1° rotation of the terminal carboxyl group of the inhibitor positions the oxygen atoms so that they both form a three-center hydrogen bond with a single hydrogen atom of the guanidine moiety of Arg 203. The positions of the guanidine group, and the inhibitor before and after minimization are shown in Figure 17. Before the minimization only O(18) hydrogen bonds to a guanidine nitrogen atom of Arg 203. The torsional shifts of the inhibitor reposition the carboxyl group to facilitate the three center hydrogen bond of O(17) and O(18) and a hydrogen atom from Arg 203.

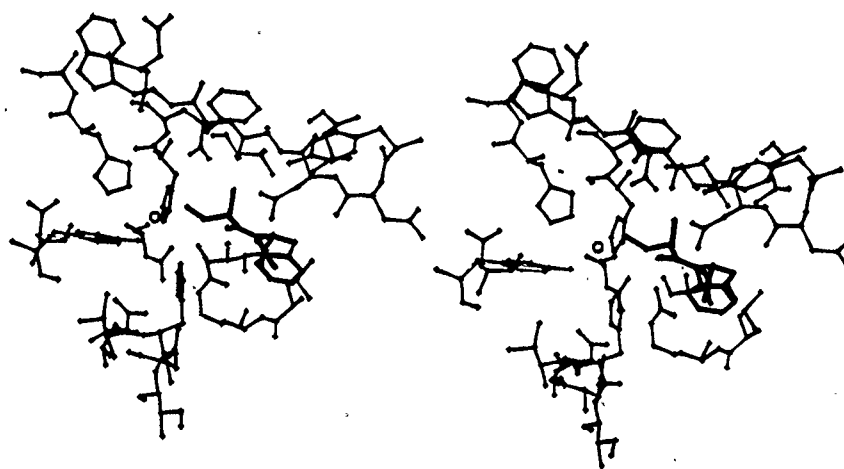
The coordination about the metal ion in the minimized structure was further from the tetrahedral geometry than the modelled structure (see Table 31). This was due to the movement of the zinc atom and the inhibitor molecule while leaving the other three residues which coordinate to the metal ion frozen in their initial positions. Comparison of the zinc atom coordination before and after minimization is in Table 31. In order to obtain the best distances for Zn-NE2(His 142) and Zn-OE1(Glu 166), the distances: Zn-NE2(His 146) and Zn-S(1) are considerably longer than their ideal values. The angles subtended by the zinc atom are all quite far from their ideal values of 109°. The best fits are obtained with angles involving S(1) of the inhibitor since this atom was free to move in the refinement. Subsequent calculations should, therefore, include torsional freedom of all of the ligands involved in coordination to the zinc atom.

The major stabilizing interactions between the inhibitor and the enzyme are, therefore, the hydrogen bonds between the carboxyl oxygen atoms and a guanidine nitrogen atom of Arg 203, the shift of the Leu 202 side chain to accommodate the indoline group of the inhibitor and the

coordination of the inhibitor sulphur atom to the zinc atom of the enzyme.



(a)



(b)

**Figure 15**

Stereoscopic drawings of (a) the modelled and (b) the minimized complexes of thermolysin and WY44221.

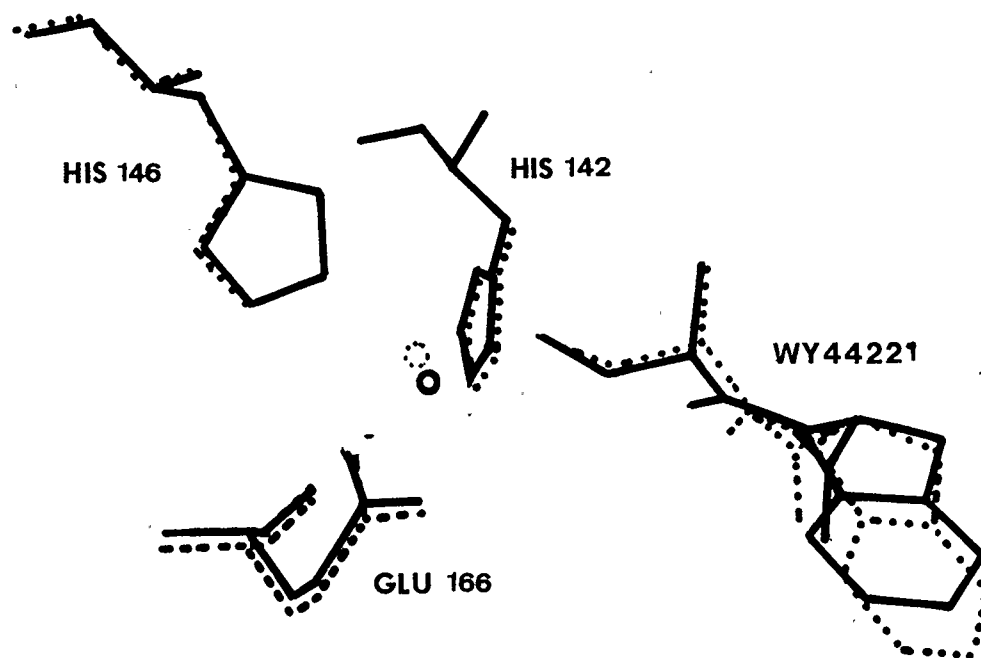


Figure 16

Superposition of the metal coordination geometry before and after minimization of the complex of thermolysin and WY44221.

The solid lines correspond to the minimized structure and the dashed lines correspond to the unminimized structure.

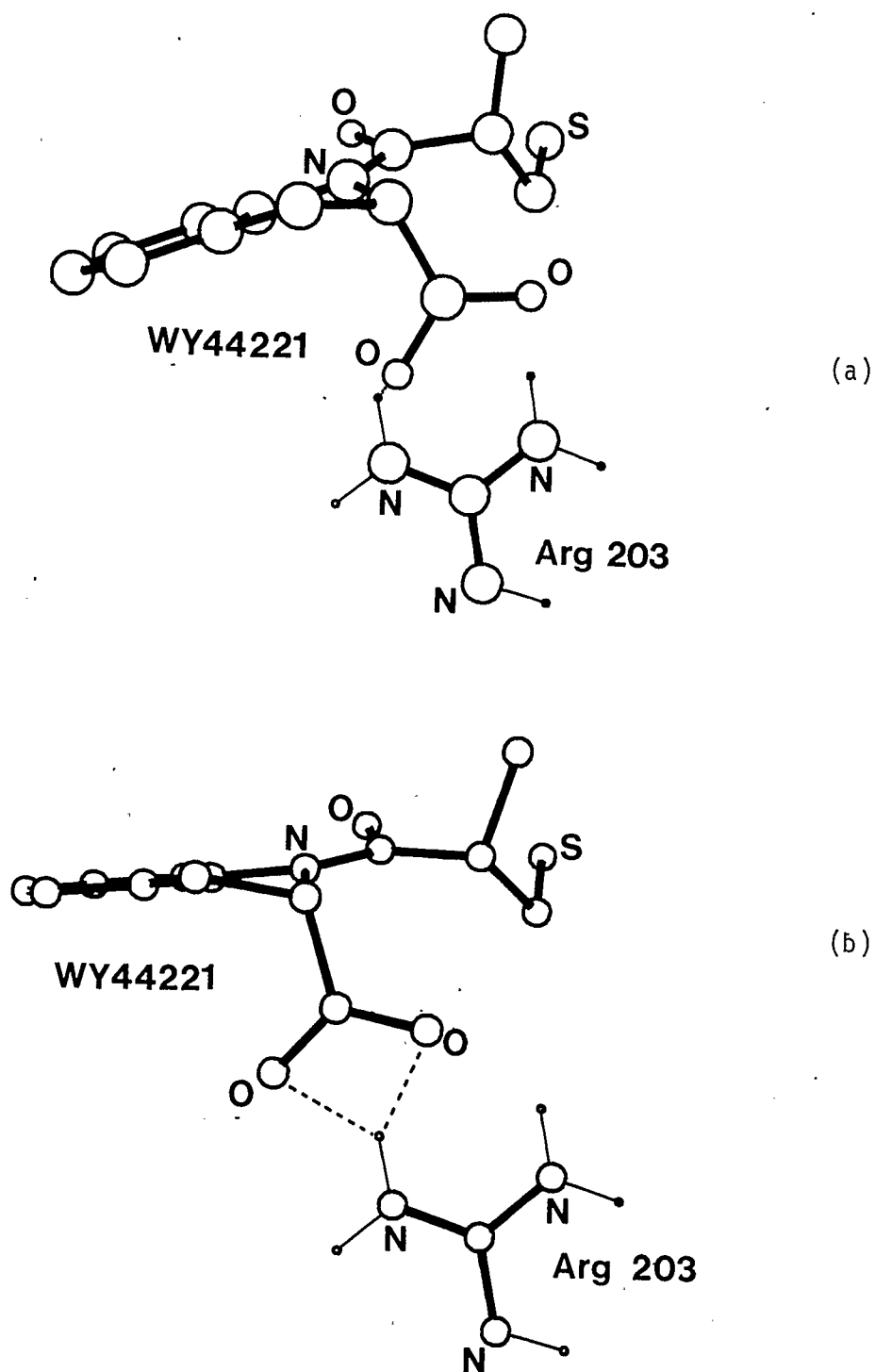


Figure 17

Hydrogen bonding interactions between Arg 203 and WY44221  
for (a) the modelled and (b) the minimized complexes of  
thermolysin and WY44221.

**Table 29**  
 Minimization Data for the Complex  
 of Thermolysin and WY44221

Number of Atoms	:	593	
Number of Residues	:	63	
Number of Dihedral			
Degrees of Freedom	:	27	
Number of Translational			
Degrees of Freedom	:	9	
Number of Rotational			
Degrees of Freedom	:	6	
Convergence Criterion	:	0.1 kcal/mole	
		Starting	Final
Coordination Fit to Ideal	:	0.748	0.555
Energies (kcal/mole)			
van der Waals	:	2653.1	-435.9
hydrogen bond	:	-22.5	-57.7
coulomb	:	-8.7	-6.7
total	:	2621.9	-500.2
Total Improvement	:	3122.1	

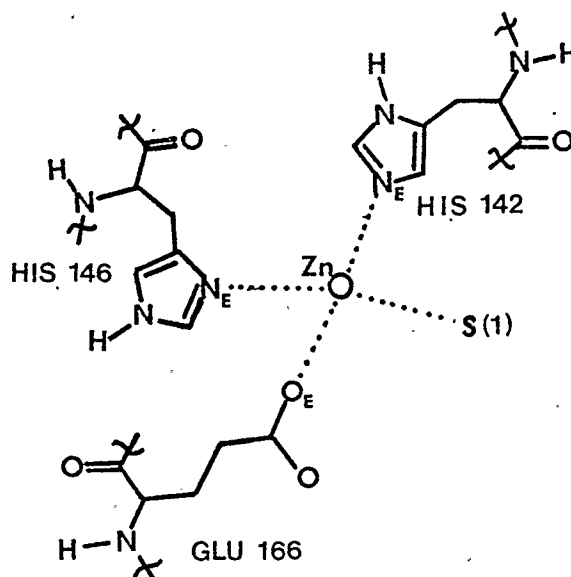
**Table 30**  
 Comparison of Torsion Angles Before and After Minimization  
 for the Complex of Thermolysin and WY44221

	Before (°)	After (°)	$\Delta$ (°)
Asn 112			
$\tau_1$	-142.0	-147.8	-5.8
$\tau_2$	155.9	142.2	-13.7
Phe 130			
$\tau_1$	-79.6	-47.7	31.9
$\tau_2$	105.9	86.8	-19.1
Leu 133			
$\tau_1$	-71.6	-80.5	-8.9
$\tau_2$	92.6	102.3	9.6
Asp 138			
$\tau_1$	58.0	65.6	7.6
$\tau_2$	178.6	167.0	-11.6
Val 139			
$\tau_1$	170.2	177.6	7.4
Glu 143			
$\tau_1$	-62.3	-49.0	13.3
$\tau_2$	-44.2	-34.1	10.1
$\tau_3$	-27.0	-54.8	-27.8
Ile 188			
$\tau_1$	178.7	178.7	0.0
$\tau_2$	-61.0	-60.8	0.6
Leu 202			
$\tau_1$	-164.1	-125.6	38.5
$\tau_2$	61.0	-6.2	-67.2
Arg 203			
$\tau_1$	-65.6	-66.8	-1.2
$\tau_2$	-179.2	-178.2	1.0
$\tau_3$	-74.3	-71.0	3.3
$\tau_4$	-75.8	-62.0	13.8
His 231			
$\tau_1$	-58.5	-64.3	-5.8

Table 30 continued:

$\tau_2$	85.6	88.7	3.1
WY44221			
S(15)-C(14)-C(12)-C(10)	94.4	69.7	-24.7
C(14)-C(12)-C(10)-N(1)	118.1	138.5	20.4
C(12)-C(10)-N(1)-C(2)	2.0	5.6	3.6
N(1)-C(2)-C(10)-O(17)	95.3	110.3	15.1

**Table 31**  
 Distances (Å) and Angles (°) for the Zinc Atom Coordination  
 Sphere for the Complex of Thermolysin and WY44221



	Before	After	$\Delta$
Distances			
Zn-NE2(His 142)	2.11	2.00	-0.11
Zn-NE2(His 146)	2.08	2.50	0.42
Zn-OE1(Glu 166)	2.08	1.96	-0.12
Zn-S(1)	2.13	2.33	0.20
Angles			
NE2(His 142)-Zn-S(1)	119.9	97.5	-22.4
NE2(His 142)-Zn-OE1(Glu 166)	127.6	142.7	15.1
NE2(His 142)-Zn-NE2(His 146)	102.4	92.1	-10.3
S(1)-Zn-OE1(Glu 166)	97.2	119.0	21.8
S(1)-Zn-NE2(His 146)	112.4	105.6	-6.8
OE1(Glu 166)-Zn-NE2(His 146)	94.7	85.6	-9.1

## V. Discussion

### 1. Comparison of the X-Ray Structures

The X-ray structures of the inhibitors, WY44088 and WY44221, are quite similar. Both structures have a *cis* conformation for the peptide bond;  $C(2)-N(1)-C(10)-C(12) = -13.4(9)^\circ$  for WY44221 and  $-1(1)^\circ$  for WY44088 (see Figures 3 and 4 for the atomic labelling schemes). The X-ray structure of captopril, however, shows a *trans* peptide bond;  $173.3(7)^\circ$  [54]. All three structures exhibit intermolecular hydrogen bonding between the carbonyl oxygen atom and the carboxylate oxygen atoms. Captopril and WY44088 show hydrogen bonding to only one oxygen atom of the carboxylate group; the separation between the oxygen atoms is 2.592(6) Å and 2.581(8) Å, respectively. This finding is substantiated by unequal C-O bond lengths in the carboxylate group: 1.19(1) Å and 1.33(1) Å for WY44088 and 1.20 Å and 1.30 Å for captopril. The structure of WY44221, however, exhibits hydrogen bonding to both carboxylate oxygen atoms,  $O(11)-O(17) = 2.742(8)$  Å and  $O(11)-O(18) = 2.98(1)$  Å. These nearly equal distances, coupled with the nearly equal C-O distances given above in the carboxylate group, are evidence for a three center hydrogen bond with the hydrogen atom shared by the three oxygen atoms.

The orientation of the carboxyl groups is the same in the two structures: WY44088 and WY44221. In WY44088, the torsion angles  $N(1)-C(2)-C(18)-O(19)$  and  $N(1)-C(2)-C(18)-O(20)$  are  $-23(1)^\circ$  and  $154.4(7)^\circ$  respectively, and for WY44221, the torsion angles:  $N(1)-C(2)-C(16)-O(17)$  and  $N(1)-C(2)-C(16)-O(18)$  are  $35.3(8)^\circ$  and  $-154.7(6)^\circ$ , respectively. This conformation is also observed in the X-ray structure of captopril. This orientation of the oxygen atoms facilitates the

three center hydrogen bond, observed in WY44221, to O(11) of a neighboring molecule without imposing unfavorable steric interactions between the molecules.

The side chains of the inhibitors are slightly different, especially in the relative position of the sulphur atoms. This difference is shown in the side chain torsion angle C(10)-C(12)-C(14)-S(15) which is  $-57.8(9)^\circ$  for WY44088 and  $175.3(5)^\circ$  for WY44221. Thus, the mercaptopropanoyl chain adopts an anti conformation whereas the benzoylthio side chain adopts a gauche conformation. In captopril, the side chain is also extended, however, due to the *trans* peptide bond, the chain is oriented in the opposite direction from that of WY44088 or of WY44221. Molecular superpositions of WY44088 and WY44221 with captopril are in Figures 18 and 19, respectively. These figures show the difference in the side chain orientation that arise from the peptide bond conformations. This conformational difference could alter the binding of these inhibitors to the active site of ACE. The sulphur atoms, that would coordinate to the zinc atom, are positioned quite differently in the superpositions; thus only one or the other of the conformations could bind to ACE.

The X-ray structure of the substrate analogue, hip-L-his-L-leu, is also in an extended conformation with all peptide bonds *trans*. A comparison of the relevant torsion angles that are equivalent to captopril shows a number of interesting similarities. A molecular superposition of captopril and hip-L-his-L-leu is in Figure 20. The equivalent peptide bond in both captopril and hip-L-his-L-leu adopts a *trans* conformation and the carboxylate groups are, in each case, on the same side of the molecule as the carbonyl oxygen atom. The leucine side



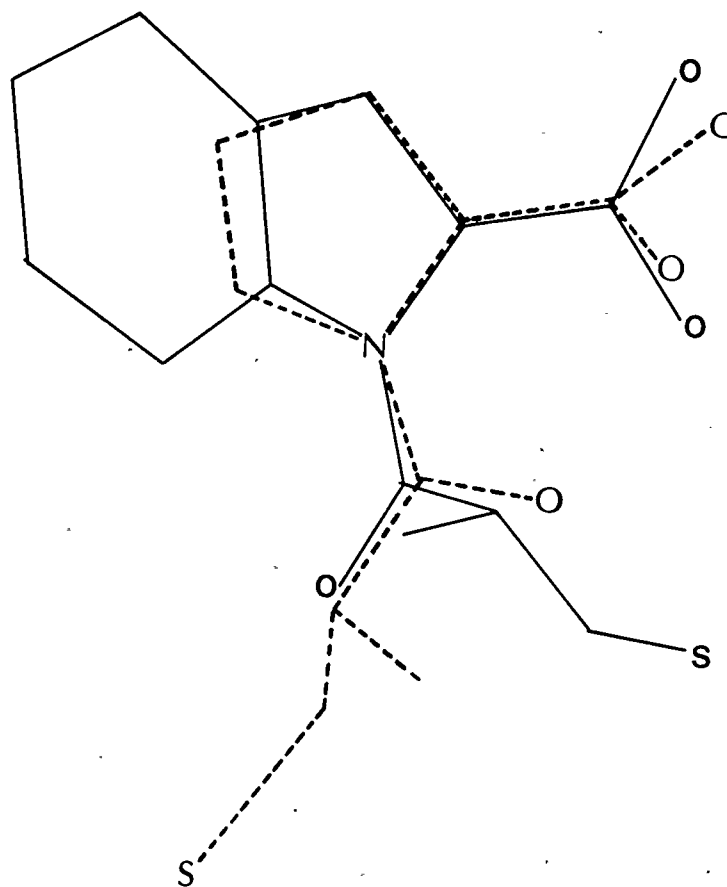


Figure 19

Molecular superposition of captopril and WY44221

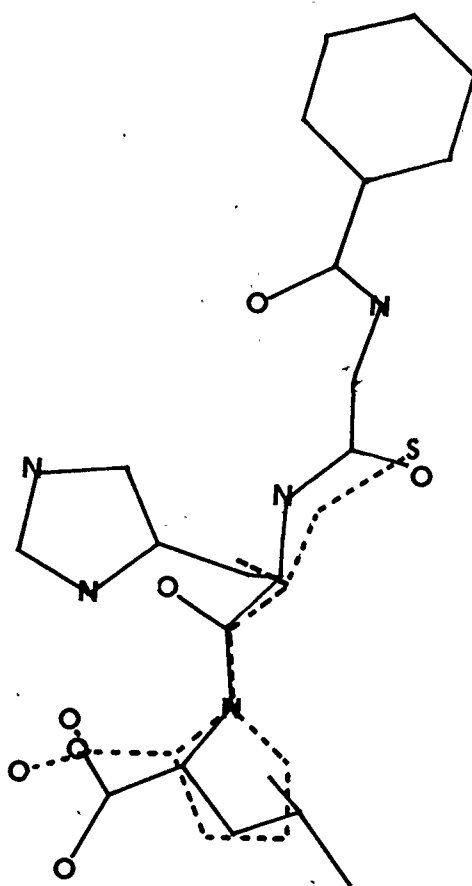


Figure 20

Molecular superposition of Hip-L-his-L-leu

chain of hip-L-his-L-leu lies in the same position as the carbon atoms of the proline ring. The alkyl side chain of captopril closely overlaps the main chain of hip-L-his-L-leu thereby placing the methyl group of captopril over the methylene group of the histidine side chain. The conformation of the substrate analogue may be due to the solvent sheath surrounding the molecule; these interactions may model the multiple interactions in the active site of the enzyme that would be required of a high affinity ligand.

Although there are striking conformational similarities between the X-ray structures of captopril and hip-L-his-L-leu, only minor similarities between captopril and the two inhibitors, WY44088 and WY44221 are observed. So, from the structural data of the inhibitors alone, no conclusions can be made regarding the active binding conformation of ACE inhibitors and substrates. The X-ray structures of the compounds reported here, as well as that of captopril, show major conformational differences due to various intermolecular and intramolecular interaction of the molecules. A larger base of structural data on ACE inhibitors may lead to more definitive conclusions regarding the active site binding conformation. In addition, other methods for determining the binding conformation should be explored as will be discussed in the next section.

## **2. Molecular Mechanics Calculations of Thermolysin Inhibitors**

The results of the molecular mechanics studies of the two thermolysin inhibitor complexes show that the energy minimized structures correspond closely to X-ray structures; however, minor changes can be effected that will enhance the binding interactions

between the inhibitor and the enzyme residues of the active site. Although both crystal structures show a distorted tetrahedral geometry, minimization can alter that coordination to one that is closer to an ideal tetrahedral geometry. The most potent inhibitor was found to have the lowest energy after minimization, although the starting energy (54 kcal/mole) was higher than that of the less potent inhibitor. Molecular mechanics, therefore, enhanced the binding interactions of BAG and thermolysin. The largest stabilizing factor for BAG over PPP is in the van der Waals energy component; the difference between the two van der Waals energy term components is 48 kcal/mole. The larger van der Waals contribution to the energy for PPP can be attributed to the two repulsions between the inhibitor atoms, C(4)-C(6); 2.50 Å and C(4)-C(10); 2.51 Å, the energies of which are 25.18 kcal/mol and 24.41 kcal/mole, respectively. These distances were not changed in the minimization since they are 1,3 interactions involving the phenyl ring. Since the molecular mechanics program fixes the bond lengths and angles at their crystallographically observed values these high energy interactions could not be minimized in the calculation.

The difference in the energy due to hydrogen bonds between PPP and BAG is 9 kcal/mole, BAG being of lower energy than PPP. This is due to the larger number of hydrogen bonds found in the BAG-enzyme complex. A symmetrical hydrogen bond is formed between the guanidine nitrogen atoms of Arg 203 and O(12) of BAG and a hydrogen bond is formed between the amine group of the side chain of Asn 112 and O(18). These hydrogen bonds may be the reason for the lower inhibition constant observed for BAG.

The difference in energy arising from the metal atom coordination

is only 6.2 kcal/mole, PPP being of lower energy. This difference in energy is due to the change in the Zn-S distance from 1.97 Å to 2.37 Å for BAG. This distance is large compared to the ideal Zn-S distance of 2.1 Å; the longer bond arising because the van der Waals and hydrogen bond interactions are optimized with the cost of a longer Zn-S distance. A comparison of the angles subtended by the zinc atom for the two complexes (Tables 24 and 27) shows little difference; the final fits to tetrahedral geometry are approximately the same for BAG and PPP; the difference is only 0.02.

Another reason for the lower energy in BAG may be the size of the inhibitor. This inhibitor extends further back along the active site cleft (see Figure 11b) so that it is more accessible to the Asn 112 and Arg 203 residues than PPP and attractive interactions with the side chain of Asp 226 are enhanced. The crystal structure of BAG showed no contacts to the terminal amine group within 4 Å, however, after minimization, the terminus of the inhibitor is brought closer to the side chain of Asp 226. This interaction, the stronger hydrogen bonds in BAG compared to PPP, and the enhanced van der Waals attractive interactions explain the inhibition constants of the two molecules.

The results of these calculations identify the residues of the active site that are most important for ligand binding as: Arg 203 and the S<sub>1</sub> subsite. Interactions with Asn 112 further enhance the binding, increasing the inhibition. This interaction, however, appears to be less important than that with Arg 203, as was shown in the refinement of PPP. Ring stacking interactions between phenyl rings on the ligands and Phe 114 also appear to enhance binding. The zinc atom plays a large role in ligand binding; the coordination geometry is optimally

tetrahedral for the cases studied.

### 3. Minimization of the Complex of Thermolysin and WY44221

Based on the molecular mechanics results, the most important enzyme residue in the active site of thermolysin is Arg 203 which hydrogen bonds to the terminal carboxyl oxygen atoms of the proline moiety of WY44221 thereby stabilizing the *cis* conformation. There is no hydrogen bond between O(11) of the inhibitor and the terminal amine group of the side chain of Asn 112. A 180° rotation of this side chain could, however, bring this amine group within hydrogen bonding distance of O(11). Then Asn 112 could contribute to the interaction with this inhibitor through hydrogen bonding, however, as observed for the PPP inhibitor, this residue is not essential for inhibition.

The zinc atom is also important; its coordination sphere is filled by an electron donating atom on the inhibitor molecule. The minimized structure tends toward a distorted tetrahedral geometry as can be seen from the decrease in the fit to an ideal tetrahedron of 0.748 to 0.555. In addition, a comparison of the results of the thermolysin inhibitors and this refinement indicates that a better fit would be achieved if the methyl group were replaced with a larger hydrophobic group that could bind in the S<sub>1</sub>' subsite and form stabilizing van der Waals interactions. The minimization results of the modelled complex of thermolysin and WY44221 samples only one conformation. Other starting conformations that were generated by computer modelling could not be refined. It is still possible that other stable conformations exist; their identification will depend on the starting structures produced by modelling the complex. The successful minimization had an inhibitor

structure with a *cis* peptide bond; attempts to model and minimize a *trans* peptide bond conformer were unsuccessful. Also, the *trans* conformer of captopril and of the substrate analogue, hip-L-his-L-leu, could not be refined. These results may indicate that the starting structure for minimization was too far from the true local minimum conformation or that the *trans* conformer is not the active binding conformation.

Since the *cis* conformer of WY44221 refined to a low energy, it is apparent that the likely binding conformation for the indoline compound is one with a *cis* peptide bond. This result suggests either that other inhibitors may bind with a *cis* peptide bond or that this binding conformation is unique for the indoline compounds. Andrews, et al. [16] have shown that the energy barrier to rotation about this bond is less than 10 kcal/mole. The cost of this torsional rotation could be recovered by the stabilization energy that arises from the formation of favorable van der Waals, hydrogen bond, and metal atom interactions.

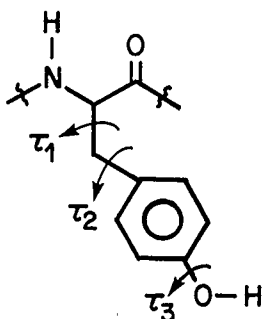
The similarities between ACE and thermolysin and the fact that WY44221 inhibits thermolysin (see Chapter IV) supports the use of thermolysin as a model for ACE. Using this model, conclusions can be drawn regarding the features essential to the active site of ACE. The active site, therefore, must contain a basic residue, such as arginine, which interacts with the carboxyl group of the proline moiety of the inhibitors or with the terminal carboxyl group of the substrate angiotensin I. A group such as asparagine may further enhance binding of the ligand by hydrogen bonding to the terminal peptide bond which is not hydrolyzed by the enzyme. The oxygen atom of the scissile peptide bond coordinates to the zinc atom. This study has only dealt with

tetrahedral complexes, however, the tolerance for less than ideal geometry for the metal coordination may indicate that a different type of coordination (possibly pentacoordination) may bind the inhibitor more strongly. The ACE inhibitor studied has only a methyl group. If the active site of ACE has a hydrophobic subsite analogous to the S<sub>1</sub> site of thermolysin, substitution of the methyl group for a larger, more hydrophobic group would enhance the binding of ACE inhibitors. Further work in the design of new ACE inhibitors could be directed towards changing the substitution on the carbon atom, as well as building pentacoordinate inhibitors such as the thermolysin inhibitors CLT [21] and phosphoramidates [24]. As predicted by Kim and coworkers, a second hydrophobic region is present in thermolysin which binds the indoline ring. This hydrophobic region may, then, also be present in ACE and the design of novel ACE inhibitors containing a hydrophobic group which would fit into this region might enhance inhibitor binding and increase the drug's potency as an antihypertensive agent.

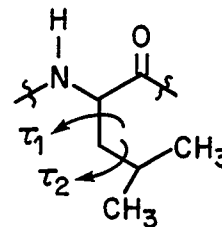
In conclusion, the combination of the methods of X-ray crystallography and molecular mechanics are powerful tools in the elucidation of the structural aspects of ligand binding.

**Appendix I**  
Torsion Angles for Amino Acid Residues

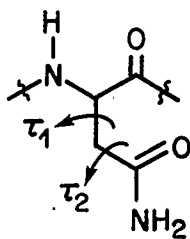
Tyrosine



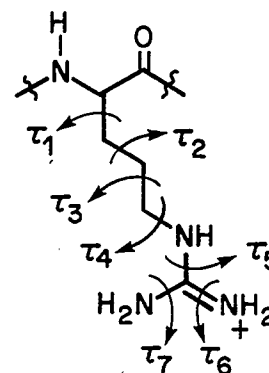
Leucine



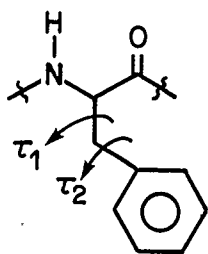
Asparagine



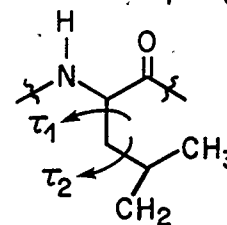
Arginine



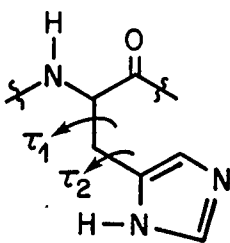
Phenylalanine



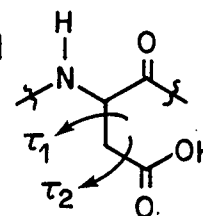
Isoleucine



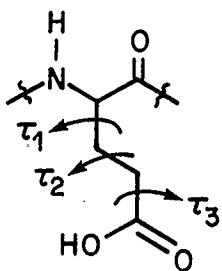
Histidine



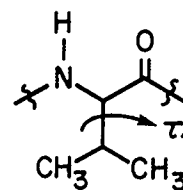
Aspartic acid



Glutamic acid



Valine



## REFERENCES

1. Ashworth, R.W., *Prog. Drug. Res.*, 26, (1982), 207.
2. Ganong, W.F., *Ann. Rev. Physiol.*, 46, (1984), 17.
3. Bunning, P., Riordan, J.F., *Isr. J. Chem.*, 21, (1981), 43.
4. Holmes, M.A., Matthews, B.W., *Biochemistry*, 20, (1981), 6912.
5. Kester, W.R., Matthews, B.W., *Biochemistry*, 16, (1977), 2500.
6. Hangauer, D.G., Monzingo, A.F., Matthews, B.W., *Biochemistry*, 23, (1984), 5730.
7. Bunning, P., Holmquist, B., Riordan, J.F., *Biochem. Biophys. Res. Commun.*, 83, (1978), 1442.
8. Ondetti, M.A., Rubin, B., Cushman, D.W., *Science*, 196, (1977), 441.
9. Cushman, D.W., Cheung, H.S., Sabo, E.F., Ondetti, M.A., *Biochemistry*, 16, (1977), 5484.
10. Byers, L.D., Wolfenden, R., *Biochemistry*, 12, (1973), 2070.
11. Condon, M.E., Petrillo, E.W., Jr., Ryono, D.E., Reid, J.A., Neubeck, R., Paur, M., Heikes, J.E., Sabo, E.F., Losee, K.A., Cushman, D.W., Ondetti, M.A., *J. Med. Chem.*, 25, (1982), 250.
12. Galardy, R.E., Kontoyiannidou-Ostrem, V., Kortylewicz, Z.P., *Biochemistry*, 22, (1983), 1990.
13. Patchett, A.A., Harris, E., Tristram, E.W., Wyvratt, M.J., Wu, M.T., Taub, D., Peterson, E.R., Ikeler, T.J., ten Broeke, J., Payne, L.G., Ondeyka, D.L., Thorsett, E.D., Greenlee, W.J., Lohr, N.S., Hoffsommer, R.D., Joshua, H., Ruyle, W.V., Rothrock, J.W., Aster, S.D., Maycock, A.L., Robinson, F.M., Hirshmann, R., *Nature (London)*, 288, (1980), 280.
14. Meyer, R.F., Nicolaidis, E.D., Tinney, F.J., Lunney, E.A., Holmes, A., Hoefle, M.L., Smith, R.D., Essenburg, A.D., Kaplan, H.R.,

- Almquist, R.G., *J. Med. Chem.*, 24, (1981), 964.
15. Kim, D.H., Guinosso, C.J., Buzby, G.C., Herbst, D.R., McCaully, R.J., Wicks, T.C., Wendt, R.L., *J. Med. Chem.*, 26, (1983), 394.
  16. Andrews, P.R., Carson, J.M., Caselli, A., Sparks, H.J., Woods, R., *J. Med. Chem.*, 28, (1985), 393.
  17. Wyvratt, M.J., Tishler, M.H., Ikeler, T.J., Springer, J.P., Tristram, E.W., Patchett, A.A., *Proc. 8th Am. Peptide Symp.*, (1983), 551.
  18. Langridge, F., Gerrin, J.E., Kuntz, I.D., Connolly, M.L., *Science* (Washington, D.C.), 211, (1981), 661.
  19. Blaney, J.M., Jorgensen, E.C., Connolly, M.L., Ferrin, T.E., Langridge, R., Oatley, S.J., Burrige, J.M., Blake, C.C.F., *J. Med. Chem.*, 25, (1982), 785.
  20. Holmes, M.A., Matthews, B.W., *J. Mol. Biol.*, 160, (1982), 623.
  21. Monzingo, A.F., Matthews, B.W., *Biochemistry*, 23, (1984), 5724.
  22. Monzingo, A.F., Matthews, B.W., *Biochemistry*, 21, (1982), 3390.
  23. Weaver, L.H., Kester, W.R., Matthews, B.W., *J. Mol. Biol.* 114, (1977), 119.
  24. Holden, H.M., Tronrud, D.E., Monzingo, A.F., Matthews, B.W., *ACA Meeting 1985*, Abstract H2.
  25. Argos, P., Garavito, R.M., Eventoff, W., Rossmann, M.G., *J. Mol. Biol.*, 126, (1978), 141.
  26. Kester, W.R., Matthews, B.W., *J. Biol. Chem.*, 252, (1977), 7704.
  27. Bernstein, F.C., Koetzle, I.F., Williams, G.J.B., Meyer, E.F., Jr., Brice, M.C., Rodgers, J.R., Kennard, O., Shimanouchi, T., Tasumi, M., *J. Mol. Biol.*, 112, (1977), 535.
  28. Hauptman, H., Karle, J., *Solution of the Phase Problem*. 1. The

- Centrosymmetric Crystal, American Crystallographic Association Monograph No. 3, Polycrystal Book Service, Pittsburg, Pennsylvania, 1953.
29. Harker, D., Kasper, J.S., *Acta. Crystallogr.*, 1, (1948), 70.
  30. International Tables for Crystallography, Volume A, Ed. T. Hahn, D. Reidel Co., Dordrecht, Holland, 1983.
  31. Wilson, A.J.C., *Nature*, 150, (1942), 152.
  32. Karle, J., Hauptman, H., *Acta. Crystallogr.*, 6, (1953), 473.
  33. Germain, G., Woolfson, M.M., *Acta. Crystallogr. Sect. B24*, (1968), 91.
  34. Germain, G., Main, P., Woolfson, M.M., *Acta. Crystallogr. Sect. A27*, (1971), 368.
  35. Ibers, J.A., Least Squares Tutorial, ACA Meeting, 1974.
  36. Dunitz, J.D., *X-Ray Analysis and the Structure of Organic Molecules*, Cornell University Press, London, 1979.
  37. Konnert, J.H., *Acta. Crystallogr., Sect. A.*, 32, (1976), 614.
  38. Konnert, J.H., Gilardi, R., Flippen-Anderson, J.L., "RESLSQ"; Laboratory for the Structure of Matter, Naval Research Laboratory, Washington, D.C., (1982).
  39. Konnert, J.H., Hendrickson, W.A., *Acta. Crystallogr., Sect. A.*, 36, (1980), 344.
  40. Hestenes, M.R., Stiefel, E., *J. Natl. Bur. Stand.*, 49, (1952), 409.
  41. Zachariasen, W.H., *Acta. Crystallogr.*, 23, (1967), 558.
  42. Larson, A.C., *Crystallographic Computing, Proceedings of an International Summer School, 1969*, ed. F.R. Ahmed, (1970), p. 291.
  43. Poland, P., Scheraga, H.A., *Biochemistry*, 6; (1967), 3791.
  44. Scheraga, H.A., *Adv. Phys. Org. Chem.*, 6, (1968), 103.

45. Hill, T.L., *J. Chem. Phys.*, 14, (1946), 465.
46. Westheimer, F.H., Mayer, J.E., *J. Phys. Chem.*, 14, (1946), 733.
47. Allinger, N.L., *J. Am. Chem. Soc.*, 99, (1977), 8127.
48. Engler, E.M., Androse, J.D., Schleyer, P.V.R., *J. Am. Chem. Soc.*, 95, (1973), 8005.
49. Fitzwater, S., Bartell, L.S., *J. Am. Chem. Soc.*, 98, (1976), 5107.
50. Ermer, O., Lifson, S.J., *J. Am. Chem. Soc.*, 95, (1973), 4121.
51. Vedani, A., Dunitz, J.D., *J. Am. Chem. Soc.*, (1985), in press.
52. Weiner, P.K., Kollman, P.A., *J. Comput. Chem.*, 2, (1981), 287.
53. McPherson, A., *Preparation and Analysis of Crystals Protein*, John Wiley and Sons, New York, 1982, pp. 214-215.
54. Fujinaga, M., James, M.N.G., *Acta. Crystallogr. Section B*, 36, (1980), 3196.
55. Kamwaya, M.E., Oster, O., Braduczek, H., *Acta. Crystallogr. Section B*, 37, (1981), 364.
56. Bravosos, A., Benedetti, E., Di Blasio, B., Pavone, V., Pedione, C., Tonido, C., Bonora, G.M., *Macromolecules*, 15, (1982), 54.
57. Cheung, H., Wang, F.L., Ondetti, M.A., Sabo, F., Cushman, D.W., *J. Biol. Chem.*, 255, (1980), 401.
58. McEvoy, F.J., Lai, F.M., Albright, J.D., *J. Med. Chem.*, 26, (1983), 381.
59. (a) Harding, M., Howieson, R.M., *Acta. Crystallogr. Section B*, 32, (1976), 633.  
(b) Di Blasio, B., Pedone, C., Sirigu, A., *Acta. Crystallogr. Section B*, (1975), 601.  
(c) Harrison, W., Rettig, S., Trotter, J., *J. Chem. Soc. Perkin Transact. II*, (1972), 1036.

- (d) Kistenmacher, T.J., Sorrell, T.J., *Cryst. Mol. Struct.*, 4, (1974), 419.
60. Brooks, B.R., Bruccoleri, R.E., Olafson, B.D., States, D.J., Swaminathan, S., Karplus, H., *J. Comp. Chem.*, 4, (1983), 187.
61. Corbett, R.J.T., Ph.D. Thesis, University of Calgary, Canada, 1984.
62. Pople, J.A., Segal, G.A., *J. Chem. Phys.*, 44, (1966), 3289.